The Henryk Niewodniczański
Institute of Nuclear Physics
Polish Academy of Sciences

University of Ferrara

Doctoral Dissertation

Spin dynamics in inhomogeneous and defected low dimensional systems

Dominika Kuźma

Supervisors:

prof. dr hab. Piotr Zieliński   *assoc. prof. Federico Montoncello*

Auxilary Supervisor: dr inż. Paweł Sobieszczyk

Kraków 2018

Acknowledgements

Contents

Abstract

Selected systems of different size scales have been studied in view of their applicability as waveguides for spin waves in various frequency ranges. Localized interface states have been found within a band of propagative waves on a junction of two ferromagnetic chains in addition to bound states in the frequency gaps. Total reflection in the whole frequency range has been found on an interface of two such chains coupled via antiferromagnetic interactions. The magnetic ground states have been found with the use of a software for micromagnetic computations for elliptically shaped flat nanoparticles (macrospins) of permalloy arranged in 1D chains. Ranges of stability/metastability of particular configurations as well as the related magnetic hysteresis loops resulting from the dipolar interaparticle interactions have been delimited. The frequencies of low lying spin waves as well as the corresponding spin precession profiles in such chains have been obtained with a software provided by the Department of Physics and Earth Sciences of the University of Ferrara. The mechanisms of the configuration switching under a homogeneous external magnetic field have been shown to be related with softening of the appropriate spin waves. A possibility of recovery of the stable antiferromagnetic configuration has been predicted by varying the anisotropy of particles. A number of configurations in the simplest two-spin model of macrospin chain have been revealed as a function of the macrospins separation in the chain. An evidence of a discontinuous transformation without, however, a hysteresis has been found.

Streszczenie

Wybrane układy magnetyczne mogące służyć jako falowody dla fal spinowych zostały zbadane pod względem konfiguracji równowagowych i wzbudzeń elementarnych. Wykryto zlokalizowane stany o częstościach w przerwie wzbronionej i - co ciekawe - w paśmie fal objętościowych na złączach łańcuchów spinowych w zależności od parametrów ich oddziaływań. Stwierdzono brak fali przechodzącej na złączu ferromagnetycznych łańcuchów spinowych sprzężonych oddziaływaniem antyferromagnetycznym. Używając oprogramowania do obliczeń mikromagnetycznych wyznaczono konfiguracje równowagowe oraz kształty histerezy magnetycznej w łańcuchach płaskich eliptycznych cząstek magnetycznych. Częstości i polaryzacje fal spinowych w takich łańcuchach zbadano za pomocą oprogramowania dostarczonego przez Wydział Fizyki i Nauk o Ziemi Uniwersytetu w Ferrarze. Mechanizm przełączania konfiguracji okazał się związany z falami spinowymi o częstościach zdążających do zera (tzw. "miękkimi" modami). Stwierdzono, że odzyskanie konfiguracji antyferromagnetycznej w takich łańcuchach jest możliwe przez zmianę parametrów anizotropii. Skonstruowano najprostszy dwuspinowy model makrospinów, zbadano jego konfiguracje równowagowe oraz wykryto przejście, które będąc nieciągłym nie wykazuje histerezy, zatem przejawia cechy przejścia drugiego rodzaju.

1

Introduction

This thesis presents studies of model low-dimensional magnetic systems treated with analytical, semi analytical, and numerical methods. The systems have been selected to be interesting for applications as guides for spin waves in various frequency regions starting from single ionic spins interacting via exchange and dipolar forces to macrospins, i.e. ferromagnetic nanoparticles that, due to their elongated shapes and the related anisotropy, behave in some analogy with single spins. Whereas the spin waves (magnons) in magnetic materials occur in the terahertz or higher frequency regions, the frequencies of magnetic excitations in macrospins can be as low as gigahertzs. This makes the latter system interesting for signal transmission in magnetic devices. The calculations of energies and of the elementary excitations in the simplest one-dimensional systems involve relatively simple analytical formulae that can be treated with routine software for symbolic and numerical calculations such as Maple Waterloo or Wolfram Mathematica. The problem is particularly simple if the system exhibits a translational invariance. The excitations then are Bloch waves, whose frequencies and polarization vectors are obtained by solving the eigenproblem for a relatively low-dimensional dynamical matrix for every wave vector from the first Brillouin zone. A difficulty arises at the presence of inhomogeneities such as surfaces and/or interfaces. A Green function technique proposed by L. Dobrzyński then is useful especially when the interactions are of a short spatial range. On the other hand, modelling of the equilibrium structure and dynamics of macrospins involves numerous degrees of freedom. The number of the degrees of freedom is related with the size of elementary cells (voxels) the macrospin, treated as a continuous magnet, should be divided into to ensure that the magnetization in a single voxel is homogeneous at all stages of computations. The numerical tools used to determine the static properties of the macrospins are The Object Oriented MicroMagnetic Framework (OOMMF) which is an open source software developed at the Information Technology Laboratory of the National Institute of Standards and Technology (ITL/NIST, USA) whereas the spin wave properties have been studied with the Dynamical Matrix Method (DMM) software provided by the Department of Physics and Earth Sciences of the University of Ferrara.

The most interesting results obtained in the thesis are

- Finding of interface localized magnon states in the frequency gap and in the band of bulk waves on an interface between two 1D ferromagnetic chains of single spins coupled in an antiferromagnetic manner.

- Prediction of singularites of wave transmission at the above interface, in particular a total wave reflection in the dispersive range of the subchain into which the wave should be in principle transmitted.

- Design of a chain of flat elliptically shaped macrospins capable of recovering the antiferromagnetic configuration by means of a homogeneous external field or anisotropy parameters.

- Systematic analysis of a chain of complexes, called here bi-spins, consisting of two single spins as the simplest model of macrospins and finding its predictive power for more developed systems.

- Finding, in the above system, of a distance-controlled transformation of a ferromagnetic configuration to an antiferromagnetic one in which a discontinuous structural change proceeds by way of second order phase transition.

The methods used in the thesis and their physical foundations are outlined in Chapter 2. Effects of interfaces on the formation of localized states and on the transmission and reflection of the travelling waves in chains of single spins interacting by exchange and magnetic anisotropy forces is the subject of Chapter 3. Chapter 4 starts with an analysis of properties of a flat elliptically shaped magnetic particle, or macrospin, under external magnetic field. In the subsequent sections of this chapter the equilibrium configurations and the selected low-frequency spin waves are studied in various chains of such particles in view of elucidation of the mechanisms of transformations and of the related soft modes. This knowledge is exploited in Chapter 5 to design optimal parameters allowing one to switch the system between its ferromagnetic and antiferromagntic configuration. The main idea relies on an interplay of the anisotropy of the adjacent macrospins; the anisotropy is controlled either by the geometry (shape anisotropy) or by a material anisotropy parameter. Chapter 6 demonstrates how the properties of a macrospin can be modelled with the use of a complex of as few as two spins (a bi-spin). The analogies turn out surprisingly close, e.g. the shape anisotropy keeping the spins within the plane of a chain of such bi-spins. Additionally, the simplicity of the model allows one to easily manipulate the parameters. The most surprising finding is that a variation of the lattice spacing in such a chain results in a discontinuous transformation which, however,

shows a mode softening at a single point and no hysteresis or phase equilibrium, i.e. properties characteristic of second order phase transition. This would be, thus, a discontinuous second order phase transition. A simple complex of four spins is used to compare the direct single-spins computations with those employing macrospin algorithms. The results and the perspectives for further research are summarized in Chapter 7.

2

Physical bases and mathematical methods

In this chapter we briefly outline foundations of the methods used in the description of the equilibrium states and elementary excitations in systems of magnetic moments.

We first outline some generalities on the magnetism of matter.

Magnetic materials					
Diamagnetic	Paramagnetic	Magnetic			
		Ferromagnetic	Antiferromagnetic	Ferrimagnetic	Antiferrimagnetic

Figure 2.1: Types of magnetic materials.

Materials can be classified into those possessing and not possessing permanent magnetic moments in their structure. The former are called magnetic and the latter non-magnetic. However, all materials show a magnetization related with mutual motions of positive and negative charges when subject to an external field. This kind of magnetization is always opposite to the applied field and the materials exhibiting but this magnetization fall into the category of diamagnetic. The reaction of the magnetic materials to an external field is much more versatile depending on the kind of ordering of the ionic permanent magnetic moments. The state of disorder of magnetic moments, characteristic of paramagnets, prevents a spontaneous magnetization and an applied field produces a coerced or forced magnetization parallel to the field. A parallel ordering of the microscopic moments defines ferromagnets. They show a spontaneous magnetization when put into a state, called monodomain state, in which the magnetic domains point in a one common direction. This is however usually not the most energetically favorable state because it produces an external field. Typical domain arrangement reduced energy are shown in Fig. 2.2 Therefore, an additional external field is often needed to make the domains parallel. However, it was shown by Brown [1] that giving an appropriate shape to a sample of appropriate size may end up in a monodomain magnet. Paradoxically such monodomain systems are often called macrospins because they contain many individual ionic spins. Apart from the ferromagnetic order a number of magnetic ordering are known some of them are presented in Fig. 2.1. Mutually antiparallel order of equal spins is characteristic of antiferromagnet. Analogous order of ionic spins of different

spins defines ferrimagntic materials. Numerous kinds of non-colinear ordering are also known: canted, helical etc. In the present dissertation we deal with ferromagnetic, antiferromagnetic and ferrimagnetic order of single individual spins typical for magnetic ions as well as of well-ordered macrospins.
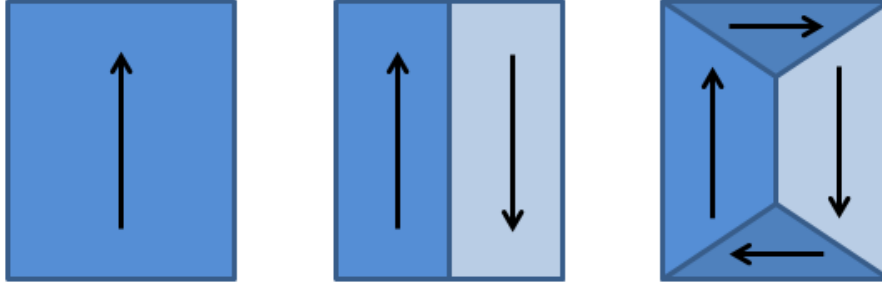
Figure 2.2: Monodomain to domain and closing domain magnetic material.

A system rests in equilibrium if its thermodynamic potential, appropriately defined to the external conditions, shows a minimum with respect to all the degrees of freedom. If the thermal fluctuations can be neglected the potential is just the potential energy. In this dissertation we consider systems of magnetic moments of constant lengths arranged in rigid lattices. Thermal macrospin are not considerate. Therefore, the relevant degrees of freedom are the spatial orientations of the moments. When driven out of its equilibrium state the system gets into motion governed by the equations discussed below.

2.1 General equations of motion for a system of coupled magnetic moments

We consider a system consisting of magnetic moments $\vec{\mu}$ that may change their spatial orientations but have fixed lengths. When reported with respect to a Cartesian reference frame, common to all the moments, the pseudovector of magnetic moment reads

$$\vec{\mu} = \mu^s \left(sin\theta cos\phi, sin\theta sin\phi, cos\theta\right) \equiv \mu^s \vec{m} \qquad (2.1)$$

Each magnetic moment is associated with the corresponding angular momentum

$$\vec{l} = \frac{\vec{\mu}}{\gamma} \qquad (2.2)$$

where γ is the gyromagnetic ratio. If the configuration of magnetic moments under study is in equilibrium the potential energy U, as a function of the angular deviations

$$(\delta\phi_k, \delta\theta_k) \equiv (q_{1k}, q_{2k}) \equiv \vec{q_k} \qquad (2.3)$$

of particular moments labeled by an index k, exhibits a minimum. Therefore it can be expressed as a positive definite quadratic form

$$U = \frac{1}{2} \sum_{k,k'} \sum_{i,i'=1}^{2} E_{kk'}^{ii'} q_{ik} q_{i'k'}. \tag{2.4}$$

The equations of motion in the Hamilton formalism read

$$\frac{\partial p_{ik}}{\partial t} = -\frac{\partial U}{\partial q_{ik}} \tag{2.5}$$

,

where the p_{ik} are the generalized momenta conjugated with the generalized coordinates q_{ik}. Because the generalized coordinates are the rotations about the unit vectors $\hat{\Phi}_{1k} = \hat{z}$, $\hat{\Phi}_{2k} = (-sin\theta_k \hat{x}, cos\phi_k \hat{y})$ by the angles $\delta\phi_k$ and $\delta\theta_k$ respectively, the conjugated momenta are the projections of the variations of the angular momenta onto these unit vectors

$$p_{ik} = \delta \vec{l_k} \cdot \hat{\Phi}_{ik} = \left(\frac{\partial \vec{l_k}}{\partial \phi_k} \delta\phi_k + \frac{\partial \vec{l_k}}{\partial \theta_k} \delta\theta_k \right) \cdot \hat{\Phi}_{ik} \tag{2.6}$$

(no summation over the repeated indices).

In accordance with $\hat{\Phi}_{1k}, \hat{\Phi}_{2k}$ one finds

$$\begin{aligned} p_{1k} &= -\frac{\mu_k^s}{l_k} sin\theta_k \delta\theta_k \\ p_{2k} &= \frac{\mu_k^s}{l_k} sin\theta_k \delta\phi_k \end{aligned} \tag{2.7}$$

.

With the generalized momenta of eqs. 2.7 and the potential energy of eq. 2.4 the equations of motion of the system are (a variant of Landau and Lifshitz equations).

$$\begin{aligned} \delta\dot{\phi_k} &= -\frac{\gamma}{\mu_k^s sin\theta_k} \sum_{k'} \left(E_{kk'}^{\theta\phi} \delta\phi_{k'} + E_{kk'}^{\theta\theta} \delta\theta_{k'} \right) \\ \delta\dot{\theta_k} &= \frac{\gamma}{\mu_k^s sin\theta_k} \sum_{k'} \left(E_{kk'}^{\phi\phi} \delta\phi_{k'} + E_{kk'}^{\theta\phi} \delta\theta_{k'} \right) \end{aligned} \tag{2.8}$$

where the second derivatives $E_{kk'}^{ii'}$ of the potential energy U with respect to the spin orientation variables form a positive definite matrix called Hessian matrix. Because of the time invariance the solutions of eq. 2.8 have an oscillatory form

$$\vec{q_k}(t) = \vec{q_k}(0) e^{-i\omega t} \tag{2.9}$$

with a frequency (pulsation) ω. The solutions are, therefore, wave-like and in the cases of spatial periodicity have a form of Bloch waves (see section 2.3). In the next subsection we discuss the relation between the eigenvalues of the Hessian matrix and the frequencies of spin waves.

2.2   Hessian to Magnon

It has been shown by Grimsditch and Montoncello [2] that the Landau- Lifshitz-Gilbert equations of motion for a system of magnetic moments of constant magnitudes, e.g. spins, can be expressed by the matrix $\overleftrightarrow{H}$ of second derivatives of the energy with respect to deviation angles $\delta\phi_n, \delta\theta_n, n = 1...N$, where N is the number of interacting spins. The equations are given in eq. 2.8 of previous section. The matrix $\overleftrightarrow{H}$ is of course symmetric and therefore it has all its eigenvalues E_k real and the eigenvectors $\vec{w}_k$ can be selected as orthonormal real vectors.

$$\overleftrightarrow{H}\,\vec{w}_k = E_k\vec{w}_k, k = 1...2N, \text{no summation} \qquad (2.10)$$

The eigenvalues E_k are positive, which is a necessary condition for the configuration being stable or at least metastable. An instability of the configuration is marked by one of the eigenvalues E_k tending to zero. The corresponding eigenvector indicates the system of the spin's deviations which costs no energy to the second order of the Taylor expansion of the energy. In practice it means that this system of deviations is the beginning of the path by which the spins quit the configuration in their search for a new, more stable configuration. The instability is, on the other hand, accompanied by a magnon frequency tending to zero. It is, therefore, interesting to study the relation between the eigenvalues of the Hessian matrix and the frequencies of the spin excitations in the system.

We can write the Landau-Lifshitz-Gilbert equations of motion in the following form

$$\overleftrightarrow{P}\overleftrightarrow{H}\,\vec{v} = -i\omega\vec{v}, \qquad (2.11)$$

where ω is the proportional to the frequency (pulsation), and the matrix $\overleftrightarrow{P}$ consists of antisymmetric 2 x 2 diagonal blocks:

$$\overleftrightarrow{P} = \begin{bmatrix} 0 & -1 & 0 & 0 & 0 & ... \\ 1 & 0 & 0 & 0 & 0 & ... \\ 0 & 0 & 0 & -1 & 0 & ... \\ 0 & 0 & 1 & 0 & 0 & ... \\ ... & & & & & \end{bmatrix}. \qquad (2.12)$$

In fact the matrix $\overleftrightarrow{P}\overleftrightarrow{H}$ is the dynamical matrix for magnons and the eq. 2.11 defines an eigenproblem for a non Hermitean matrix.

We shall discuss how the eigenvectors $\vec{v}$, i.e. the vectors of spatial profiles of the spin motion or polarization vectors of magnons, are related with the eigenvectors $\vec{w}_k$. To check it we expand the vector $\vec{v}$ in the basis of vectors $\vec{w}_k$

$$\vec{v} = \sum_{k=1}^{2N} a_k \vec{w}_k. \tag{2.13}$$

Inserting the expansion 2.13 into eq. 2.11 we obtain a homogeneous system of equations, for the coefficients a_k

$$\sum_{k=1}^{2N} \left(\overleftrightarrow{P} E_k + i\omega \overleftrightarrow{I} \right) \vec{w}_k a_k = 0. \tag{2.14}$$

If we left multiply the eq. 2.14 by $i\vec{w}_l^T$ we arrive at the eigenproblem

$$\sum_{k=1}^{2N} \overleftrightarrow{\widetilde{M}}_{lk} a_k = \omega a_l \tag{2.15}$$

with the matrix

$$\overleftrightarrow{M} = \overleftrightarrow{\widetilde{M}} \overleftrightarrow{L} \tag{2.16}$$

where

$$\widetilde{M}_{lk} = i\vec{w}_l^T \overleftrightarrow{P} \vec{w}_k \tag{2.17}$$

is a purely imaginary antisymmetric but at the same time Herimitean matrix, $\overleftrightarrow{L}$ is the diagonal matrix with the eigenvalues E_k on its diagonal

$$L_{nm} = \delta_{nm} E_m \tag{2.18}$$

.

We have to find the eigenvectors $\vec{a}$ and eigenvalues ω of the product $\overleftrightarrow{M} = \overleftrightarrow{\widetilde{M}} \overleftrightarrow{L}$ of two Hermitean matrices

$$\overleftrightarrow{\widetilde{M}} \overleftrightarrow{L} \vec{a} = \omega \vec{a}. \tag{2.19}$$

For this purpose it is useful to introduce a transformation

$$b_k = \sqrt{E_k} a_k. \tag{2.20}$$

which can be abbreviated

$$\vec{b} = \overleftrightarrow{L}^{1/2} \vec{a}. \tag{2.21}$$

Substituting eq. 2.21 into eq. 2.19 and multiplying both sides by the matrix $\overleftrightarrow{L}^{1/2}$ yields:

$$\overleftrightarrow{L}^{1/2} \overleftrightarrow{\widetilde{M}} \overleftrightarrow{L}^{1/2} \vec{b} \equiv \overleftrightarrow{D} \vec{b} = \omega \vec{b}. \tag{2.22}$$

The matrix $\overleftrightarrow{D}$ is antisymmetric, but because it is purely imaginary it is at the same time Hermitean. Therefore all the eigenvalues ω are real as it should be for the

frequencies in a conservative system. On the other hand, for each eigenvalue ω there exists an opposite one $-\omega$. The eigenvectors corresponding to such opposite eigenvalues are mutually complex conjugate. Indeed $\overleftrightarrow{D}^T = -\overleftrightarrow{D} = \overleftrightarrow{D}^*$. Consequently, taking a complex conjugate of eq. 2.22 and remembering that the eigenvalues ω are real we obtain

$$\overleftrightarrow{D}^* \vec{b}^* = -\overleftrightarrow{D}\,\vec{b}^* = \omega^* \vec{b}^* = \omega \vec{b}^* \tag{2.23}$$

which is equivalent to

$$\overleftrightarrow{D}\,\vec{b}^* = -\omega \vec{b}^* \tag{2.24}$$

The essential step between the Hessian matrix and the calculus of the frequencies of the spin excitations lie in the relations 2.17 and 2.18.

2.2.1 The case of soft mode

A special treatment is needed when one of the eigenvalues of eq.2.10, say $E_1 = 0$, i.e. the system is on the verge of its stability. Because the transformation 2.20 does not define the coefficient a_1 we have to come back to the generic eigenproblem of eq. 2.19. We remark that the first column of the matrix $\overleftrightarrow{M}\overleftrightarrow{L}$ consists exclusively of zeros. Therefore, the solution of eq. 2.19 then is $a_1 = 1$, $a_k = 0$ for $k \neq 1$ and $\omega = 0$. Bearing in mind the relation 2.13 and the fact that the eigenvectors of the Hessian matrix are real we conclude that the space profile of the soft mode is identical with the eigenvector corresponding to the vanishing eigenvalue of the Hessian matrix. The eigenvector is real, which is a degenerate limit of an ellipse whose long axis becomes infinitely longer than its short axis. This result facilitates study of soft modes in magnetic systems

2.3 Bloch waves

Many systems considered here show a spatial periodicity in that the equilibrium configuration of the relevant degrees of freedom fulfill the relation.

$$\vec{w}(\vec{r}) = \vec{w}(\vec{r} + \vec{a}m + \vec{b}n + \vec{c}p), \tag{2.25}$$

where $\vec{a}, \vec{b}, \vec{c}$ are the periods in three spatial dimensions and m, n, p are integer numbers. In the cases considered here the quantities $\vec{w}_0(\vec{r})$ are usually pseudovectors of magnetization. A very general Bloch's theorem [3] states that the elementary excitations in such systems, i.e. the solutions of equations of motion in the absence of external disturbances, take on the following form called Bloch's wave

$$\delta\vec{w}(\vec{r}, t) = \delta\vec{w}(\vec{r})e^{-i\omega t + i\vec{k}\vec{r}}, \tag{2.26}$$

where $\vec{k}$ is a wave vector within the first Brillouin zone, i.e. the Wigner-Seitz unit cell in the reciprocal space. The prefactor $\delta\vec{w}_0(\vec{r})$ shows the same periodicity as the original lattice

$$\delta\vec{w}(\vec{r}) = \delta\vec{w}(\vec{r} + \vec{a}m + \vec{b}n + \vec{c}p), \tag{2.27}$$

It is clear from eqs. 2.26 and 2.27, that the actual displacements from equilibrium in the unit cell located at the radius vector $\vec{a}m + \vec{b}n + \vec{c}p$ away from the one corresponding to $m = n = p = 0$ are

$$\delta\vec{w}(\vec{r} + \vec{a}m + \vec{b}n + \vec{c}p, t) = \delta\vec{w}(\vec{r})e^{-i\omega t + i\vec{k}\vec{r}}, \tag{2.28}$$

In practical calculations it is useful to write the eq. 2.26 in the form

$$\delta\vec{w}(\vec{r}, t) = \delta\vec{w}(\vec{r})e^{-i\omega t + i\vec{k}(\vec{a}m + \vec{b}n + \vec{c}p)}, \tag{2.29}$$

where the displacements within the unit cell labeled by $m = n = p = 0$ are directly given as $\delta\vec{w}_0(\vec{r})$. The latter quantity is usually called polarization vector because it is an analogue of the polarization vector in an acoustic or electromagnetic wave that should be multiplied by the phase factor $e^{-i\omega t + i\vec{k}(\vec{a}m + \vec{b}n + \vec{c}p)}$ to obtain the displacements in other unit cells and in the time instant selected as $t = 0$.

The excitations of magnetic moments from equilibrium are called spin waves even though the magnetic moments are macroscopic and not quantum spins. The appellation is, however, adequate in that the excited magnetic moments effectuate precession about their equilibrium orientations. When a wave-corpuscular dualism comes into play, the spin waves are called magnons.

In the macrospin calculations the polarization vectors of the spin waves are represented by the precession ellipses of the magnetic moments as functions of the position in the macrospin. The maps or profiles of the parameters characterizing the ellipses are discussed in Chapters 4 and 5.

2.4   Symmetry of the Bloch waves

The foundations of the Bloch's theorem lie in the group theory [4]. The space of all the displacements of the system's degrees of freedom from equilibrium values is invariant under the symmetry operations (symmetry elements) of the system's symmetry group. This means that any symmetry operation (symmetry element) applied to this space transforms it into the same space. The space splits into subspaces each corresponding to a star $\vec{k}$ of wave vectors generated from a given wave vector $\vec{k}$ by the

symmetry elements of the group. This fact, resulting from the translational periodicity, is sometimes summarized by saying that the wave vector (quasi momentum) is a "good quantum number". Further, the subspace corresponding to one arm $\vec{k}$ of the star generally splits under the subgroup leaving this arm invariant (so called wave vector group) into smaller subspaces. The smallest such subspaces, called irreducible, which cannot be further split, correspond to a given frequency ω (energy $\hbar\omega$). In other words every frequency (energy) of elementary excitation corresponds to an irreducible representation[4] of the symmetry group of the system. The frequencies of the excitations of different irreducible representations are generally different, and they may exceptionally coincide (accidental degeneracy). The symmetry analysis is particularly simple for the wave vector $\vec{k} = 0$, i.e. at the Brillouin zone centre and at the Brillouin zone border. In the former case the displacements in all the unit cells are identical, and in the latter they are opposite in the adjacent cells.

An important simplification occurs when the symmetry group contains an operation, say i which when composed with itself produces the identity operation $i^2 = e$. Such are: spatial inversion, mirror reflections and rotations by 180°. Also the spin reversal operation, called time reversal operation, shows this property. At the presence of such an operation every mode of elementary excitation is either pair (symmetric) or impair (antisymmetric), i.e. either invariant or changing in sign when subjected to this operation. When considered as depending on some parameters the modes of different symmetry (different irreducible representation, e.g. symmetric and antisymmetric) may cross. In contrast to that the modes of the same symmetry generally show an anticrossing also called avoided crossing or repulsion. When their frequencies approach they often show a hybridization, i.e. the same type of polarization displaces from one branch to the other.

2.5 Micromagnetic computations - Dynamical Matrix Method

As explained above the analysis of each system consists of two stages. First an equilibrium configuration must be determined. It corresponds to a minimum of the potential energy. If the minimum is global, the configuration is called stable. Local minima correspond to metastable configurations. If thermal agitation is considered a thermodynamical potential (free energy) adapted to the experimental conditions should be used instead of energy. To practically deal with macrospins the continuous medium approximation is used. The system then is divided into cells (voxels) so small in size that their magnetization can be treated as homogeneous. The details of this approach can be found in ref. [5, 6]. In every (meta-) stable configuration each

macrospin exhibits a distribution of elementary spins (voxels). In the present work the minima of energy are found with the use of the software OOMMF [7, 8]. If global and local minima coexist in the given external conditions, the result of application of the OOMMF program depends on the initial configuration imposed by the user. The external parameter mostly used in this study is the applied magnetic field.

The second step of the study of the spin dynamics is the calculus of the matrix of the second derivatives of energy, in other words the Hessian matrix involved in the equations of motion 2.17. The DMM software involving hybrid of micromagnetic and analytical methods developed in Ferrara performs this calculus and then provides the frequencies of the spin waves for every desired wavevector. The following diagram illustrates the routine way of using the numerical methods.
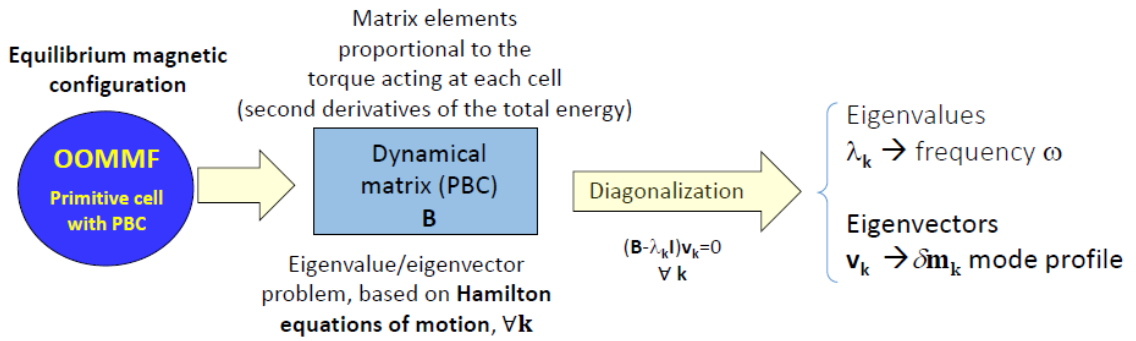

Figure 2.3: Schematic diagram of Dynamical Matrix Method.

In the case of flat macrospins considered in Chapter 4 the equilibrium orientations of the magnetic moments of all the voxels lie in the plane of the macrospin. In our coordinate system this is the (x, y) plane. The perpendicular z axis is always considered to point out of the plane of the figure. Because the motion of the moments involved in the elementary excitations are precessions of the moments around their equilibrium axes the z component of the precessing magnetic moment is always shifted by $\pi/2$ with respect to the (x, y) component. This is illustrated in the following scheme,
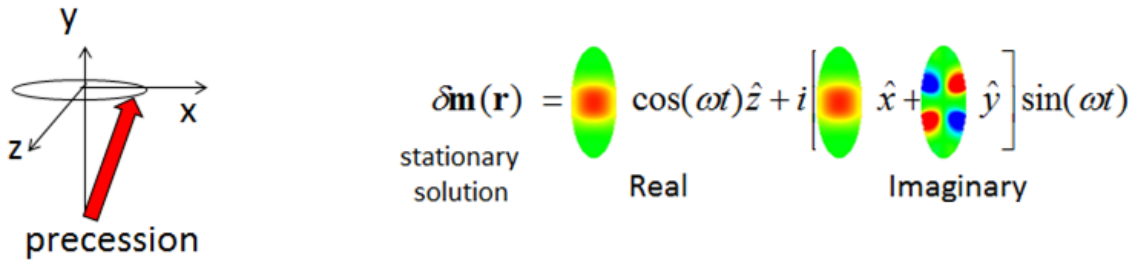

Figure 2.4: Reference system in description and example of complex polarization vector.

An example of polarization vector of a $k = 0$ modes in an AF configuration of

oval-shaped flat macrospins is shown in Fig 2.5. The z component of the precession ellipses is represented with the use of a color code: blue corresponds to negative and red to positive values whereas green stands for zero. The modes are both symmetric with respect to an inversion center denoted by the letter A. They are at the same time antisymmetric with respect to the point B. Of course both points A and B are inversion centers in equilibrium. One can easily see that the frequencies of both modes must be different.
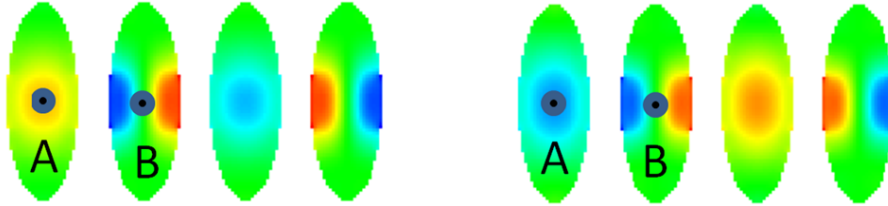

Figure 2.5: Example of precession profiles (polarization vectors) of two centrosymmetric (and at the same time centroantisymmetric) modes at $k = 0$ in chain of identical flat macrospins in AF configuration.

3

Dynamics of 1D magnetic chain

Modern nanotechnology finds nowadays more and more efficient methods of design and fabrication of well-defined systems of interacting magnetic moments. The moments may be those of nanoparticles [9] but they may also originate from magnetic ions embedded in more or less sophisticated organic matrices [10]. Materials of this kind, generally called molecular magnets, are the subject of studies of the Department of Magnetic Research of The Institute of Nuclear Physics. Both kinds of systems are intensively studied in view of the size reduction of memory storage devices [11] and other applications, spintronics, quantum computers included. In the present thesis we present the simplest 1D systems that may be called "composite". They consist of distinct regions of different magnetic arrangement and coupling. The surfaces and interfaces may involve still different magnetic interactions. It has been recently reported that propagation of spin waves (even though the magnetic moments are not necessarily spins) or magnons is possible and observable in the kind of systems [12]. Therefore, in what follows, we study transmission and reflections of the waves at such inhomogeneities.

Using the Green function technique developed by L. Dobrzyński [13] we predict the frequencies of magnons localized on selected interfaces of 1D ferromagnetic, antiferromagnetic, ferrimagnetic, antiferrimagnetic systems. We then find the coupling strengths at which the localized, infinitely lived ("true" [14, 15]) magnetic waves transform into interface resonances marked by finite life times ("leaky waves" [14, 15]). An interesting finding is that in some of the systems the localized true magnons occur for frequencies belonging to bulk radiative bands. To exploit the propagative properties of the systems we calculate the transmission and reflection coefficients for given incident magnons. It turns out that the degrees of freedom excited in the reflection/transmission are orthogonal to those involved in the localized magnon.

3.1 Model of 1D chain of identical magnetic moments with exchange interactions

The simples dynamics of any system in equilibrium is the find by the matrix of second derivatives of the energy or hessian matrix. The values of the coefficients $E^{ii'}_{kk'}$ should be calculated from the specific model of interactions of the magnetic moments. In the 1D case of the exchange interactions limited to the nearest neighbours, with the same exchange constants J throughout the volume considered, the energy is a sum of the scalar products of the neighbouring moments

$$U = J\left(\mu^s\right)^2 \sum_k \left(1 - \vec{m}_k \cdot \vec{m}_{k+1}\right), \tag{3.1}$$

Expanding the reorienting normalized moments $\vec{m}_k$ to the second order in the generalized coordinates

$$\vec{m}_k \approx \vec{m}_k + \sum_{i=1}^{2} \frac{\partial \vec{m}_k}{\partial q_{ik}} \delta q_{ik} + \frac{1}{2} \sum_{i=1}^{2} \sum_{i'=1}^{2} \frac{\partial^2 \vec{m}_k}{\partial q_{ik} q_{i'k}} \delta q_{ik} \delta q_{i'k}. \tag{3.2}$$

One finds the expansion of energy eq. 3.1

$$U = \frac{J\left(\mu^s\right)^2}{2} \sum_k \left(\vec{q}_{k+1} - \vec{q}_k\right)^T \overleftrightarrow{H'} \left(\vec{q}_{k+1} - \vec{q}_k\right) \tag{3.3}$$

with the 2 x 2 matrix $\overleftrightarrow{H'} = \begin{bmatrix} sin^2\theta & 0 \\ 0 & 1 \end{bmatrix}$. The matrix is particularly simple for $\theta = \pi/2$. The corresponding model is depicted in Figure 3.1.
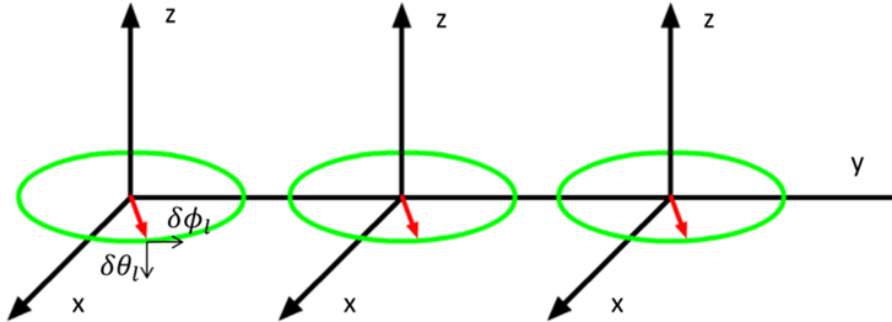

Figure 3.1: Linear infinite chain of magnetic moments

The non-zero coefficients are

$$E^{\theta\theta}_{kk\pm1} = E^{\phi\phi}_{kk\pm1} = -\frac{J\left(\mu^s\right)^2}{2}$$
$$E^{\theta\theta}_{kk} = E^{\phi\phi}_{kk} = J\left(\mu^s\right)^2, \tag{3.4}$$

Recalling the definition eq. 2.3 one can write down the equations of motion for an infinitely long chain of identical magnetic moments

$$\delta\dot{\phi}_k = \frac{\gamma J \mu^s}{2}\left(\delta\theta_{k+1} + \delta\theta_{k-1} - 2\delta\theta_k\right)$$

$$\delta\dot{\theta}_k = -\frac{\gamma J \mu^s}{2}\left(\delta\phi_{k+1} + \delta\phi_{k-1} - 2\delta\phi_k\right),$$

(3.5)

For the sake of brevity we define an effective coupling constant

$$\beta = -\frac{\gamma J \mu^s}{2}.$$

(3.6)

3.1.1 Green function for the infinite chain

The equations of motion 3.5 in expanded form read

$$
\begin{bmatrix}
\ddots & & 0 & -\beta_1 & 0 & 0 & 0 & 0 & 0 & 0 \\
 & & \beta_1 & 0 & 0 & 0 & 0 & 0 & 0 & 0 \\
0 & -\beta_1 & i\omega & 2\beta_1 & 0 & -\beta_1 & 0 & 0 & 0 & 0 \\
\beta_1 & 0 & -2\beta_1 & i\omega & \beta_1 & 0 & 0 & 0 & 0 & 0 \\
0 & 0 & 0 & -\beta_1 & i\omega & 2\beta_1 & 0 & -\beta_1 & 0 & 0 \\
0 & 0 & \beta_1 & 0 & -2\beta_1 & i\omega & \beta_1 & 0 & 0 & 0 \\
0 & 0 & 0 & 0 & 0 & -\beta_1 & i\omega & 2\beta_1 & 0 & -\beta_1 \\
0 & 0 & 0 & 0 & \beta_1 & 0 & -2\beta_1 & i\omega & \beta_1 & 0 \\
0 & 0 & 0 & 0 & 0 & 0 & 0 & -\beta_1 & & \\
0 & 0 & 0 & 0 & 0 & 0 & \beta_1 & 0 & & \ddots
\end{bmatrix}
\begin{bmatrix}
\vdots \\
\delta\phi_{-1} \\
\delta\theta_{-1} \\
\delta\phi_{0} \\
\delta\theta_{0} \\
\delta\phi_{1} \\
\delta\theta_{1} \\
\delta\phi_{2} \\
\delta\theta_{2} \\
\vdots
\end{bmatrix}
= \vec{0}
$$

(3.7)

or

$$\overleftrightarrow{H}\vec{w} = \vec{0},$$

(3.8)

where the matrix $\overleftrightarrow{H}$ is a band-type.

Because of the translational invariance (all the pairs of rows of the matrix $\overleftrightarrow{H}$ are identical) the solution of this equation of motion is given as a travelling wave

$$\delta\phi_l = w_0 e^{-i\omega t + ikal}$$

$$\delta\theta_l = v_0 e^{-i\omega t + ikal}.$$

(3.9)

The angular frequency ω is related with the propagation vector k through the dispersion relations

$$\omega = \pm 2\beta\left(1 - \cos\left(ka\right)\right).$$

(3.10)

It is seen that there exist one positive and one negative (opposite) frequency. Physically both solutions correspond to two modes, each involving a rotation of the moment around its equilibrium orientations. The rotation in one mode is clockwise and in the other anticlockwise. Nevertheless, it is worthwhile to keep a negative

frequency because it corresponds to a band of bulk magnon waves useful in further considerations. The dispersion curves are depicted in the following graph.
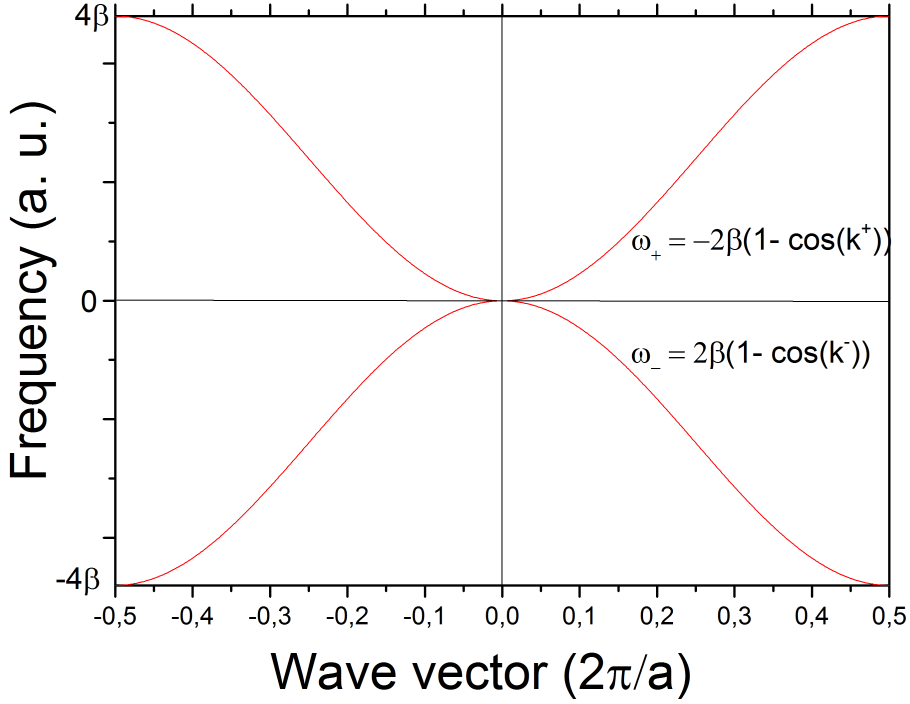

Figure 3.2: The dispersion relations in a chain of ferromagnetically coupled magnetic moments

The plot is symmetric with respect to omega. A negative value of frequency corresponds to the precession of spins in opposite direction. One can see that the modes with $k = 0$ have $\omega = 0$. This is a consequence of the translational invariance of the system; a rotation of all the moments by the same angle costs no energy. It should be kept in mind, however, that such a system is in principle unstable according to the Mermin, Wagner, Berezinsky theorem. This drawback may be easily healed by adding a magnetic anisotropy term at each site. This would introduce a frequency gap at $\omega = 0$. The effect of the gap will be discussed further.

If we want to study the behaviour of the system at a given frequency we have to calculate the corresponding wave vectors. Because we have two separate frequency bands there will be two real wave vectors (one for a wave propagating to the right and one for the wave propagating to the left) and two imaginary wave vectors (one for a wave evanescent to the right and one for a wave evanescent to the left). Generally, if the frequency under study lies in bands of propagative waves, there is as many real wave vectors as there are the bands this frequency belongs to. For the particular system of eq. 3.1 this is depicted in Fig. 3.3.
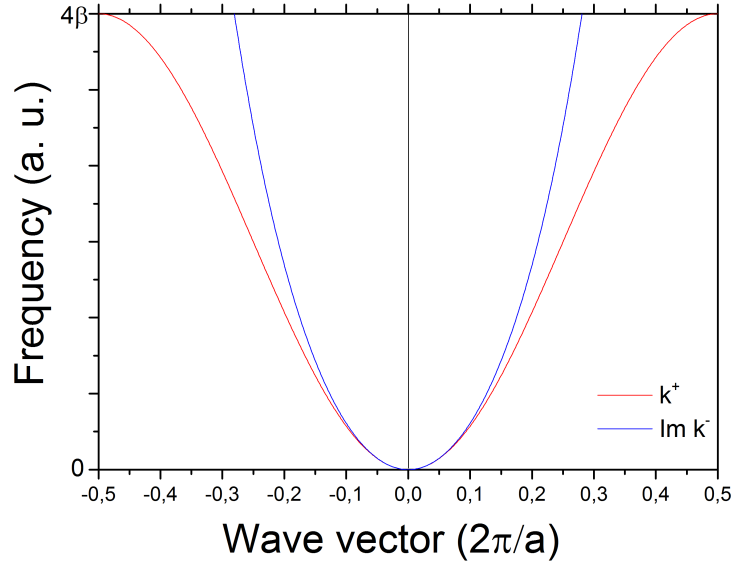
Figure 3.3: The magnon dispersion relations useful in calculations of the wave vectors corresponding to a given frequency. The ordinate shows a positive real frequency, the abscissa shows the wave vector for this frequency (red curve) and the imaginary part of the wave vector corresponding to the negative branch of the dispersion relation.

The wave vectors are needed in calculation of the response function (Green function) for this infinite chain. By definition the Green function is the matrix $\overleftrightarrow{G}$ inverse to the matrix $\overleftrightarrow{H}$

$$\overleftrightarrow{G} = \overleftrightarrow{H}^{-1} \tag{3.11}$$

Physically, the element $\overleftrightarrow{G}_{ll'}$ represents the response of the system at the site l to a harmonic perturbation applied to the site l'. We have obtained the explicit expression for the Green function in the general form

$$\overleftrightarrow{G}_{ll'}(\omega) = \overleftrightarrow{A}_1 z_1^{|l-l'|} + \overleftrightarrow{A}_2 z_2^{|l-l'|} \tag{3.12}$$

where

$$
\begin{aligned}
\overleftrightarrow{A}_1 &= \frac{1}{2\beta\left(z_1 - z_1^{-1}\right)} \begin{bmatrix} i & 1 \\ -1 & i \end{bmatrix} \\
\overleftrightarrow{A}_2 &= \frac{1}{2\beta\left(z_2 - z_2^{-1}\right)} \begin{bmatrix} -i & 1 \\ -1 & -i \end{bmatrix}
\end{aligned} \tag{3.13}
$$

where

$$z_1 = e^{ik^+}, z_2 = e^{ik^-}. \tag{3.14}$$

The correctness of these equations can be checked by a direct multiplication

$\overleftrightarrow{G}\overleftrightarrow{H}^{-1} = 1$. The quantities z_1 and z_2 , related to the wave vectors schematized in Fig. 3.3 must be such that $|z_i| < 1$ or when $|z_i| = 1$ the corresponding wave propagate in the direction from the perturbation to the observation of the response. This "bulk" response function is a starting point for obtaining the Green function of any 1D composite system.

3.1.2 A single interface between two chains - Interface Green function

Now we consider two different ferromagnetic chains coupled in a ferromagnetic or antiferromagnetic manner.
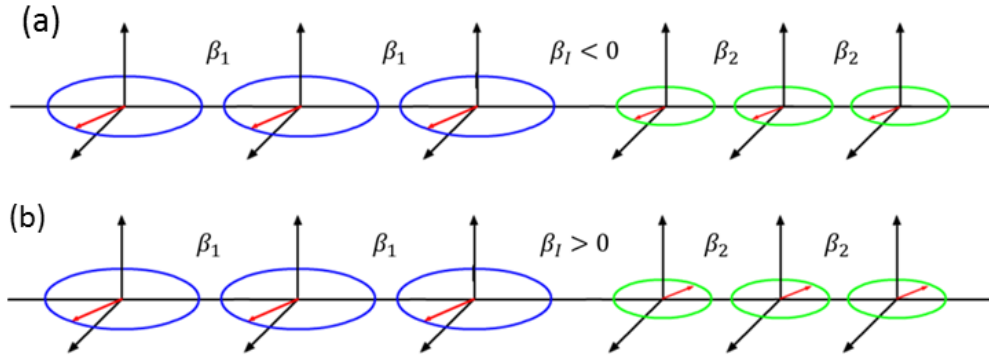

Figure 3.4: (a) Ferromagnetic chain coupled in a ferromagnetic manner, (b) ferromagnetic chain coupled in an antiferromagnetic manner.

Now the matrix $\overleftrightarrow{h}$ of equations of motion consist of semi-infinite segments of the general form of eq. 3.7 $\overleftrightarrow{H}$, with the intrachain parameters β_1 and β_2 respectively. Additionally the matrix is modified in the region of interface by the presence of the interchain coupling parameter β_I. It has been shown by L. Dobrzynski that the Green function g for the interface satisfies a Dyson type equation

$$\left(\overleftrightarrow{I} + \overleftrightarrow{A}\right) g = \overleftrightarrow{G}_s \tag{3.15}$$

where $\overleftrightarrow{G}_s$ is a block diagonal matrix corresponding to elements (eq. 3.11) with the parameters of sub-chain "1" in the region $l \leqslant 0$ and $l' \leqslant 0$ and the parameters of sub-chain "2" in the region $l \geqslant 1$ and $l' \geqslant 1$. The remaining elements of $\overleftrightarrow{G}_s$ vanish. The matrix $\overleftrightarrow{A}$, involving the modifications introduced to the interactions by the interface, has non-zero elements if its second index lies in the region where the equations of motion differ from those in the infinite chains. The region, denoted by $\overleftrightarrow{M}$, encompasses in our case only $l' = 0, l' = 1$ because we assume that the interface spins interact with their nearest neighbours only. Denoting the whole index range by D we can write

$$(I\,(DD) + A\,(DD))\ g\,(DD) = G_s\,(DD)\,, \tag{3.16}$$

or

$$g\,(DD) + A\,(DM)\ g\,(MD) = G_s\,(DD)\,, \tag{3.17}$$

in parentheses we indicate the region of indices of nonzero elements. In particular restricting the first index to M we get

$$
\begin{aligned}
G_s\,(MD) = g\,(MD) + A\,(MM)\,g\,(MD) &= (I\,(MM) + A\,(MM))\,g\,(MD) \\
&\equiv \Delta\,(MM)\,g\,(MD)\,,
\end{aligned}
\tag{3.18}
$$

where we have defined a relatively small matrix

$$\Delta\,(MM) = I\,(MM) + A\,(MM)\,, \tag{3.19}$$

which in our case is a 4×4 matrix. Then

$$g\,(MD) = \Delta^{-1}\,(MM)\,G_s\,(MD)\,. \tag{3.20}$$

When inserted into 3.17 the obtained $g\,(MD)$ of 3.20 allows one to write the explicit expression for $g(DD)$:

$$g\,(DD) = G_s\,(DD) - A\,(DM)\,\Delta^{-1}\,(MM)\,G_s\,(MD)\,. \tag{3.21}$$

3.1.3 Magnons localized at the interface

It is well known that the singularities of the Green function correspond to system's eigenstates. According to eq. 3.21 all the singularities of G_s are also present in g. They correspond to the bulk states. Additionally, however, new eigenstates may appear when $\det \Delta(MM)$ vanishes. Such solutions with real ω represent the states occurring due to the existence of the interface. An example of the interface magnon states calculated numerically for the semi-infinite ferromagnetic chains coupled in the ferromagnetic and antiferromagnetic manner according to Fig. 3.4 are depicted in Fig 3.5.
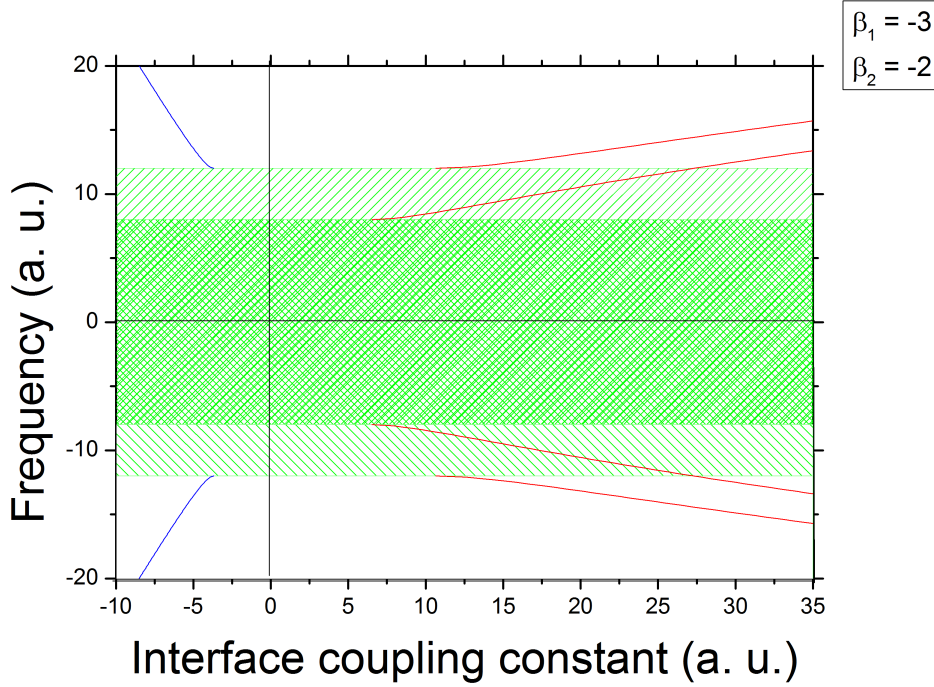
Figure 3.5: The frequencies of localized magnons in ferromagnetic chains coupled in ferromagnetic manner ($\beta_I < 0$) and antiferromagnetic manner ($\beta_I > 0$). The lightly shaded area is the band of bulk waves in the left part, and intensely shaded are is the bulk band of the right part.

In the case of two ferromagnetic chains coupled in a ferromagnetic manner, i.e. for $\beta_1 < 0$, $\beta_2 < 0$, $\beta_I < 0$, there is only one localized state above the band of "bulk" waves, i.e. for $\omega > max(4|\beta_1|, 4|\beta_2|)$. (Mind that the bulk waves are here 1D waves). The mirror reflection symmetry of the graph, $\omega \to -\omega$, implies the existence of a state also below the bands. One can notice that a condition for the existence of the localized state is that $\beta_I < \frac{2\beta_1(\beta_1 - \sqrt{\beta_1(\beta_1 - \beta_2)} + \beta_2)}{3\beta_1 + \beta_2}$, i.e. the interchain coupling must be harder than both intrachain couplings. The polarization vectors of these states can be also calculated with the same theory. Because in the absence of anisotropy and/or external magnetic field the dispersion relations are gapless ($\omega = 0$ at $k = 0$), there is no possibility of a localized state below the bulk band. If the same ferromagnetic chains are coupled in an antiferromagnetic manner, i.e. $\beta_I > 0$ (the spontaneous magnetizations of both sub-chains must be mutually opposite to ensure a minimum of energy), the situation is different. There are, firstly, up to two localized states. The higher of them occurs above both bulk bands. The condition for its existence is $\omega > max(4|\beta_1|, 4|\beta_2|)$ and $\beta_I > -\frac{\beta_1\beta_2\left(\beta_1 + \sqrt{\beta_1(\beta_1 - \beta_2)}\right)}{\beta_1^2 + \frac{\sqrt{2}}{2}\beta_1\beta_2 + \sqrt{\beta_1(\beta_1 - \beta_2)}\left(\beta_1 - \frac{\sqrt{2}-1}{2}\beta_2\right)}$. There is, however, another localized state whose existence condition is $\beta_I > -\frac{\beta_1(\beta_1 + \beta_2 - \sqrt{\beta_1(\beta_1 + \beta_2)})}{\beta_1 + \beta_2}$. There exists, therefore, a region of β_I where the state occurs "on the background" of the band of the bulk waves

of the "harder" chain. The phenomenon is known in the realm of acoustic waves as secluded surface wave [16]. An isolated true surface wave has been found by D.Trzupek and P. Zielinski [17]. The mechanism of such phenomena resides in the fact that the degrees of freedom involved in the surface excitation involve evanescent partial waves only. These degrees of freedom are orthogonal to those involved in the bulk waves of the background.

3.1.4   Local density of states

It is known that the local density of states (LDOS) is proportional to the imaginary part of the Green function [13],

$$\eta = Im \ g \left(\omega + i \ \epsilon \right), \tag{3.22}$$

where ϵ denotes and infinitesimal positive quantity. Physically, the LODS amounts to the energy rate absorbed by the system once excited with an oscillatory forcing. Generally LDOS vanishes outside the bulk bands and takes finite values inside. The localized states are marked by Dirac delta peaks. Fig. 3.6 provides examples of LDOS calculated at the interface of our chains at some characteristic coupling strengths.
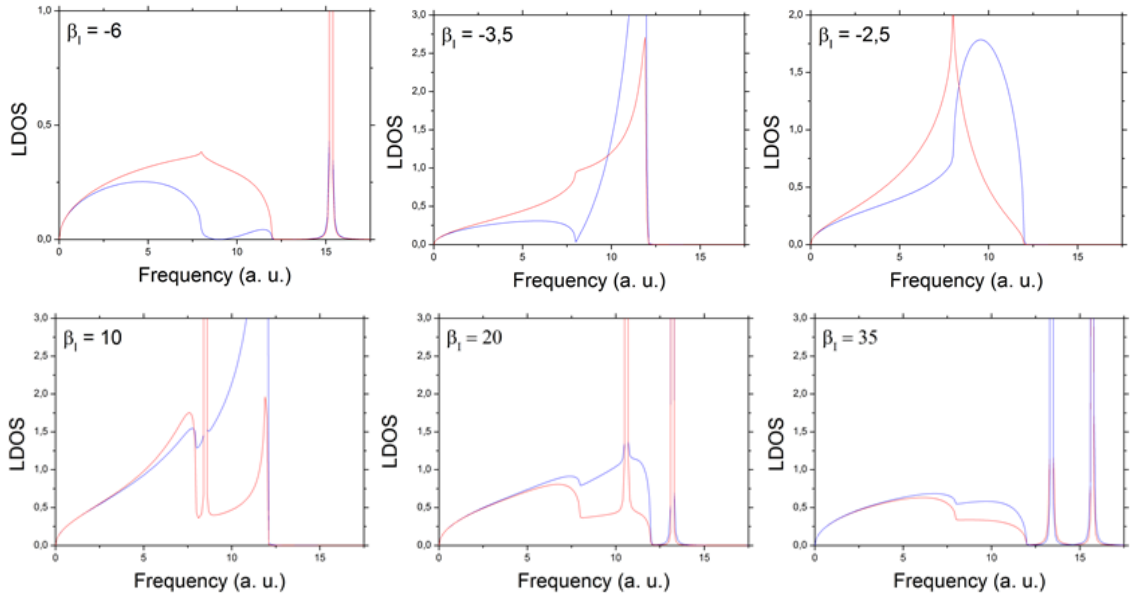

Figure 3.6: LDOS polarized $\delta\phi$ (equal to those polarized in $\delta\theta$) at nodes "0" (blue lines) and "1" (red lines) for the ferromagnetic chains coupled in a ferromagnetic manner (upper row) and antiferromagnetic manner (lower row). The delta-like peaks are artificially broaden by taking a non-zero epsilon in eq. 3.9

Looking at the upper row of Fig. 3.6 one notes the localized state represented by a delta peak outside the bulk band for a strong interchain coupling. The peak is artificially broadened by a finite value of ϵ . With decreasing coupling strength

the peak merges into the band of the bulk waves. The density of states within the bulk band then becomes modified that is characteristic of an interface resonance. However, in contrast with many mechanical cases [15] we have not found any solution of the equation $\Delta(\omega) = 0$ with a complex ω. The question of the existence of a surface resonance in this case remains, therefore, open. The lower row of Fig. 3.6 depicts analogous behaviour for the antiferromagnetic coupling of ferromagnetic chains. When the coupling is strong enough two localized states occur above the bulk bands. For weaker couplings one of the states occurs "on the background" of one of the bulk bands. We have not found solutions with complex ω either.

3.1.4.1 The transmission and reflection of magnons from the interface

A magnonic wave incident on the interface generally transforms partly into a number of transmitted and partly into a number of reflected waves. In the present case, due to the existence of two bulk bands at every sub-chain (positive and negative frequency) one expects two transmitted and two reflected waves. If the frequency falls into a band of bulk waves, the corresponding transmitted/reflected wave is propagative, i.e. it has a real wave vector. In the opposite case the transmitted/reflected wave is evanescent or, in other words, forms a kind of near fields. A schematic representation of the transmission/reflection effects in the case of frequency lying within bulk bands of both sub-chains is depicted in Fig. 3.7.
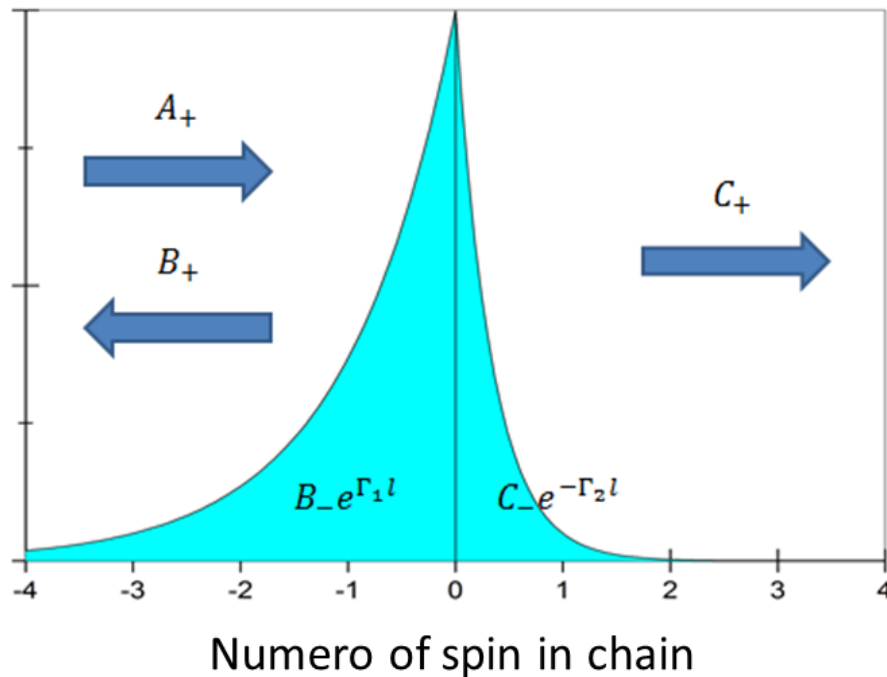

Figure 3.7: Schematic representation of the transmission/reflection effects. Arrows represent incoming, reflected and transmitted propagative waves. The cyan regions correspond to evanescent partial waves (near fields) that can also arise in this scattering experiment.

Noteworthy is that if $\omega > 0$ the wave fields B_- and C_- are near fields originated from the existence of the negative frequency bulk band. The amplitudes B_+, B_-, C_+ and C_- relative to the amplitude of the incident wave define the reflection and transmission coefficients respectively. The calculus of the transmission and reflection coefficients stems from the boundary conditions. It involves solving the following system of linear equations

$$\overleftrightarrow{M} \begin{pmatrix} B_+ \\ B_- \\ C_+ \\ C_- \end{pmatrix} = \vec{a}\, A_+. \tag{3.23}$$

The matrix $\overleftrightarrow{M}$ corresponding to a ferromagnetic interchain coupling and the vector $\vec{a}$ are

$$\overleftrightarrow{M} = \begin{pmatrix} \beta_1\, e^{-ik_1^+} - \beta_1 + \beta_I & -\beta_1\, e^{-ik_1^-} + \beta_1 - \beta_I & -\beta_I\, e^{ik_2^+} & \beta_I\, e^{ik_2^-} \\ -\beta_1\, e^{-ik_1^+} + \beta_1 - \beta_I & -\beta_1\, e^{-ik_1^-} + \beta_1 - \beta_I & \beta_I\, e^{ik_2^+} & \beta_I\, e^{ik_2^-} \\ -\beta_I & \beta_I & e^{ik_2^+}(\beta_2\, e^{-ik_2^+} - \beta_2 + \beta_I) & e^{ik_2^-}(-\beta_2\, e^{-ik_2^-} + \beta_2 - \beta_I) \\ \beta_I & \beta_I & e^{ik_2^+}(-\beta_2\, e^{-ik_2^+} + \beta_2 - \beta_I) & e^{ik_2^-}(-\beta_2\, e^{-ik_2^-} + \beta_2 - \beta_I) \end{pmatrix},$$

$$\vec{a} = \begin{pmatrix} -\beta_1\, e^{ik_1^+} + \beta_1 - \beta_I \\ \beta_1\, e^{ik_1^+} - \beta_1 + \beta_I \\ \beta_I \\ -\beta_I \end{pmatrix}. \tag{3.24}$$

In the case of an antiferromagnetic coupling they read

$$\overleftrightarrow{M} = \begin{pmatrix} \beta_1\, e^{-ik_1^+} - \beta_1 - \beta_I & -\beta_1\, e^{-ik_1^-} + \beta_1 + \beta_I & -\beta_I\, e^{ik_2^+} & \beta_I\, e^{ik_2^-} \\ -\beta_1\, e^{-ik_1^+} + \beta_1 + \beta_I & -\beta_1\, e^{-ik_1^-} + \beta_1 + \beta_I & -\beta_I\, e^{ik_2^+} & -\beta_I\, e^{ik_2^-} \\ -\beta_I & \beta_I & e^{ik_2^+}(\beta_2\, e^{-ik_2^+} - \beta_2 - \beta_I) & e^{ik_2^-}(-\beta_2\, e^{-ik_2^-} + \beta_2 + \beta_I) \\ -\beta_I & -\beta_I & e^{ik_2^+}(-\beta_2\, e^{-ik_2^+} + \beta_2 + \beta_I) & e^{ik_2^-}(-\beta_2\, e^{-ik_2^-} + \beta_2 + \beta_I) \end{pmatrix},$$

$$\vec{a} = \begin{pmatrix} -\beta_1\, e^{ik_1^+} + \beta_1 + \beta_I \\ \beta_1\, e^{ik_1^+} - \beta_1 - \beta_I \\ \beta_I \\ \beta_I \end{pmatrix}. \tag{3.25}$$

Fig. 3.8(a) represents the frequency dependence of the moduli of the coefficients in the case of ferromagnetic coupling. Noteworthy is that none of the near fields are present on both sides except for the region above the bulk band on the transmission side. As expected the modulus of the reflection coefficient amounts to unity in the latter cases.
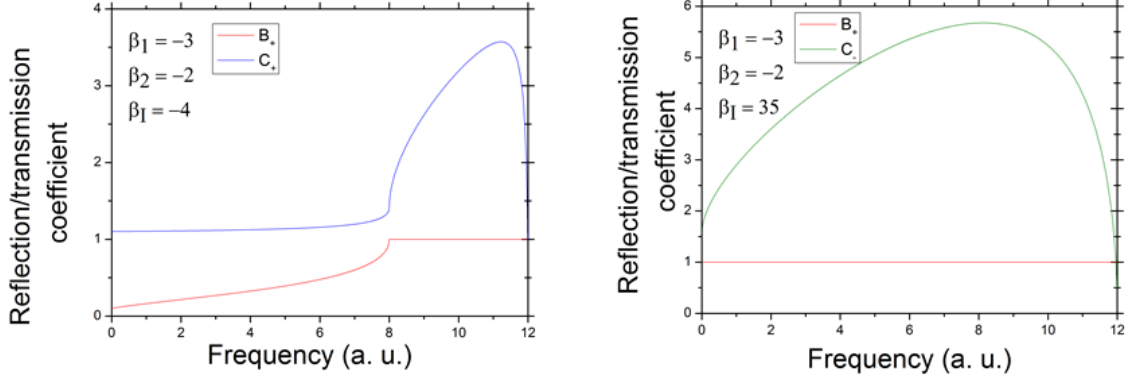
Figure 3.8: Moduli of amplitude reflection (red) and transmition coefficients (propagative wave - blue and near field - green) as functions of frequency of the incident wave in case of (a) ferromagnetic coupling and (b) antiferromagnetic coupling

.

Fig. 3.8b represents analogous results for the ferromagnetic chains coupled in an antiferromagnetic manner. Interestingly enough there is no transmitted propagative wave at all. What arises at the transmission side is a near field only. In turn, there is no near field on the incident side. The amplitude of the reflection coefficient is equal to 1 for all frequencies.

3.1.5 Partial waves involved in localized states

The condition $A_+ = 0$ and $det(M) = 0$ correspond to the localized states whose frequencies are reported in Fig. 3.5. The eq. 3.23 then becomes homogeneous, and the amplitudes $B_\pm$ and $C_\pm$ define the partial waves forming the localized wave. We have checked that in the case of a ferromagnetic interchain coupling the only localized state consists of the wave fields proportional to B_+ and C_+ i.e. the same that participate in the transmission-reflection, when the frequency is in the band of propagative waves. The z-parameters of these wave fields are negative so that the waves are alternating with the distance from the interface. This is analogous to many mechanical cases. A different behaviour is shown for an antiferromagnetic coupling visible on the right side of Fig. 3.5. A high-frequency localized state is visible on the right side of Fig. 3.5. The wave field of the high-frequency localized state consists of B_+ and C_-, i.e. the same involved in the transmission-reflection. Now, however, the excitation is dumped alternating on the incidence (harder coupling) side and monotonous on the transmission (weaker coupling) side. It should be born in mind that C_-, corresponds to an evanescent wave in the whole range of frequencies. The wave fields forming the low-frequency localized state are B_- and C_+. The wave field is then monotonous on the incident (harder) side and alternating on the transmission (weaker) side. There is no localized state in which the wave field would be monotonous on both sides of the interface. Such states can be expected

in the presence of a gap at $k = 0$. These are the partial waves that are absent from the transmission- reflection. In particular, by lowering frequency below $4\beta_2$ no propagative wave C_+ arises.

3.1.6 Summary of results with exchange interaction only

We have adopted the Green function technique due to L. Dobrzynski to determine the frequencies of the localized states and the local densities of states in any composite chain of coupled magnetic moments. (The same techniques allows one to calculate the polarization vectors of the localized states [18] which is not discussed here). We have exemplified the method on two ferromagnetic chains coupled in a ferromagnetic and antiferromagnetic manner. A single localized magnon state, alternating on both sides of the interface, has been found for a strong enough ferromagnetic interchain coupling. When the coupling is antiferromagnetic two localized states may arise. The low-frequency one, alternating on the weak coupling side, occurs "on the background" of the bulk band of the strong coupling part of the system. An incident wave coming from the strong-coupling side does not produce any propagative transmitted wave. An interesting effect is the non-existence of the transmitted waves in the case of the ferromagnetic chains coupled in an antiferromagnetic manner.

3.2 Anisotropy

The previous calculations, involving only exchange interactions, concerned in fact an unstable system in that any rotation of all the spins by the same angle costed no energy. In reality any magnetic moment in condensed matter is subjected to a local potential. Minima of the potential define the magnetic anisotropy. The orientations of the spin that correspond to the minimum define an "easy axis". We start with the ferromagnetic chains and assume that the equilibrium orientation of the spins, say x (Fig. 3.1) corresponds to the minimum of the local potential. The matrix of the second derivatives of the magnetic energy (see Eq. 2.4) should now be completed with the local term. A priori there are three types of the local term, i) degenerate (axisymmetric), ii) perpendicular and iii) twisted. The corresponding matrix in the three cases reads:

- Degenerate (axisymmetric)

$$E_{ani} = \left[\begin{array}{cc} H_1 & 0 \\ 0 & H_1 \end{array} \right], \tag{3.26}$$

here the energy of the spin increases as a function of the angle of the spin with the unique axis only;

- Perpendicular, (non rotated)

$$E_{ani} = \begin{bmatrix} H_1 & 0 \\ 0 & H_2 \end{bmatrix}, \tag{3.27}$$

here the eigenvectors of the local energy matrix are parallel and perpendicular to the chain, this means that the energy depends also on the orientation of the projection of the spin onto the plane perpendicular to the easy axis (and to the spin);

- Twisted (rotated with respect to chain axes)

$$E_{ani} = \begin{bmatrix} H_1 & H_3 \\ H_3 & H_2 \end{bmatrix}, \tag{3.28}$$

here the eigenvectors point any directions perpendicular to the spin. In all the cases the matrix should be positive definite. The effect of the anisotropy on the dispersion relations in infinite chains is as follows.

3.2.1 Coupling of two chains with anisotropy identical at each site of each subchain

- Degenerated anisotropy

The matrix of second derivatives of energy density is

$$E_{ani} = \begin{bmatrix} H_1 & 0 \\ 0 & H_1 \end{bmatrix}. \tag{3.29}$$

Then dispersion relations are given by the following formula:

$$\omega = \pm\sqrt{(2\,\beta(1 - \cos{(ka)}) - H_1)^2}. \tag{3.30}$$

The polarization vectors of the magnons are the same as in the case without anisotropy. The dispersion curves are depicted in the following graph:
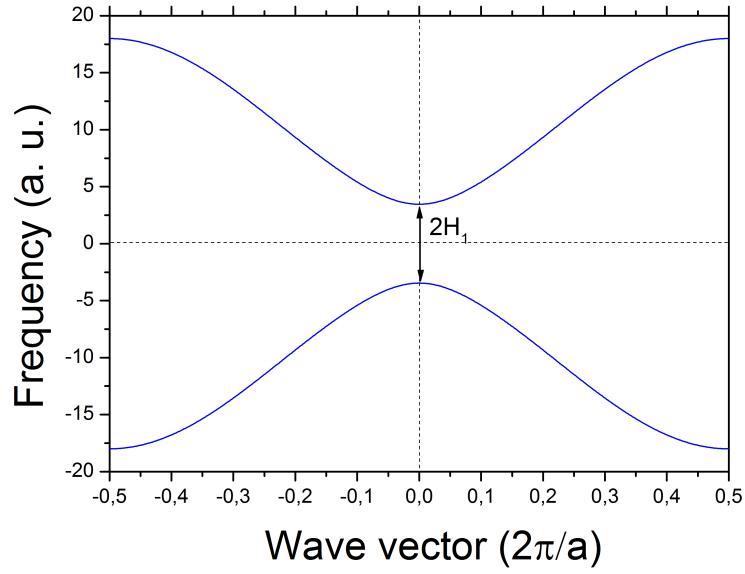
Figure 3.9: The dispersion relations in the case of degenerate anisotropy.

The plot is symmetric with respect to ω (as without anisotropy), but now it has a frequency gap (width $2H_1$). The dispersion curves are shifted by $H_1 = (H_1)_1$. The internal index corresponds to the number of the chain and the outer to the position in the matrix $(H_k)_1$; $k = 1, 2$.

If we couple two such chains in a ferromagnetic manner we have found one localized state above the band of bulk waves for $\omega > max\{(4\ |\beta_1| + (H_1)_1)\,,\ (4\ |\beta_2| + (H_2)_1)\}$
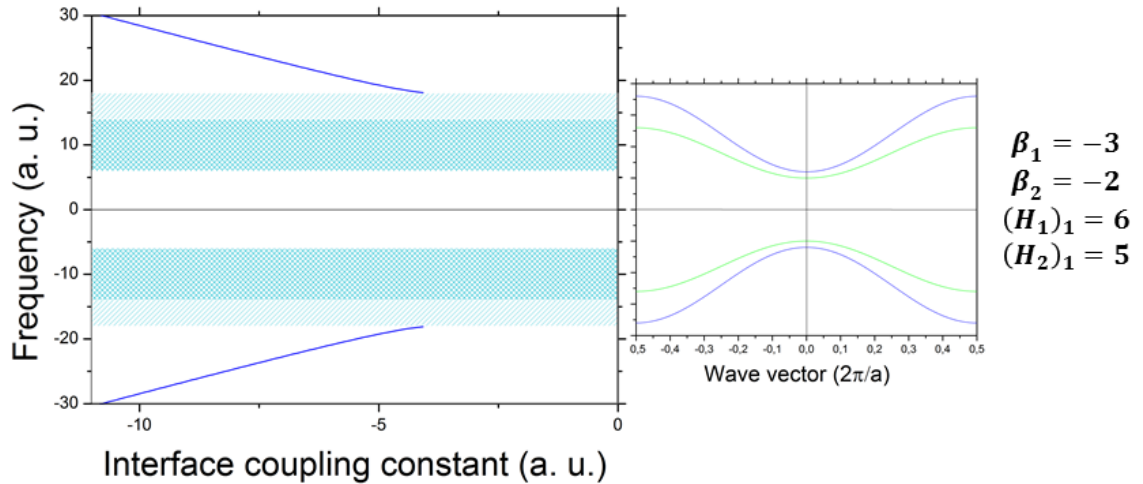

Figure 3.10: The bulk bands and localized states frequencies for two ferromagnetic chains with degenerated anisotropy as a function of coupling constant β_I (left). The dispersion relations of both subchains (right).

29

● Perpendicular anisotropy

In this case the matrix of second derivatives of energy density is as follows

$$E_{ani} = \begin{bmatrix} H_1 & 0 \\ 0 & H_2 \end{bmatrix}. \tag{3.31}$$

(this matrix must be positive definite, i.e. $H_1 > 0$ and $H_2 > 0$)

Then the dispersion relations are given by the formula.

$$\omega = \sqrt{(2\beta\left(1 - \cos\left(ka\right)\right) - H_1)\left(2\beta(1 - \cos\left(ka\right)) - H_2\right)}. \tag{3.32}$$

The polarization vectors of the magnon waves are now dependent on the wave vector k.
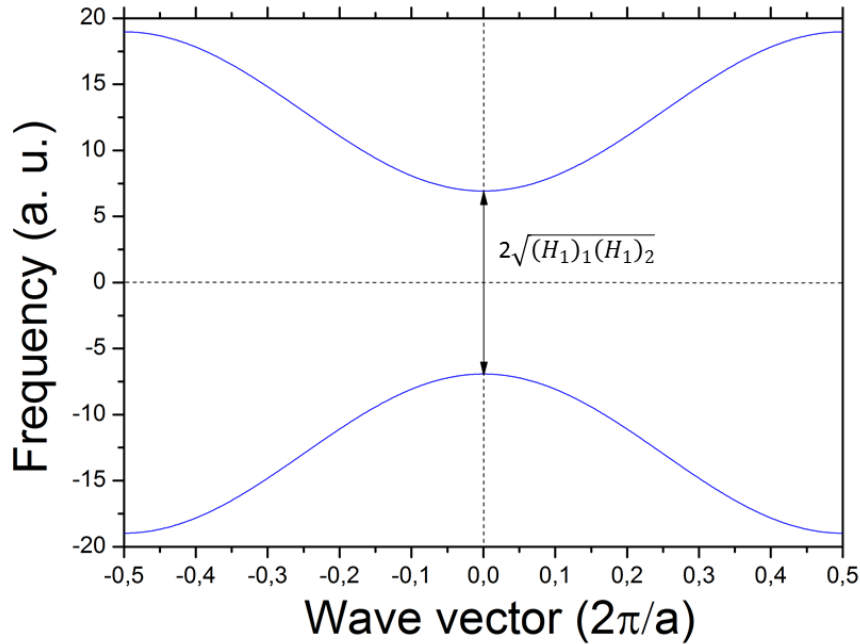
The dispersion curves are depicted in the following graph:

Figure 3.11: The dispersion relations of spin waves for magnetic chain with perpendicular anisotropy

.

The plot is also symmetric with respect to ω (as without anisotropy), but now the frequency gap is defined by the geometric mean of both eigenvalues (width: $2\sqrt{(H_1)_1(H_1)_2}$). The width of the bulk band, i.e. the distance between the minimum and maximum of the dispersion curve increases.

There is one localized state above the band of "bulk" waves for

30

$$\omega > max\{\sqrt{\left(4\ |\beta_1| + (H_1)_1\right)\left(4\ |\beta_1| + (H_1)_2\right)},\ \sqrt{\left(4\ |\beta_2| + (H_2)_1\right)\left(4\ |\beta_2| + (H_2)_2\right)}\}$$
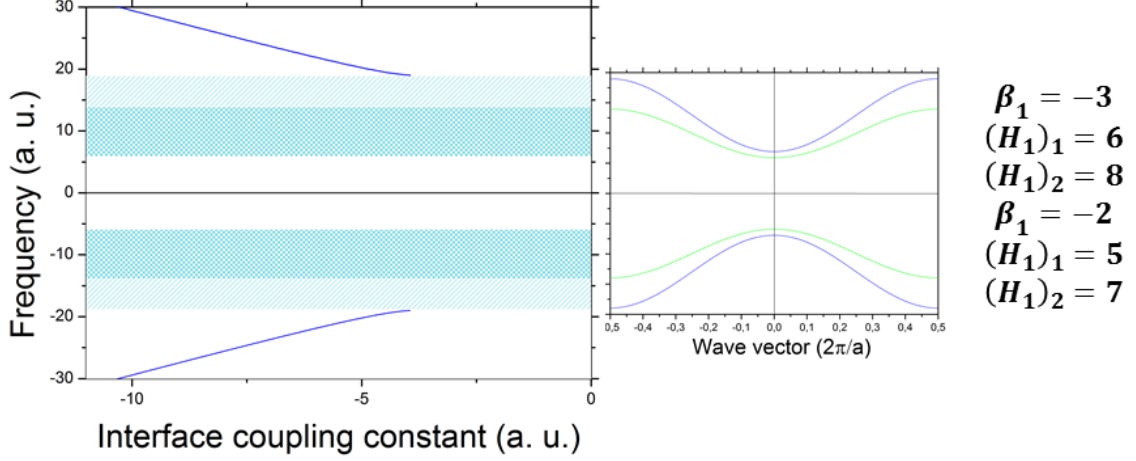
$$(3.33)$$

Figure 3.12: The bands of bulk waves and frequencies of localized states for two ferromagnetic chains with perpendicular anisotropy as a function of coupling constant β_I (left). The dispersion relations of both subchains (right).

- Twisted anisotropy

In this case the matrix of second derivatives of energy density is as follows

$$E_{ani} = \left[\begin{array}{cc} H_1 & H_3 \\ H_3 & H_2 \end{array}\right].$$

$$(3.34)$$

(this matrix must be positive definite)

Then the dispersion relations:

$$\omega = \sqrt{\left(2\beta\left(1 - \cos\left(ka\right)\right) - H_1\right)\left(2\beta(1 - \cos\left(ka\right)) - H_2\right) - H_3^2}.$$

$$(3.35)$$

The dispersion curves are depicted in the Fig. 3.13. The plot is symmetric with respect to ω (as without anisotropy), but now it has a frequency gap of the width $2\sqrt{((H_1)_1(H_1)_2 - H_3^2)}$, once again the geometric mean of the eigenvalues. Here again the interval between the minimum and maximum increases. When one of the eigenvalues of the anisotropy energy matrix tends to zero, i.e. when $(H_1)_1(H_1)_2 - H_3^2 \to 0$ the minimum at $\omega = 0$ becomes more and more sharp. There is one localized state above the band of "bulk" waves for

$$\omega > max\{\sqrt{\left(4\ |\beta_1| + (H_1)_1\right)\left(4\ |\beta_1| + (H_1)_2\right) - (H_1)_3^2},\ \sqrt{\left(4\ |\beta_2| + (H_2)_1\right)\left(4\ |\beta_2| + (H_2)_2\right) - (H_2)_3^2}\}$$
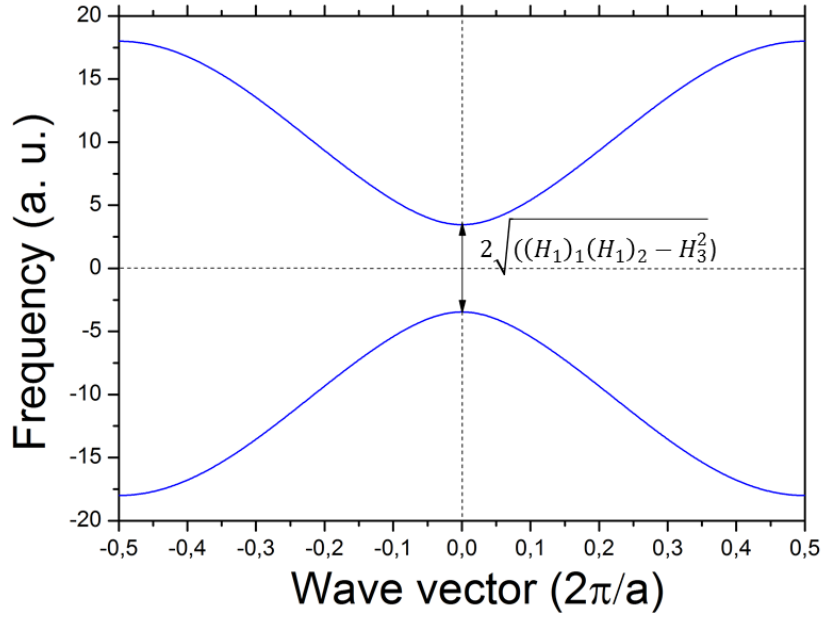
$$(3.36)$$

Figure 3.13: The dispersion relations of spin waves for ferromagnetic chain with twisted anisotropy.
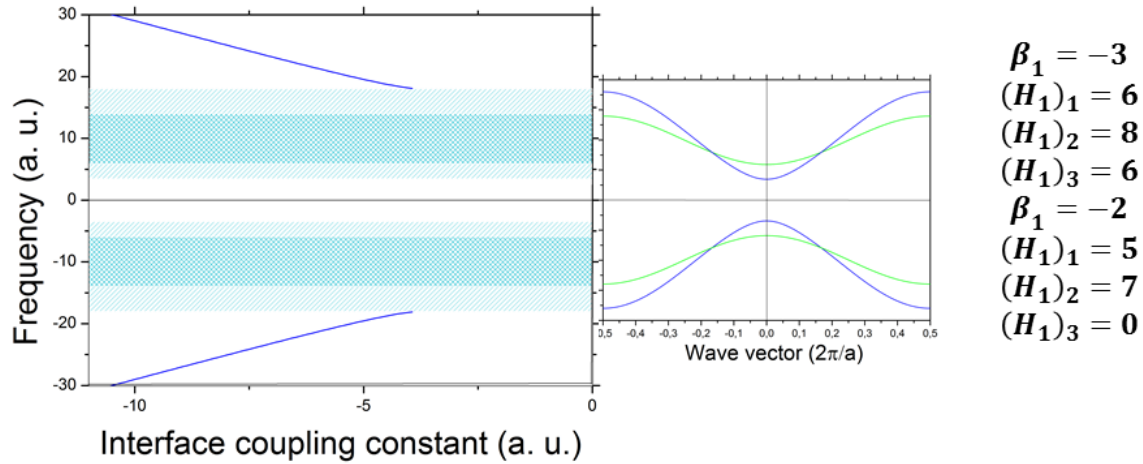

Figure 3.14: The bands of bulk waves and frequencies of localized states for two ferromagnetic chains with twisted anisotropy as a function of coupling constant β_I (left). The dispersion relations of both subchains (right).

3.2.2 Effect of modification of anisotropy in the interface region

The above examples of the coupled chains assumed a uniform anisotropy in both subchains independently of the distance from the interface. However, one can expect that the local energy term can be different at the sites adjacent to the interface

because the chemical surrounding is different there from the one within each chain. We expect the appearance of localized states in the gap in the cases where the anisotropy in the vicinity of the interface is weaker than in the bulk. In the specific case where both interface spins show an anisotropy different than in the bulk we determine the frequencies and polarizations of the localized states by finding zeros of the determinant of a 8 x 8 matrix, whose columns are labelled by the unknowns of the problem: $B_+, B_-, \delta\phi_0, \delta\theta_0, \delta\phi_1, \delta\theta_1, C_+, C_-$, where B_+ and B_- are the amplitudes of waves (evanescent if the frequency is outside the bands of the bulk waves) propagating into the subchain 1 and C_+, C_- are the analogous amplitudes in the subchain 2. The variables $\delta\phi_0, \delta\theta_0$ and $\delta\phi_1, \delta\theta_1$ describe the motion of the interfacial moments that cannot be associated with the waves. Below we discuss some characteristic examples.

Example 1: Two different ferromagnetic chains with anisotropy weaker at the interface sites

We consider a degenerate anisotropy in both subchains. The anisotropy energy keeps the moments in the ferromagnetic configuration in both subchains independently of their angular displacements. The anisotropy in both subchains is identical so that the chains differ in the exchange energy only. Thus, the anisotropy energy term away from the interface is given by the matrix

$$E_{ani} = \begin{bmatrix} H^c & 0 \\ 0 & H^c \end{bmatrix}, \tag{3.37}$$

and on the sites adjacent to the interface:

$$E_{ani} = \begin{bmatrix} H^s & 0 \\ 0 & H^s \end{bmatrix}. \tag{3.38}$$

Thus, the matrix of the equations of motion reads

$$h = \begin{bmatrix}
0 & -\beta_1 & i\omega & -H^c + 2\beta_1 & 0 & -\beta_1 & 0 & 0 & 0 & 0 & 0 & 0 \\
\beta_1 & 0 & H^c - 2\beta_1 & i\omega & \beta_1 & 0 & 0 & 0 & 0 & 0 & 0 & 0 \\
0 & 0 & 0 & -\beta_1 & i\omega & -H^s + \beta_1 + \beta_I & 0 & -\beta_I & 0 & 0 & 0 & 0 \\
0 & 0 & \beta_1 & 0 & H^s - \beta_1 - \beta_I & i\omega & \beta_I & 0 & 0 & 0 & 0 & 0 \\
0 & 0 & 0 & 0 & 0 & -\beta_2 & i\omega & -H^s + \beta_2 + \beta_I & 0 & -\beta_I & 0 & 0 \\
0 & 0 & 0 & 0 & \beta_2 & 0 & H^s - \beta_2 - \beta_I & i\omega & \beta_I & 0 & 0 & 0 \\
0 & 0 & 0 & 0 & 0 & 0 & 0 & -\beta_2 & i\omega & -H^c + 2\beta_2 & 0 & -\beta_2 \\
0 & 0 & 0 & 0 & 0 & 0 & \beta_2 & 0 & H^c - 2\beta_2 & i\omega & \beta_2 & 0
\end{bmatrix}. \tag{3.39}$$

We consider an example with the parameters of the exchange interactions: $\beta_1 = -3$, $\beta_2 = -2$. The sites in the left subchain are labelled by $l \in (-\infty, 0\rangle$, and in the right subchain $l \in \langle 1, +\infty)$. The anisotropy term in the bulk regions $H^c = 6$, for $l \neq \{0, 1\}$ is the same in both subchains whereas it takes a value $H^s = a$, at $l = 0$ and $l = 1$. We vary this parameter in the range $a \in \langle 0, 10 \rangle$.

If the anisotropy term at the interface is equal or greater than that in the bulk

the only localised states exist above the bulk bands. However, if the anisotropy in the interface region is weaker, the localized states appear also in the low frequency gap as a function of the coupling constant β_I. In the figure below we depict the frequencies of the localized states for the parameters

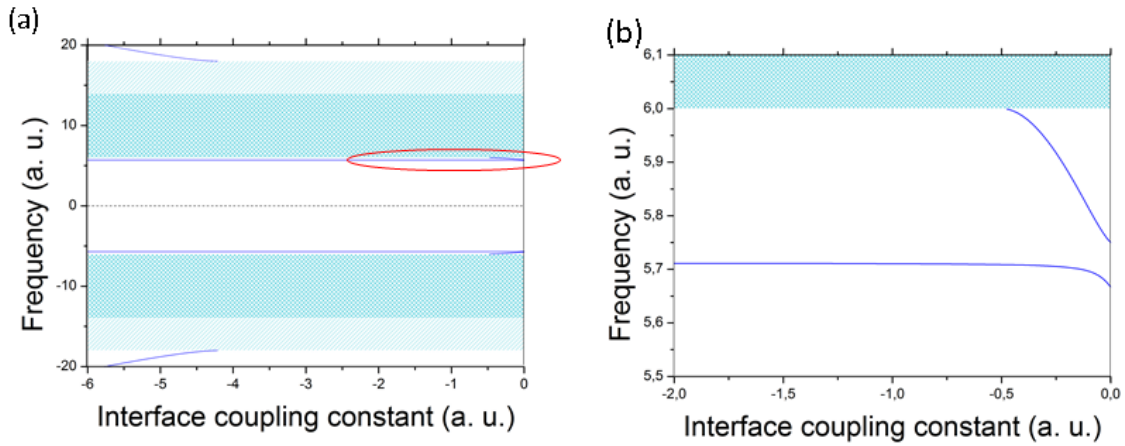$$\beta_1 = -3,$$
$$\beta_2 = -2,$$
$$H^c = 6,$$
$$H^s = 5.$$

Figure 3.15: (a) Frequencies of localized states on interface of two different ferro-magnetic chains with $\beta_1 = 3$ and $\beta_2 = 2$ respectively, identical bulk anisotropies $H_c = 6$ and interface anisotropies $H_s = 2$ as functions of the coupling parameter β_I. (b) Enlarged detail of (a) marked with red ellipse.

The scale on the right allows one to discern the structure of the localized states in the gap.

The scale on the right allows one to discern the structure of the localized states in the gap. There are generally three dispersion branches of the localized interface states. The lowest branch (bottom) occurs in the whole region $\beta_I = (-\infty,\ 0)$. The corresponding frequency region is $= (5.6667,\ 5.7122)$. The asymptotic behaviour of the polarization is such that $\begin{pmatrix} \delta\phi_0 \\ \delta\theta_0 \end{pmatrix} = \begin{pmatrix} \delta\phi_1 \\ \delta\theta_1 \end{pmatrix}$ in this mode in the limit $\beta_I \to -\infty$. This means that both interface spins remain parallel when rotating about their axes. Generally the displacements of both spins are

$$\begin{pmatrix} \delta\phi_1 \\ \delta\theta_1 \end{pmatrix} = d \begin{pmatrix} \delta\phi_0 \\ \delta\theta_0 \end{pmatrix}$$

where $d = C_+ z_{2+}$.

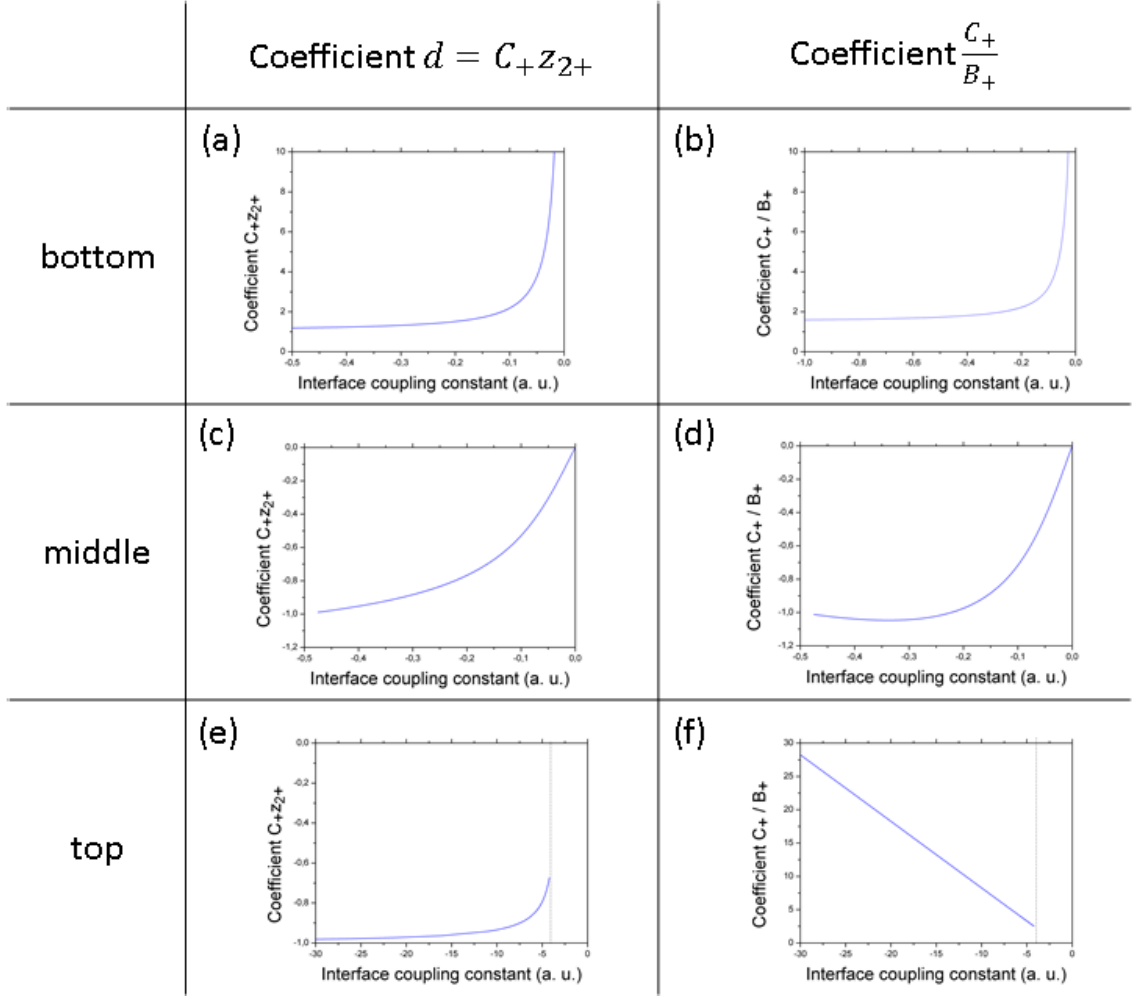The dependence of the parameter d on β_I is depicted in fig. 3.16

Figure 3.16: Dependences of ratios C_+z_{2+} and C_+/B_+ on coupling constant β_I for three dispersion branches of the localized interface states.

Its asymptotic behaviour at $\beta_I \to -\infty$ is easily visible. In the limit $\beta_I \to 0$, i.e. for the decoupled chains the coefficient d tends to infinity. Bearing in mind that in the present calculation the value B_+ has been kept $B_+ = 1$ one easily sees that this symmetric mode becomes a surface wave in the subchain 2, i.e. the one with a weaker exchange interactions, whereas no motion is observed in the subchain 1.

The quotient $\frac{C_+}{B_+}$, i.e. the ratio of the amplitudes of the waves propagating in both subchains as a function of β_I is depicted in Fig. 3.16(b).

The result means that the coupling between the chains controls the amplitudes of the partial evanescent waves penetrating the both subchains.

As it is seen from the Fig. 3.15 there is another localized state (middle) in the frequency gap provided that the coupling parameter is weak enough, here $\beta_I > -0.5$. In the very limit $\beta_I \to -0.5$, $\omega = 6$ and the angular displacements of both interfacial moments satisfy the condition

$$\begin{pmatrix} \delta\phi_1 \\ \delta\theta_1 \end{pmatrix} = -\begin{pmatrix} \delta\phi_0 \\ \delta\theta_0 \end{pmatrix},$$

i.e. the moments rotate in opposite directions (see. Fig. 3.17)

For weaker couplings the displacements are related by the following formula

$$\begin{pmatrix} \delta\phi_1 \\ \delta\theta_1 \end{pmatrix} = C_{+}z_{2+} \begin{pmatrix} \delta\phi_0 \\ \delta\theta_0 \end{pmatrix}.$$

Fig 3.16(c) gives the values of the coefficient $C_{+}z_{2+}$ as a function of β_I.

As one can see the coefficient vanishes at $\beta_I = 0$, i.e. in the case of decoupled subchains where the chain 2 rests motionless. This corresponds to a surface state in subchain 1. Its frequency turns out to be $\omega = 5.7501$. The ratio $\frac{C_{+}}{B_{+}}$ as a function of β_I is shown in Fig. 3.16(d). The behaviour is not monotonous.

The character of the displacements in both modes in the gap are illustrated in Fig. 3.17.
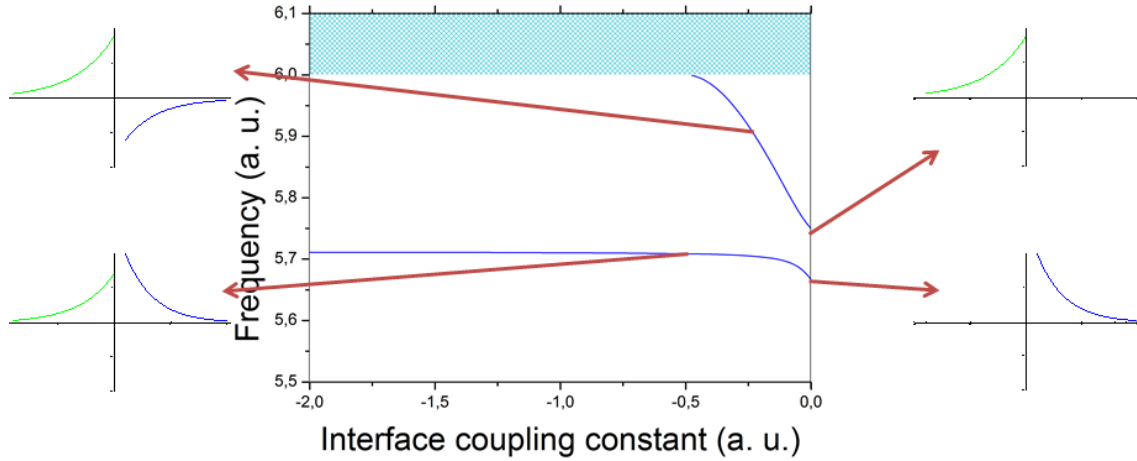

Figure 3.17: Schematic of displacements in interfaces modes on both sides of interface.

The mode (top) above the bands of the bulk waves exists in the range of the chain coupling $\beta_I \in (-4.21, -\infty)$. It consists of two partial waves of the length $2a$, where a is the spin separation, enveloped by damped exponential functions.

The motion of the interfacial spins is still related by the formula $\begin{pmatrix} \delta\phi_1 \\ \delta\theta_1 \end{pmatrix} = C_{+}z_{2+} \begin{pmatrix} \delta\phi_0 \\ \delta\theta_0 \end{pmatrix}$ This time, however, $z_{2+} < 0$, (as usually above the bulk band if its top corresponds to the wave vector $k = \frac{\pi}{a}$) and $C_{+} > 0$. Fig. 3.16(e) shows that in the limit of a very strong coupling, $\beta_I \to -\infty$ the coefficient $C_{+}z_{2+}$ tends to -1, i.e. the motion of the interface spins becomes opposite. The ratio of the amplitudes of the interfacial spins C_{+}/B_{+} shows a behaviour as depicted in Fig. 3.16(f).

In summary:

The coupling between the chains controls existence of the interface states as well as the amplitudes of the partial evanescent waves that consitute the localized state. We can see that at $\beta_I =0$ our solutions represent surface excitations. In this limit the upper mode from Fig. 3.15 corresponds to the surface wave in subchain 1 (stronger coupling) and the lower mode to the surface wave in the subchain 2. With increasing coupling β_I one can see the conversion of the surface mode to the interface modes.

4

1D systems of magnetic nanoparticles

It is well known that macroscopic magnets are seldom monodomain because a domain structure reduces the energy of the resulting magnetic field [19]. However, W.F. Brown [1] stated conditions for so called micrmicromagnetism or nanonmagnetism. It turns, namely, out that some shapes of a micro- or nanoparticle may make the material magnetized almost uniformly. Experimental observations and theoretical predictions indicate that the most favorable shapes for that are those axially elongated. The spontaneous magnetic moment then is oriented parallel to the long axis. Thus, such particles show properties of single spins, so that they may be legitimately called macrospins. In particular, their excitations form equilibrium configurations resemble magnons. A difference is that the frequencies of magnons in solid state systems fall in the range of tens and hundreds of Terahertzs, whereas in the micro or nanomagnets they are placed in the Gigahertzs region. The reason for that lies in the interactions. Whereas the ordering of single ionic spins in a magnet are due to exchange forces, the micro or nanomagnets, interact as magnetic dipoles. The Gigahertz region of excitations make them interesting for telecommunication.

When arranged in a 1D chain perpendicular to their long axes the macrospins are preferentially ordered in an antiparallel manner, head-tail sequence of neighbouring macrospins, in analogy to a microscopic antiferromagnet. This can be easily understood bearing in mind that the most stable configuration of two dipoles is the head-tail one. We shall call this configuration antiferromagnetic (AF). An external magnetic field applied perpendicular to the chain and parallel to the macrospin axes may transform the configuration into a parallel one, i.e. ferromagnetic (FM). This resembles a matamagnetic phase transition [20]. It is interesting that, with the magnetic field switched off, the FM structure of macrospins is locally (marginally) stable, i.e. it corresponds to a local energy minimum. This is in contrast with single magnetic dipoles which when parallel, and perpendicular to their position vector, are in a maximum of energy. Moreover, the return to the most stable AF configuration is rather difficult with the use of external magnetic field. This section will deal with the behviour of chains of macrospins in magnetic field.

4.1 Macrospin

A macrospin is comprised of a large number of spins belonging to a single magnetic domain. In what follow we consider thin oval shaped nanoparticles, i.e. elliptical cylinders of a very small height. The system can be practically realized by depositing elliptic dots of permalloy on a diamagnetic substrate. The size of the ovals are mostly 66 x 24 x 1 cells, each cell being 5 nm x 5nm x 5nm large. The magnetic parameters of permalloy are saturation magnetization M_s=800 kA/m, exchange stiffness parameter $A = 10^{-11}$ J/m, gyromagnetic ratio γ=185 rad GHz/T , and the damping coefficient is $\alpha = 0.5$.
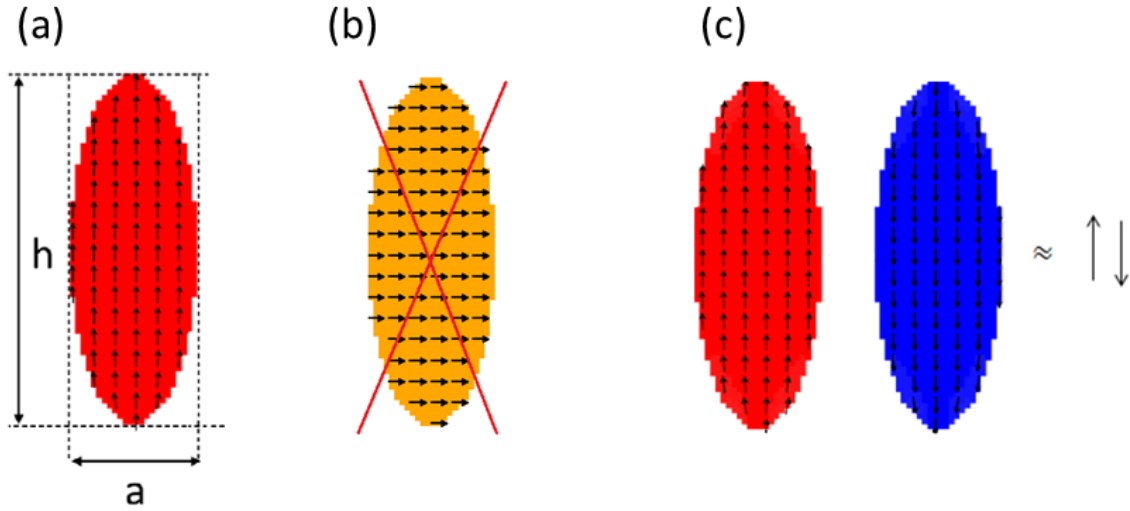

Figure 4.1: Schematic magnetization maps in thin cylindric macrospins: (a) uniformly magnetized macrospin of length $h = 330$ nm and width $a = 120$ nm magnetized along the easy axis, (b) hard axis magnetization (c) a pair of macrospins in antiferromagnetic configuration.

As represented in Fig. 4.1 the easy axis is in the y direction and the x direction is a hard axis. The reason for that, being in fact a manifestation of a shape anisotropy, is that in the case of magnetization in x direction a strong demagnetization field is created. A magnetization in the z direction is even more energy consuming. In contrast with that, the regions of homonymous magnetic poles is minimal if the magnetization is parallel to the y axis. Additionally, the elliptical shape minimizes the demagnetization energy. In practical calculations we adopt a slight deviation of magnetic field from the very exact y-direction to avoid numerical problems with symmetric minima versus saddle points. The value of the tilt angle 0.001° ensures the removal of the artificial problem and at the same time, does not afflict the symmetry of the magnetic excitations.

4.1.1 Statics: equilibrium configurations, hysteresis, coercive fields

As stated above the systems under study consist of macrospins, i.e. magnets that should behave like a single spin. Therefore a starting point is a single macrospin. The magnetization map of an elliptically shaped thin cylinder under an external magnetic field is depicted in 4.1. The magnet is treated in a continuous approximation and divided into cubic pixels 5 nm x 5 nm x 5 nm. The cylinder is one pixel thick. The adjacent pixels are assumed to interact by exchange forces and all the voxels by dipolar interactions. Because of the cubic shape the voxels exhibit also higher multipoles. The configuration corresponding to the minimum of energy is found with the use of the software OOMMF. Examples of the equilibrium configuration are depicted in 4.2 in such a way that every arrow represents the average magnetization over four voxels. As one can see the magnetization is fairly uniform in all the three values of the external field. The average magnetic moments are, however deviated from the y-axis. To visualize the deviations we have applied a colour code. The deviation to the right are marked red and to the left - blue. In other words the intensity of the blue colour corresponds to a negative x-component and red to a positive x component of the magnetic moment. Noteworthy is that the z component (perpendicular to the figures plane) is practically zero everywhere as a result of a strong shape anisotropy. The regions of blue and red are readily symmetric in the absence of the external field and in the field strictly parallel to the y-axis.
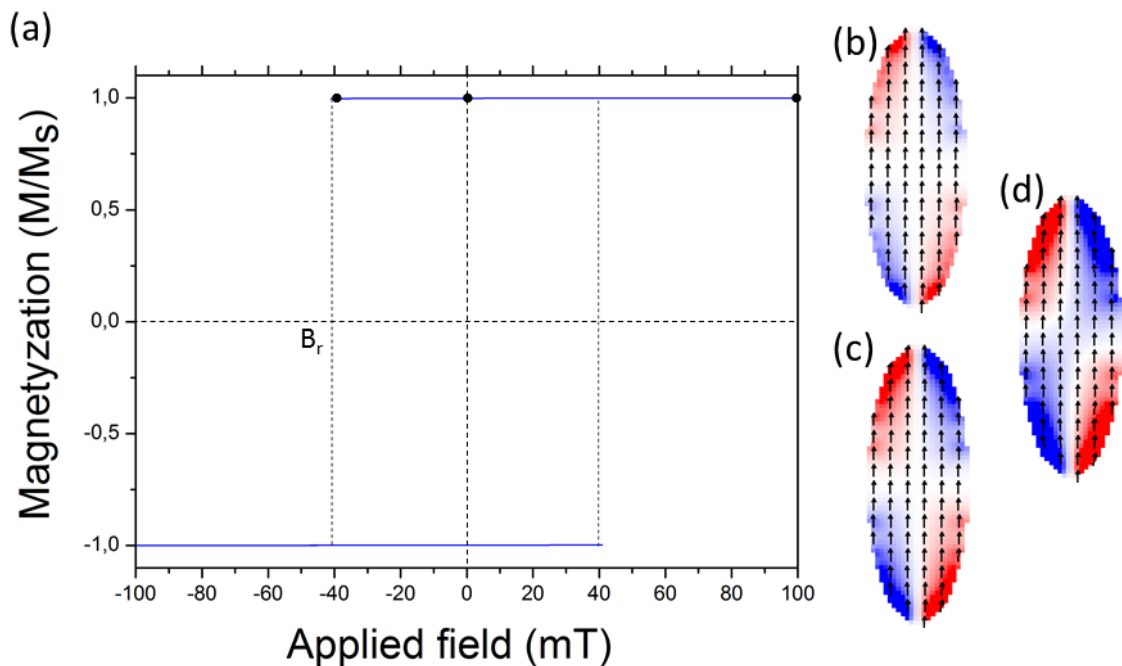

Figure 4.2: (a) Hysteresis loop for a single macrospin. Magnetization maps for (b) $B = 100mT$, (c) $B = 0mT$ and (d) $B_r = -41.5mT$.

Being well monodomain the marcospin does not behave entirely like a single spin in that it shows a hysteresis. This means that there exists a range of magnetic fields in which a configuration antiparallel to the field, energetically less favorable than the parallel one, is metastable. Fig 4.2 shows this hysteresis. Negative value of the field indicates that the field is opposite to the magnetization. The switching fields (critical fields) are $B_r = -41.5[mT]$. The shape of the hysteresis loop is close to rectangular but a bit rounded in the vicinity of the critical fields. It is related, at least in part, with reverse S-shaped region of deviated spins. A region like that can be seen in Fig. 4.2(d). The most significant effect of the field are the spin deviation regions in four quadrants of the ellipse. The region increase in intensity with decreasing and negative external field, i.e. opposite to the average magnetisation. At the same time the spins located close to the regions of the short and long axes are practically parallel to y-axis (see Fig. 4.2 (b,c)). We have checked that the employed tilt is small enough as to not produce other static or dynamic consequences.

4.2 Chain of identical magnetic nanoparticles

Now we construct a chain of the macrosopins. The macrospins are parallel to the y direction and equidistant in x direction as shown in Fig. 4.3
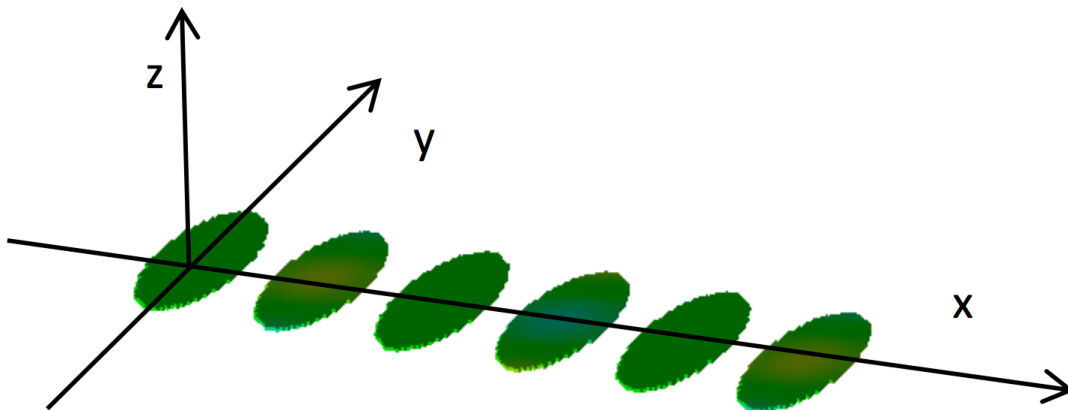

Figure 4.3: Infinite chain of nanoparticles

.

In a zero magnetic field the macrospins can be all parallel - ferromagnetic configuration or exhibit an alternating antiferromagnertic configuration. Because the interparticle interactions are dipolar the stable configuration is the antiferromagnetic one whereas the ferromagnetic is metastable.
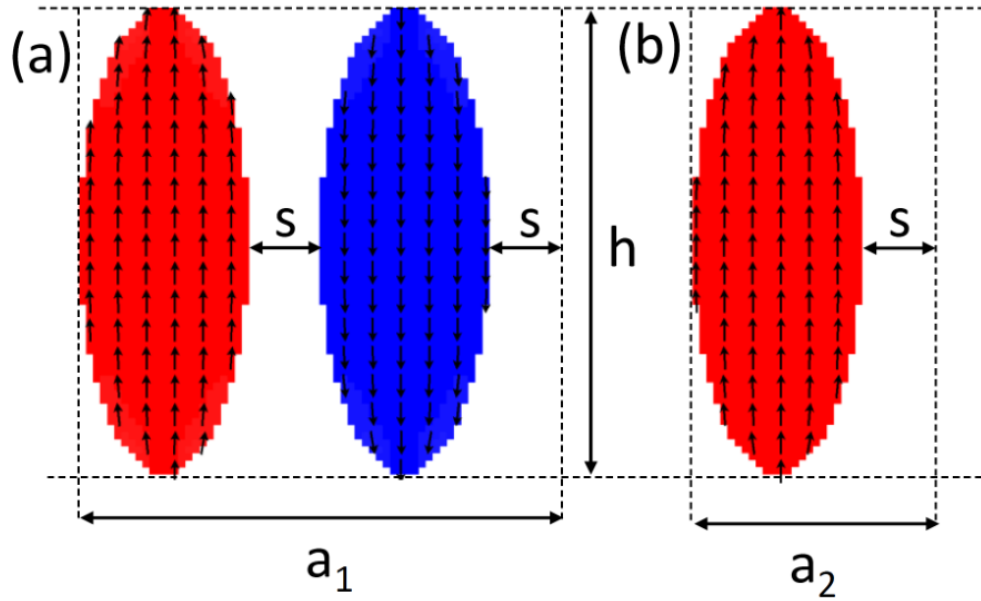
Figure 4.4: Schematic magnetization maps in unit cell for (a) antiferromagnetic and (b) ferromagnetic configuration chain of macrospin where h=330 nm, S=50 nm, a_1=340 nm, a_2=170 nm

.

The lattice constant a_1 of the antiferromagnetic configuration is twice as long as in the ferromagnetic configuration a_2. This has been depicted in Fig. 4.4

4.2.1 Statics

The equilibrium configuration of the chain described in the previous section is calculated with the use of the OOMMF program. To study the switching phenomenon we apply the external magnetic field quasi parallel to the macrospins long axes. The results are summarized in Fig 4.5. The critical field for the AF $\rightarrow$ FM switching is $B_c = 42.05$ mT, FM$\rightarrow$FM reversal B_r=-30 mT. (b) In comparison with the reversal field for the single macrospin, $|B_r|$=41.5 mT, the analogous field for AF $\rightarrow$ FM is higher and for FM$\rightarrow$FM is markedly smaller.

The mechanism of the switching is partly depicted in Fig. 4.5. One should notice a difference in the magnetisation map between the macrospin parallel and antiparallel to the field close to the critical field. Not only is the antiparallel macrospin marked by an inverted S-shape but its right side is much more strongly deviated than its left side as a result of the tilt angle of the magnetic field with respect to the y-direction. An abrupt reversal ends up in a ferromagnetic configuration. With the decreasing field the FM configuration persists down to zero and even to negative values until $B_r = -30$ mT when the system quits its antiparallel magnetization to arrive at a reverse FM configuration parallel to the field. The hysteresis loop between both FM configurations is narrower than for the single macrosopin (compare B =-41.5 mT

for the single macrospin). The evolution of the magnetization map in the chain is similar to that for a single macrospin. We have studied the dependence of the width of the hysteresis on the width, or horizontal diameter, of the elliptic macrospins.
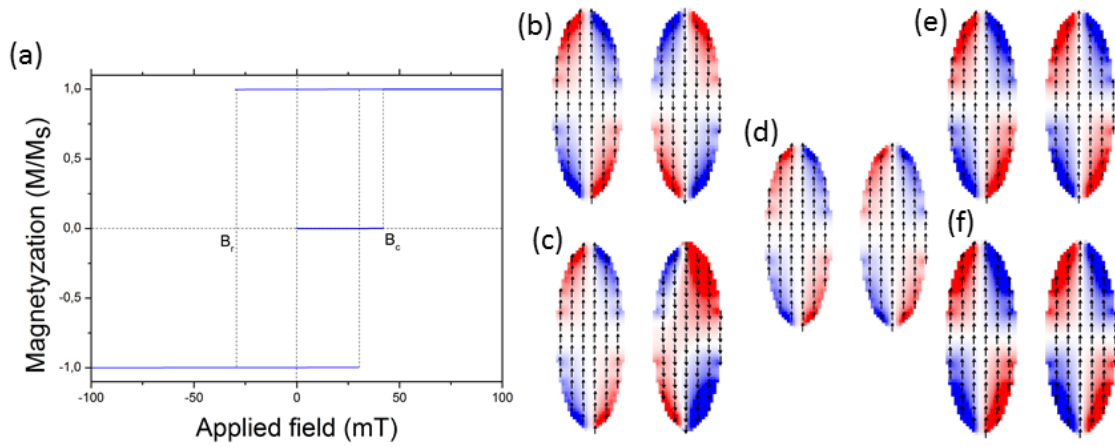

Figure 4.5: (a) Hysteresis loop for infinite chain of macrospins. Magnetization maps for antiferromagnetic configuration in (b) $B=0$ mT, (c) $B=42,05$ mT and antiferromagnetic configuration in (d) $B=100$ mT, (e) $B=0$ mT, (f) $B=-30$ mT
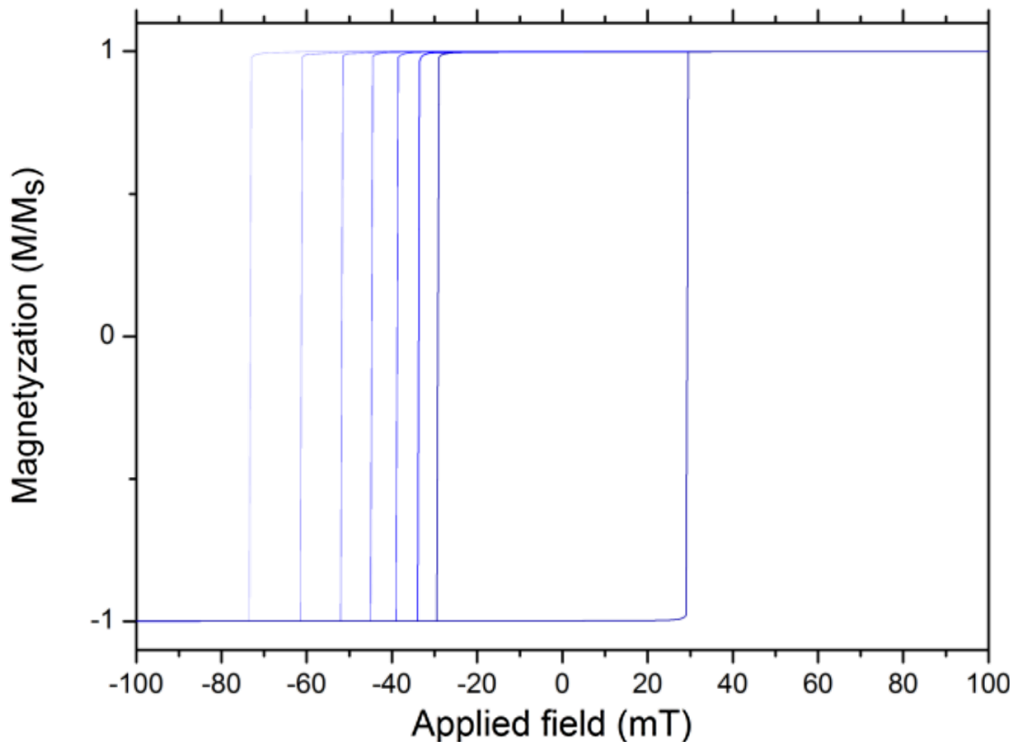
.

Figure 4.6: Half-hysteresis loops (entire loop for the oval's horizontal diameter 120 nm) for different horizontal diameters 110 nm, 100 nm, 90 nm, 80 nm, 70 nm and 60 nm. The color intensity corresponds to the dianometer length.

For the sake of clarity, in the Fig. 4.6, we have reported only halves of the loops

starting from the FM configuration. The hysteresis becomes wider with decreasing short axis of the macrospin as it has been depicted in Fig. 4.6. The reason for that behaviour is that a wider oval produces higher demagnetization field.

4.2.2   Dynamics

We consider small magnetic excitations of the most stable AF configuration of identical macrospins in the harmonic approximation. Because of the translational invariance of the chains the excitations are Bloch waves. The waves are characterized by their frequencies and polarization vectors. The former are eigenvalues and the latter are eigenvectors of the corresponding dynamic matrix related with the Hessian matrix of the system by the Landau-Lifshitz-Gilbert equations of motion (see. sec 2.2). The polarization of such magnetic excitations, spin waves or magnons can be visualized as profiles or maps of the amplitudes of precessing magnetic moments. It is clear that the number of the modes in systems of macrospins is very large as a result of a large number of degrees of freedom involved in each macrospin. Therefore we have to select the lowest-frequency ones, because one of them becomes soft to drive the instability of a configuration. Secondly, the lowest modes fall into the gigahertz frequency regions.

It turns out that the profiles obtained are characterized by the number of nodes (zero amplitude) across the macrospins long axes. Obviously the modes with even and odd number of nodes differ in symmetry. It should be born in mind that because of the inversion invariance all the modes are either symmetric or antisymmetric.One could expect that the lowest modes will be those with the lowest possible number of nodes. From among all the eigenfrequences we have selected those of minimal number of nodes. Surprisingly, the lowest mode is not always the uniform (nodeless) Kittel mode. The lowest modes can be classified as "bulk modes" and "end modes". The former involve mainly central parts of the ovals whereas the latter rather distal upper and lower parts. Fig. 4.7 shows a comparison of an ideal Kittel mode with symmetric and antisymmetric as well as bulk and end modes.
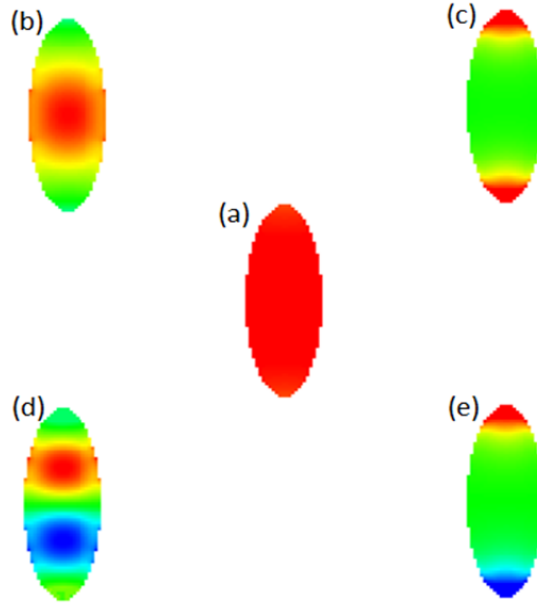
Figure 4.7: Illustration of the ideal Kittel mode (a) and the simplest symmetric bulk (b), symmetric end (c), antisymmetric bulk (d) and antisymmetric end (e) modes

The classification "bulk" and "end" as well as the one based on the number of nodes is not symmetry protected and can change with the applied magnetic field as well as across the Brillouin zone. Generally one speaks of hybridization of modes of the same symmetry. On the other hand the modes of different symmetry do not hybridize and their dispersion curves cross.

The excitations involve precession of the magnetic moments around their equilibrium orientations. To illustrate a profile of such an excitation we draw a map of the maximal value of the z-component of the precessing magnetic moment. Fig. 4.8 exhibits the profiles of the lowest modes in the AF configuration without applied external field. Because the unit cell comprises two ovals the modes at the Brillouin zone centre can be classified as acoustic and optic. The mode is called acoustic if both ovals of the unit cell vibrate in phase. In turn an optical mode is marked by an antiphase vibrations of both ovals that is reflected by opposite signs of the corresponding regions. All the unit cells vibrate in the same way (in phase) at the centre of the Brillouin zone ($k = 0$) whereas at the zone Border ($k = \pi/a_1$) the signs of the vibration on neighbouring unit cells is opposite.
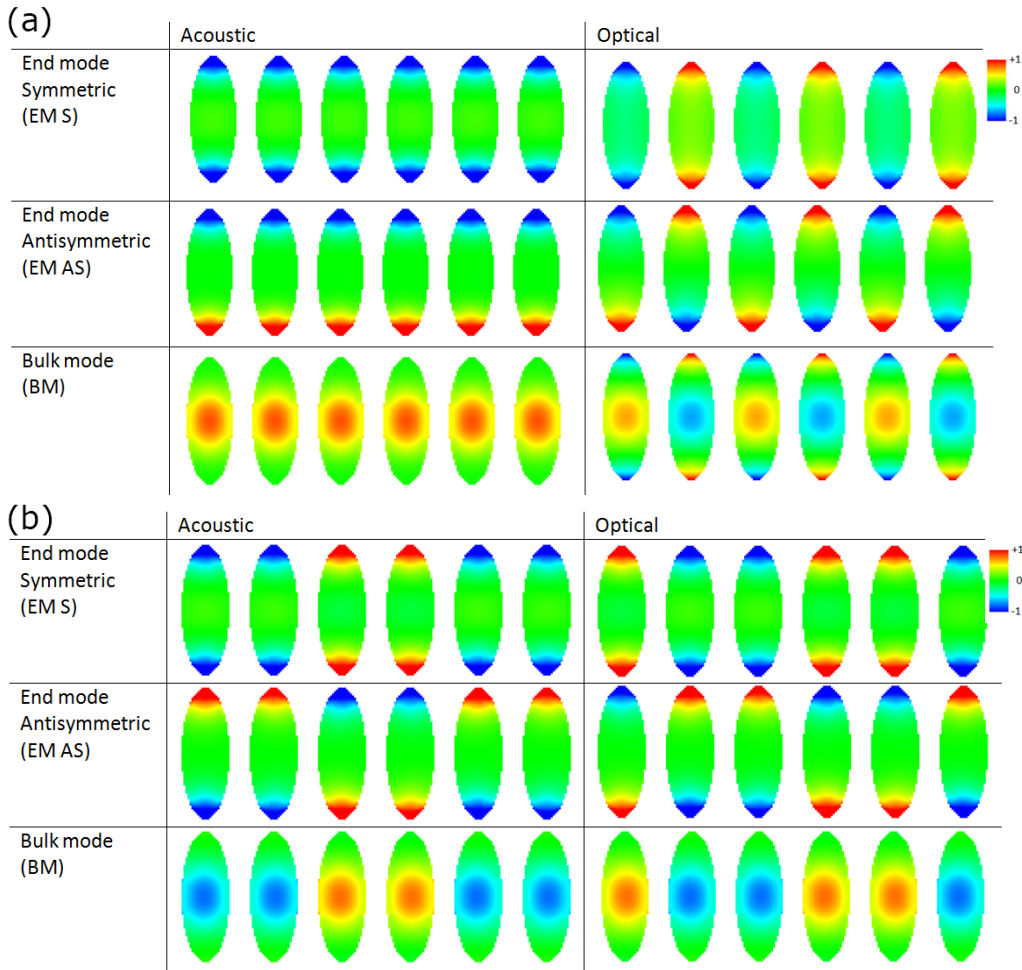
Figure 4.8: Profiles of precesion intensity in the three lowest modes for acustic and optical branches in the absesce of external field at (a) $k = 0$ and (b) $k = \pi/a_1$

.

Looking at the optical modes one can remark that the mode EM S has no nodes, the EM AS has one node whereas the BM has two nodes. The situation is different for acoustic modes: EM S has two nodes and the one BM none. This corroborates the observation that the acoustic mode shows a higher frequency than the optical one at $k = 0$ in contrast with a usual mechanical (phonon) case. On the Brilloiun zone border the branches degenerate (see Fig. 4.9) that is reflected in the dynamic magnetic profiles for $k = \pi/a$. In what follows we have studied the dispersion relations of the modes and their dependence on the applied magnetic field.

The effect of magnetic field quasi parallel to the ovals' long axes is represented in Figs 4.9.

The results for three values of the field are shown: B=0 mT, the field B =42 mT, i.e. close to the switching field (coercive field) and a slightly higher $B = 42.5$ mT just after the switching to the FM configuration. The field lifts the degeneracy of the acoustic and optic modes at the zone border. The curves EM S and EM AS
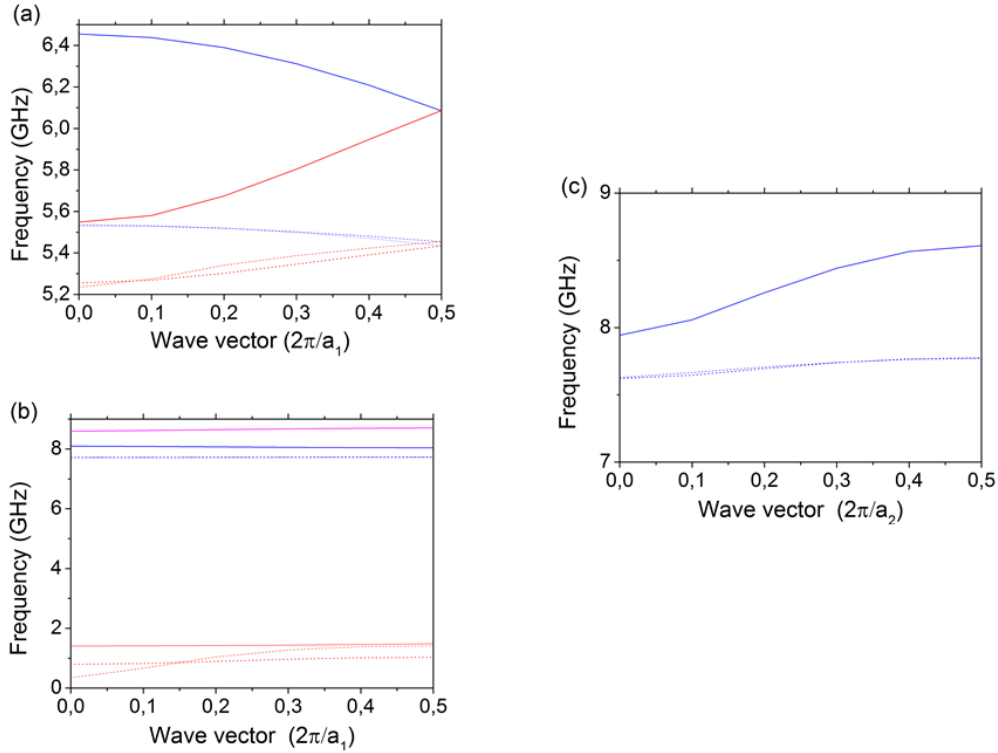
Figure 4.9: Dispersion relations acoustic (blue lines) and optical (red lines) BMs (solid lines), EMs S(dashed lines) and EMs AS(doted lines) for (a) AF order at B=0 mT and (b) AF order at B=42 mT (c) F order at B=42,5 mT.

lie steadily very close. Because their symmetry is different the curves cross at some points of the Brillouin zone. All the modes at B=0 show a relatively high dispersion, i.e. a slope responsible for the group velocity. This means that the modes can propagate along the chain at relatively high speed. The slope markedly reduces with the increasing field to become very weak at the instability point. This is characteristic of a "memory type" modes. The only mode of significant dispersion at $B = 42$ mT is the one EM S. As one can see its frequency at $k = 0$ is very low. In fact it is this mode that becomes eventually soft at the instability point. The dependence of the group speed of the modes on the applied field indicates a possibility of controlling the propagativity of the modes that is interesting for applications in magnonic logical gates [21, 22, 23, 24, 25]. In particular an increasing external field enhances the memory regime at the expense of the propagative one. Additionally, a non-zero applied field engenders a stop band across the whole Brillouin zone, i.e. makes the system magnonic. At the coercive field $B = 42$ mT one sees two acoustic modes that both show a BM character because a hybridization. Once the ferromagnetic order is attained all the modes become acoustic, because the unit cell contains but one macrospin. The structure being entirely reconstructed there is no continuation of

the dispersion curves from the AF configuration. Out of the three lowest modes the higher BM shows a significantly higher dispersion. The two lower weakly dispersive modes are in fact two interwoven EM A and EM AS modes.

4.2.3 Soft modes and mechanisms of switching

The transformation from the antiferromagnetic configuration is discontinuous. A signature of that is the lack of a group subgroup relation. Indeed a translation by the distance between the neighboring ovals is a symmetry element of the FM structure, which element disappears in the AF structure. However, a new symmetry element arises, i.e. a composition of the translation with the spin reversal. The kind of transition reminds what is known as metamagnetic transition [26, 27]. We know that even a single macrospin remains metastable under a magnetic field oriented antiparallel to its magnetization. Analogous statement is valid for the chain of macrospins. Under an increasing applied magnetic field the energy minimum corresponding to the magnetic configuration along the field deepens to become the absolute minimum characteristic of a stable structure. At the same time the initial AF state becomes metastable. A perturbation or thermal agitation may throw it to the stable one. In the absence, however, of such factors the AF structure persists until the stationary point of the AF structure ceases to be a minimum and transforms into a saddle point. This is marked by the lowest eigenvalue of the Hessian matrix crossing zero to become negative. At the same time one of the spin wave frequencies tends to zero. The phenomenon is called mode softening and the spin wave with frequency tending to zero is called soft. The initial AF structure cannot exist beyond the softening. The respective value of the magnetic field is, therefore, the critical field or switching field. We have shown that the corresponding eigenvector of the Hessian matrix coincides with the precession ellipse of the magnetic moments degenerated to a straight line. Therefore this eigenvector defines the polarization vector of the soft spin wave.

Fig 4.10 shows the evolution of selected modes at the Brillouin zone center and zone border in the AF configuration of the infinite chain of identical elliptic macrospins under an increasing external magnetic field. Generally, the optical modes show a decreasing tendency whereas the acoustic ones visibly harden except for the branch BM at $k = \pi/a_1$ in the field range $B \in (36, 42.05)$ mT which declines downwards as a result of a hybridization and the consequent anticrossing (level repulsion) of two modes of the same symmetry.

A hybridization concerns also modes at the zone center. In particular the symmetric optical modes interact in such a way that at about $B = 36$ mT the lower branch takes over an amplitude in the centre of the oval from the upper branch.
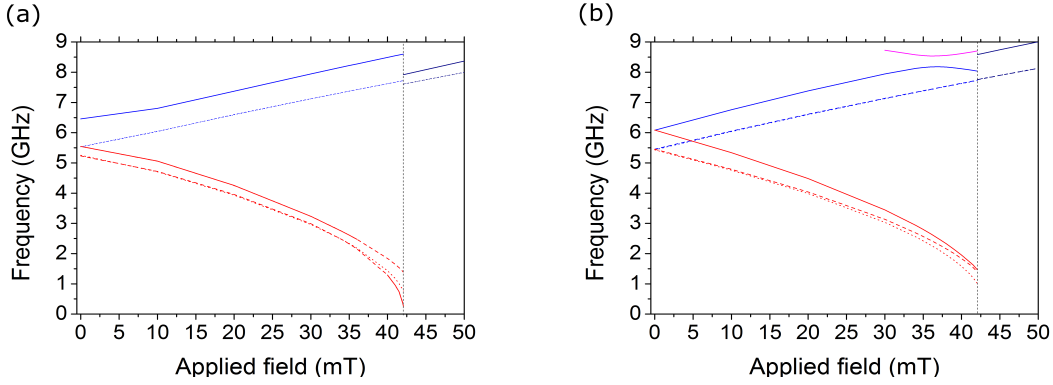
(a)

(b)

Figure 4.10: Frequency vs. applied field curves for acoustic (blue lines) and optical (red lines) BMs (solid lines), EMs S (dashed lines) and EMs AS (dotted lines): (a) $k = 0$ and (b) $k = \pi/a_1$.

The feature of a significant amplitude at the oval center is marked by a solid line in contrast with dashed line for EM S. The frequencies of the symmetric and antisymmetric modes EM lie generally close to each other except for the optical modes in the very vicinity of the instability point. The calculated value of the critical field for the parameters applied amounts to $B_c = 42.05$ mT. The leading soft mode whose frequency crosses zero as the first one is a BM at $k = 0$. It is interesting that the polarization of the soft mode depends on intensity of the applied field so that at weak fields the mode is practically of EM nature and near to the coercive field it becomes a BM with, however, a significant precession amplitude close to oval's ends. The latter property makes the soft mode somewhat similar to the uniform Kittel mode (compare Fig. 4.11). Every two-oval unit cell behaves in the same way. To better illustrate the properties of the soft mode the amplitudes of the spin declination in the three spatial directions x, y and z have been reported in Fig. 4.11 for selected values of the magnetic field. The positive displacements are represented by the red colour and the negative by the blue one. An intensity scale is always given. The acoustic vs optical nature of the modes can be readily understood from this Figure. First one has to remark that all the solutions conserve the time arrow, i.e. every spin effectuates precession in the same sense about its equilibrium spatial orientation. The term "acoustic" concerns the kind of motion that the spins in the first and the second oval of the unit cell are in phase. Similarly, a mode is called optical if the motion in both members of the unit cell are shifted in phase by π.

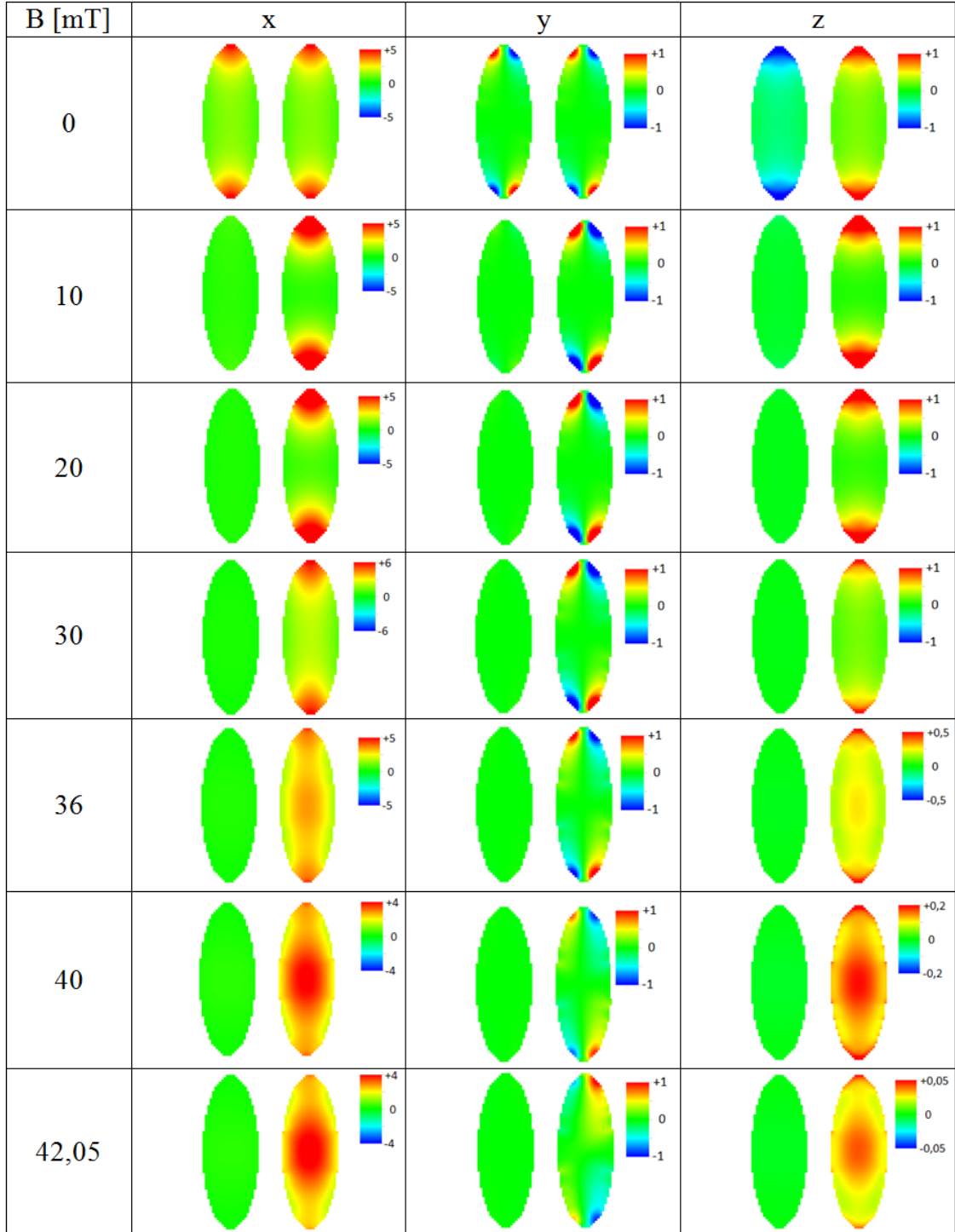| B [mT]	x	y	z
0			
10			
20			
30			
36			
40			
42,05			

Figure 4.11: Precession amplitude of the profile of soft mode in centre of Brillouin zone as a function of the applied magnetic field.

The symmetric soft mode changes its nature when increasing the applied field. At $B = 0$ mT the amplitudes at both ovals within the unit cell are similar. For non-zero magnetic field precession is mostly pronounced on the ovals magnetized opposite to the field, whereas the spins on the oval magnetized along the field rest practically motionless. When looking at the y component one sees a non-zero region close to

the rounded ends of the ovals. This is a result of an equilibrium deviation of the spins in these regions from the y orientation. Otherwise the precession takes place in the plane (x, z). An insight into the x component map one notes that for relatively weak fields, from B= 0 mT to B=20 mT the spin motion occurs at the ends of the macrospins only. A faint streak appears along the long axis starts to be visible at B = 30 mT. With still increasing field intensity, $B = 36$ mT the precession overwhelms the whole macrospin so that the mode becomes more and more comparable to the Kittel mode. Noteworthy is that the z component diminishes with the increasing field intensity. The reader should mind the scale difference at B=42.05 mT; the scale for the z component is 80 times enlarged in comparison with the scale for the x component. On the other hand the precession close to $B = 0$ mT is described by quite a fat ellipse. The behavior reflects a gradual elongation of the precession ellipses; they approach the limiting shape with the vanishing z semiaxes, i.e. a degeneracy to a straight line in the plane of the oval. This is at the same time the eigenvector of the zero eigenvalue of the Hessian matrix.
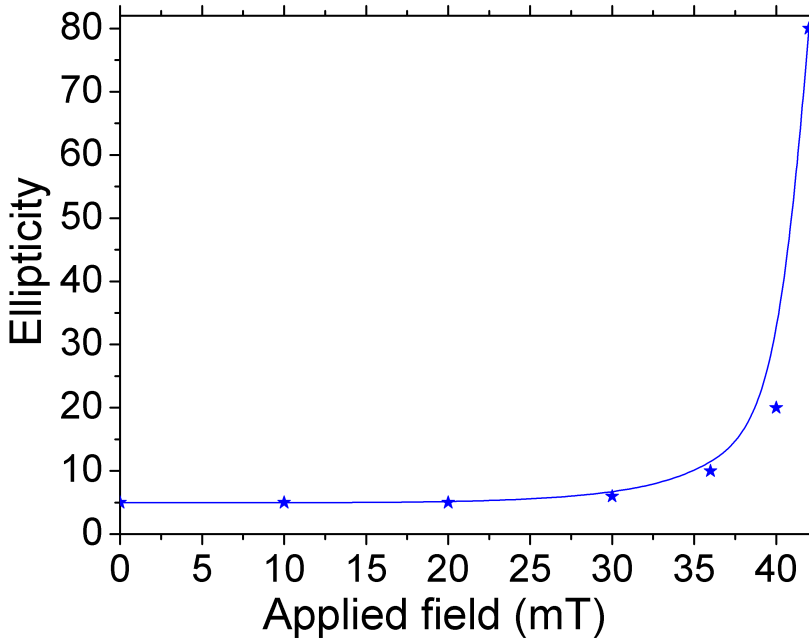

Figure 4.12: Behaviour of ellipticity when approaching the coercive field for the lowest mode in AF configuration.

The dependence of the ellipticity parameter, i. e. the horizontal/vertical of $\frac{max\{m_x\}}{max\{m_z\}}$ ratio on the applied field intensity for the soft mode driving the AF→FM transformation as represented in Fig.4.12.

4.2.4 Robustness of the F configuration in chains of identical nanoparticles

Once the FM configuration is atteined it persists in spite of the fact that one can reduce the intensity of the magnetic field and even make it negative. At $B = 0$ mT the system remains in the metastable FM configuration although the stable one is the AF. With our assumptions the only way to quit a configuration is to change the parameter of the system to make the configuration unstable, i.e. to find the point where the Hessian matrix ceases to be positive definite.

There is, thus, a question of how the AF configuration can be regained starting from the FM one. A variation of the uniform magnetic field does not work because of the metastability which persists to negative fields down to a switching value (coercive field). Even then, however, with the parameters employed in our calculations, the final configuration is the reversed FM. Of course defects or other perturbations may drive the system to the most stable configuration, that can be similar to a spin glass. Various strategies may be invented to provoke a FM→AF transition out of which the one with an inhomogeneous alternating magnetic field seems theoretically simplest but difficult to put into practice. What we propose in the subsequent sections is to make every second macrospin different either in shape or in anisotropy parameters.

In our considerations we assume that the only way to quit a metastable configuration is to vary the system's parameters so as to make the configuration unstable, i.e. the Hessian matrix must cease to be positive definite. It happens that in many cases the instability of a FM configuration under the field opposite to the magnetization occurs at the field in which the FM configuration parallel to the field is the most stable state. This make the recovery of the AF state stable at $B = 0[mT]$ is quite a problem.

Towards reversible ferro - antiferro switching in 1D chains of macrospins

As discussed above, there is a problem to recover the most stable AF configuration of the chain starting from a metastable state FM. A solution is to make every second oval different that imposes a desired reduction of symmetry. This can be attained by varying some parameters out of which we first select those related with shape bearing in mind the shape anisotropy. In particular the reversal is the more difficult - and the oval is more assimilated to a single spin - the shorter is its horizontal semiaxis. In the present section we will show two cases of regaining the stable AF structure.

5.1 Chains of nanoparticles of alternating width

Let us consider a system in which every second nanoparticle is a narrower oval. The unit cell contains two particles from the beginning as it has been shown in 5.1.
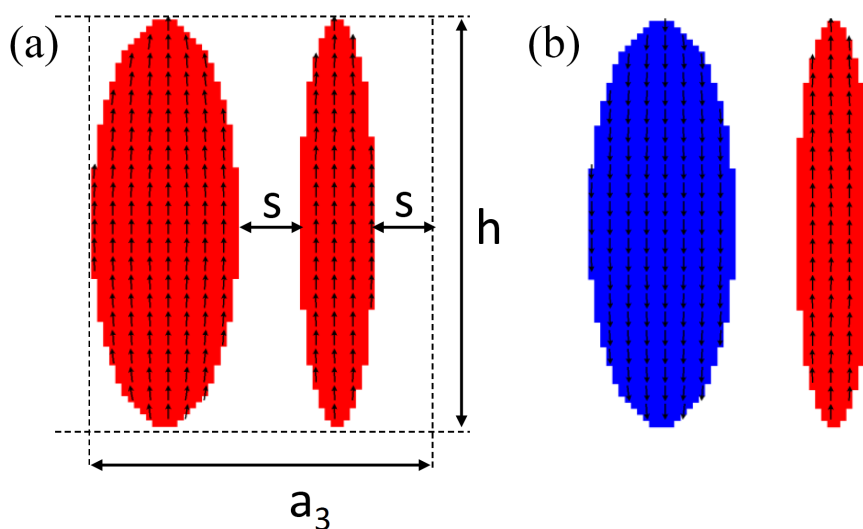

Figure 5.1: Static magnetization maps in elementary cell of a di-particle chain in (a) parallel (ferrimagnetic) configuration and (b) antiparallel (antiferrimagetic) configuration (b). The parameters are h=330 nm, S=50 nm, a_3=280 nm.

Making the horizontal diameters of the ovals different introduces a dissymmetry and different switching fields for every diameter. Namely, narrower particles reverse at higher fields. Following the analogy to microscopic magnets we have denoted the parallel configuration in 5.1 (a) ferrimagnetic and (b) antiferrimagnetic.

5.1.1 Statics

As a first step we study how the change of diameter of every second nanoparticle affects the behaviour of the ferrimagnetic configuration in the external magnetic field.
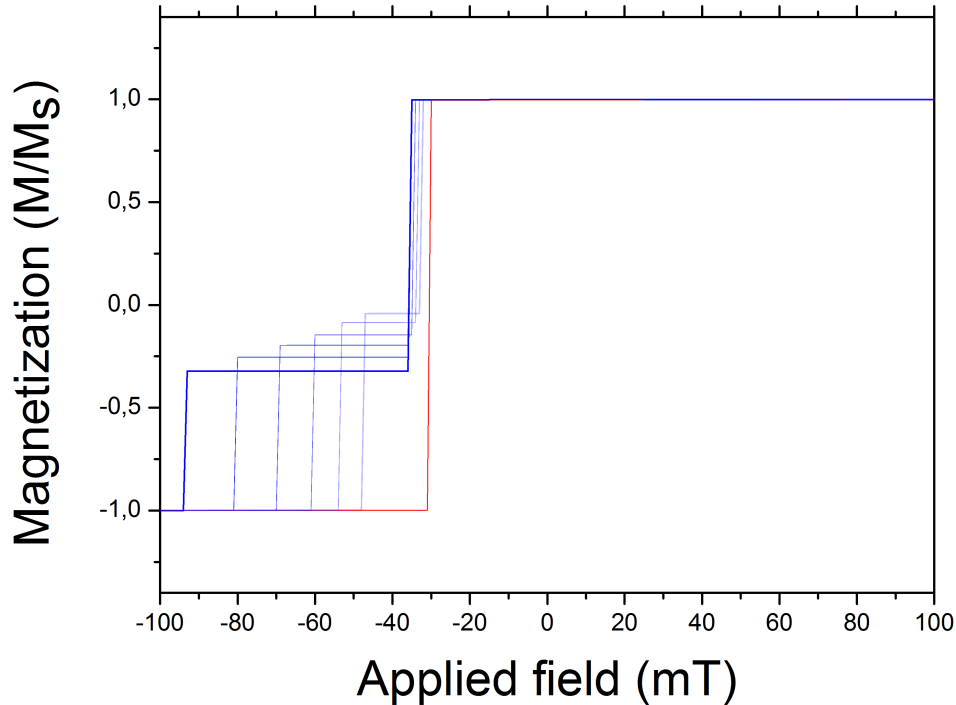

Figure 5.2: Hysteresis half-loops with widths of narrower oval 110, 100, 90, 80, 70, 60 nm. The width is marked with the intensity of blue. Red curve correspond to identical macrospins of diameter 120 nm (see section 4.5)

In Fig. 5.2 the red line corresponds to the half loop of histeresis for identical ovals with width 120 nm in unit cell. An analogous half loop for the diameter ratio 1/2 is marked with the most intense blue color, the next line exhibit effect of consecutive diminishing the diameter of the narrower nanoparticle. The intermediate cases show the evolution of the hysteresis loop with varying the width of the second nanoparticle, looking from the left this parameter amounts to 70, 80, 90, 100 and 110 nm respectively. Even a slightest difference in the diameter of the neighbouring ovals allows the AF structure to be recovered. One can see that the coercive field

increases with decreasing oval breadth. It is consistent with the observation of the single macrospin. The reentrant antiparallel configuration occurs at the field which is the stronger the lower is the breadth of the narrower component. One can easily see that the magnetization of the configuration in which two different ovals are ordered antiparallel to each other does not compensate to zero. That is why we call it anti-ferrimagnetic (AF to indicate antiparallel arrangement of neighbouring macrospins irrespectively to their individual magnetization). This is a simple consequence of the fact that the number of spins in the wider oval is larger. Noteworthy is also that increase in the diameter difference makes the region of the AF configuration to grow. The residual magnetization in the AF configuration is visibly oriented along the applied field. This allows one to conclude that the macrospin that reverses as the first in the opposite field is the wider one as it can be expected from its lower coercive field. The observation is corroborated by the magnetization maps obtained with the program OOMMF and presented in Fig. 5.1 (b). We shall now study in more detail the system in which every second nanoparticle is twice as wide as the neghbouring ones. Their horizontal diameters are 120 and 60 nm respectively. The entire hysteresis loop is exhibited in Fig. 5.3.
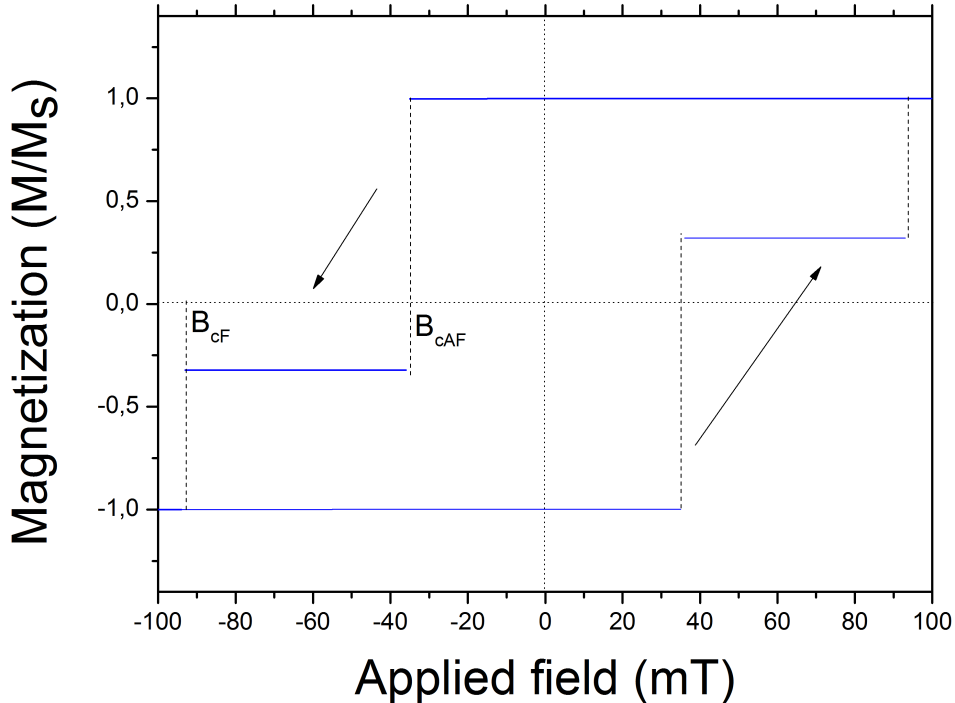

Figure 5.3: Hysteresis loop for infinite chain of macrospins of alternating horizontal diameters 120 and 60 nm.

There are in fact two characteristic fields in such a system: B_{cAF} one for the switching from the FM configuration to the AF state and B_{cF} for the AF → FM

transition. In the present case the corresponding values are B_{cAF}=-35 mT and B_{cF}=-93 mT. The hysteresis loop is symmetric with respect to the reversal of the applied field. One can easily see that the region of te AF configuration is relatively large. We shall now analyse the dynamical properties of these transitions following the bold line of Fig. 5.3 in the direction starting from strong positive field that subsequently decreases to become negative(i.e. antiparallel to initial magnetization).

5.1.2   Dynamics

The dispersion relations of the three lowest modes localized on wider ovals and the three lowest modes localized on narrower ovals in the chain of ovals of different widths at the most characteristic points of the hysteresis loop are collected in Fig. 5.4.
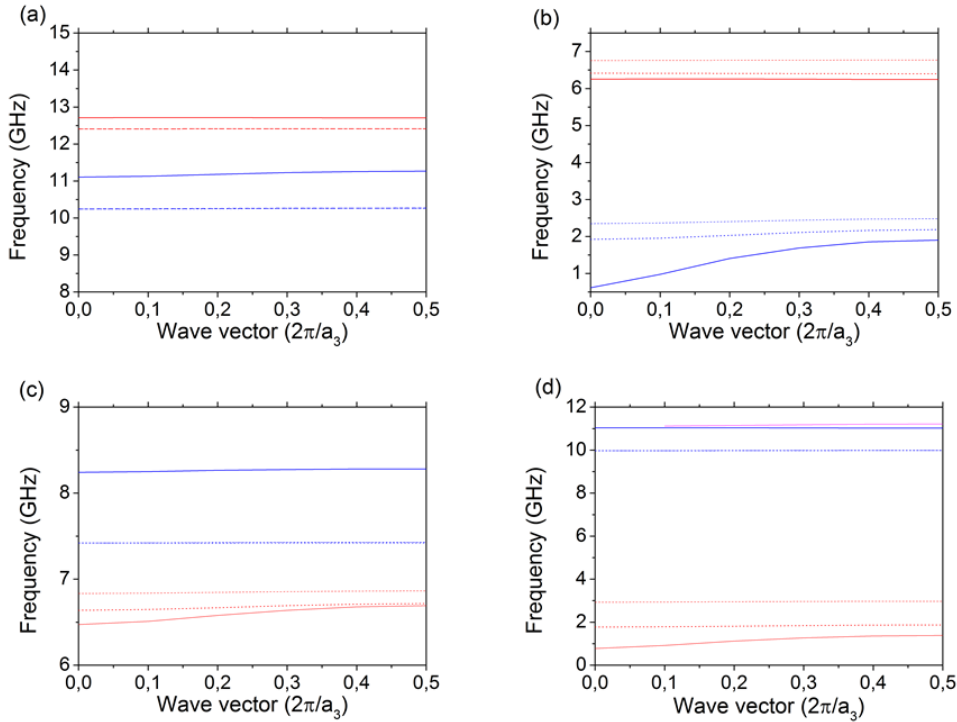

Figure 5.4: Dispersion relations acoustic (blue lines) and optical (red lines) BMs (solid lines), EMs S(dashed lines) and EMs AS(doted lines) for FM order at (a) B=100 mT and (b) B=-35 mT and AF order at (c) B=-36 mT and (d) B=-93 mT.

The first diagram (Fig. 5.4(a) is made in a strong field B=100 mT where the FM configuration is well established. The respective dispersion relations in the same configuration but at the verge of stability, i.e. for B = -35 mT are visible in Fig. 5.4(b). In Fig. 5.4(c) one can see the dispersion relations at B=-36 mT in the AF configuration just after the transition from the FM configuration. The value B=-

93 mT is close to the instability of the AF phase before its reversal to the stable Ferromagnetic configuration. The dispersion relation at this field are given in Fig. 5.4(d) . The negative value of the field indicates a field applied antiparallel to the initial FM configuration.

The appellation "acoustic" and "optical" modes at the Brillouin zone centre is not adequate here, because no modes show identical in-phase or out-of-phase displacements on both members of the two-oval unit cell as it is the case for a chain of identical nanoparticles. Instead, the analogues of the acoustic modes are now concentrated at the wider oval and the analogues of the optical ones at the narrower one. The frequencies of EMs S and AS in FM configuration lie very close at fields far from the coercive field, so that they are hardly distinguishable in the diagrams. The same mode are however clearly separated near to the switching field. In contrast to that in AF configuration EMs S and AS for pseudo-optical branches are well separated in all the values of the field studied. The pseudo-acoustics EMs branches are very close to each other also in AF configuration. The branch marked in magenta (Fig 5.4(d) very near the AC BMs represents another symmetric mode. It will be shown that these modes hybridize close to the reversal field B_{cF}. It is apparent that most of the modes reported in Fig. 5.4 show a weak dispersion, i.e. a memory regime related with low group velocity. The only exceptions are the pseudo-acoustic (centred at the wider oval) mode and the pseudo-optical (centred at the narrowerr oval) mode in Fig. 5.4 (b, d). In fact the curves become more and more dispersive when the instability, i.e. the complete eventual softening of the mode at the Brillouin zone centre, is aproached. This effect is interesting in view of possible applications of such chains as logical gates. A rule can be stated that the soft modes are at the same time the most dispersive ones. The gap between the pseudo-acoustic and pseudo-optic branches is generally weak for strong enough fields and significantly broadens close to the critical points. The ability of controlling the stop band by means of magnetic field is a desirable property for spintronics. The soft mode behaviour accompanying the transitions from FM configuration to AF and from AF configuration to the reversed FM one in the chain of alternating macrospins is depicted in Fig. 5.5.

The figures 5.5 show the dependence of the spin motions in selected modes on the applied field. The end modes EM S and EM AS lie very close to each other in a wide range of applied fields except for the very vicinity of the critical field. The dispersion branches are particularly close to each other at $B = 0$ mT that results in a strong hybridization of the modes of the same symmetry. As a consequence the polarization of the modes changes and the one of the lowest energy becomes BM. There are two critical fields B_{cF} and B_{cAF} in the system of alternating ovals. Both of the instabilities are marked by soft modes. The soft mode at the field $B_{cAF} = $ -35
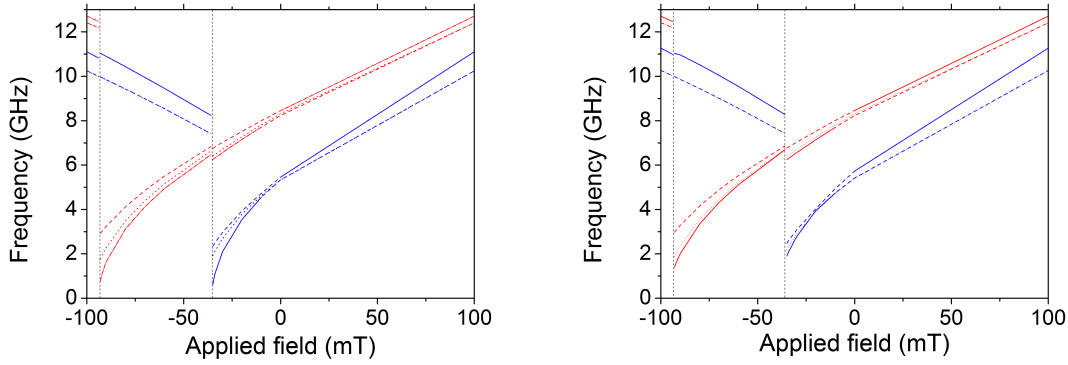
Figure 5.5: Frequency vs. applied field curves for pseudo-acoustic (blue lines) and pseudo- optical (red lines) BMs (solid lines), EMs S (dashed lines) and EMs AS (doted lines), at (a) $k = 0$, and (b) $k = \pi/a_3$.

mT turns out to be the one pseudoacoustic (localized on the wider oval) BM. This is consistent with the wider oval reversing at this field. In turn the transition from the antiferrimagnetic configuration AF to the FM one at $B_{cF} = $ -93 mT is a BM pseudo-optical one localized at the narrower oval, which reverses at this transition. A slight deflection of a BM of the pseudo-acoustic branch at $k = \pi/a_3$ close to the critical field BcF is a result of the proximity, and the consequent hybridization, of another symmetric mode reported in Fig 5.4(b) in magenta color. We shall now watch the variations of the precession amplitude profiles of the soft modes with the applied field.

In Fig. 5.6 we present the evolution of the precession profiles of the lowest pseudo-optical and pseudo-acoustic modes in the chain of ovals of different widths. Generally the precession of spins is fairly circular at fields far from the instability, e.g. at $B >$ 100 mT. The semiaxes of the precession ellipses in the x and z directions are equal as it is seen from the same scale ± 2. When approaching the instability one observes a progressive reduction of the semi axis in favour of that in-plane. E.g. at $B = $ -35 mT the semi major axis in x direction is 40 times longer than the z semi minor axis. This is an effect of the shape anisotropy: the low-frequency modes are preferentially polarized in-plane. One can also appreciate a hybridization of branches of the same symmetry. Namely, at $B = 0$ mT the lowest mode is of an end-mode character with only a faint streak at the oval's center. With the field increased to $B = $ -10 mT the precession amplitude are significantly different from zero in the whole area of the oval. With still stronger field the visible motions are present in the central part of the macrospin only.
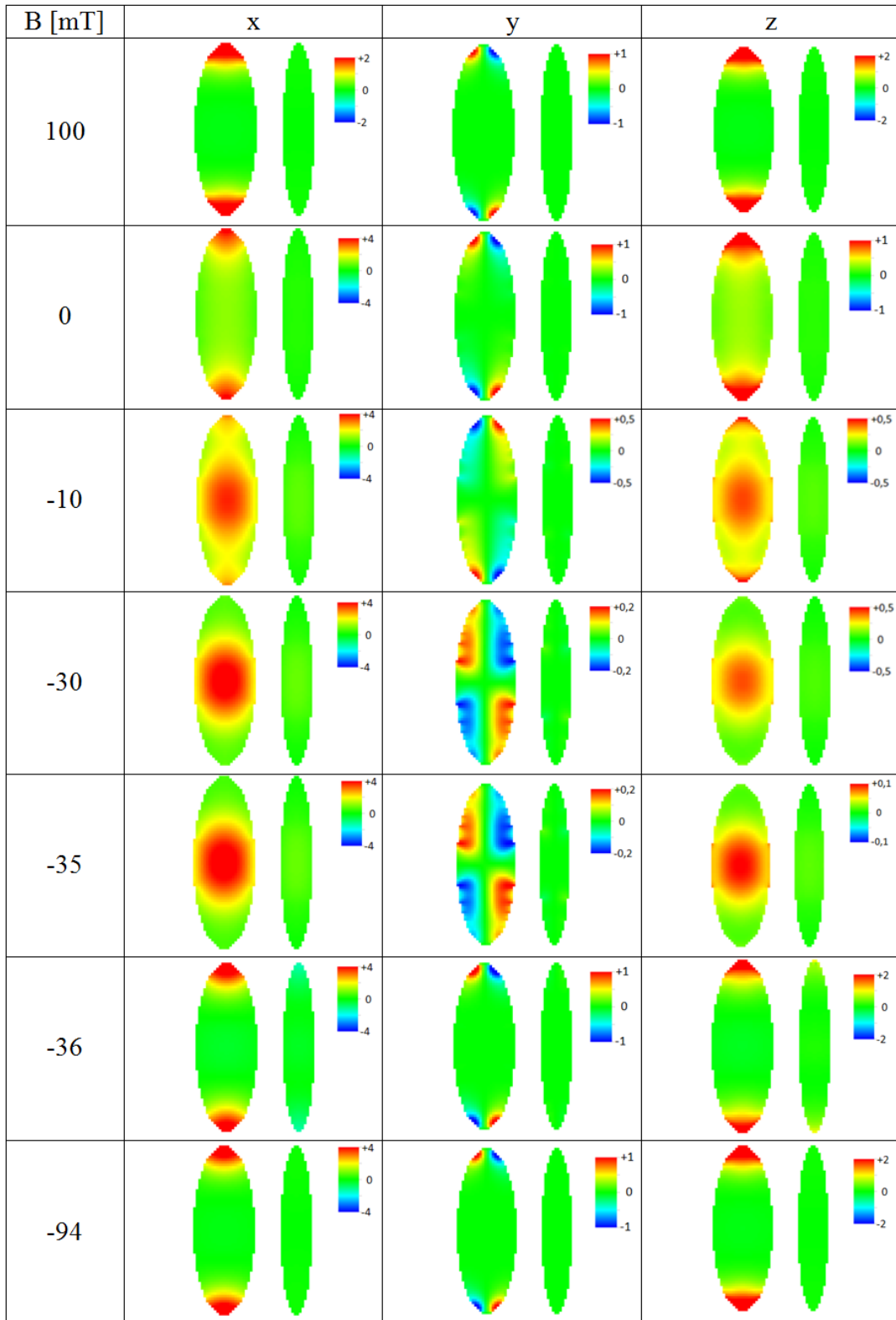
Figure 5.6: Precession amplitude profile for the lowest pseudo-acoustic mode in chain of ovals of different width at $k = 0$ as a function of applied field.

The precession amplitudes in the pseudo-optical mode are gathered in Fig. 5.7 as functions of the applied magnetic field.
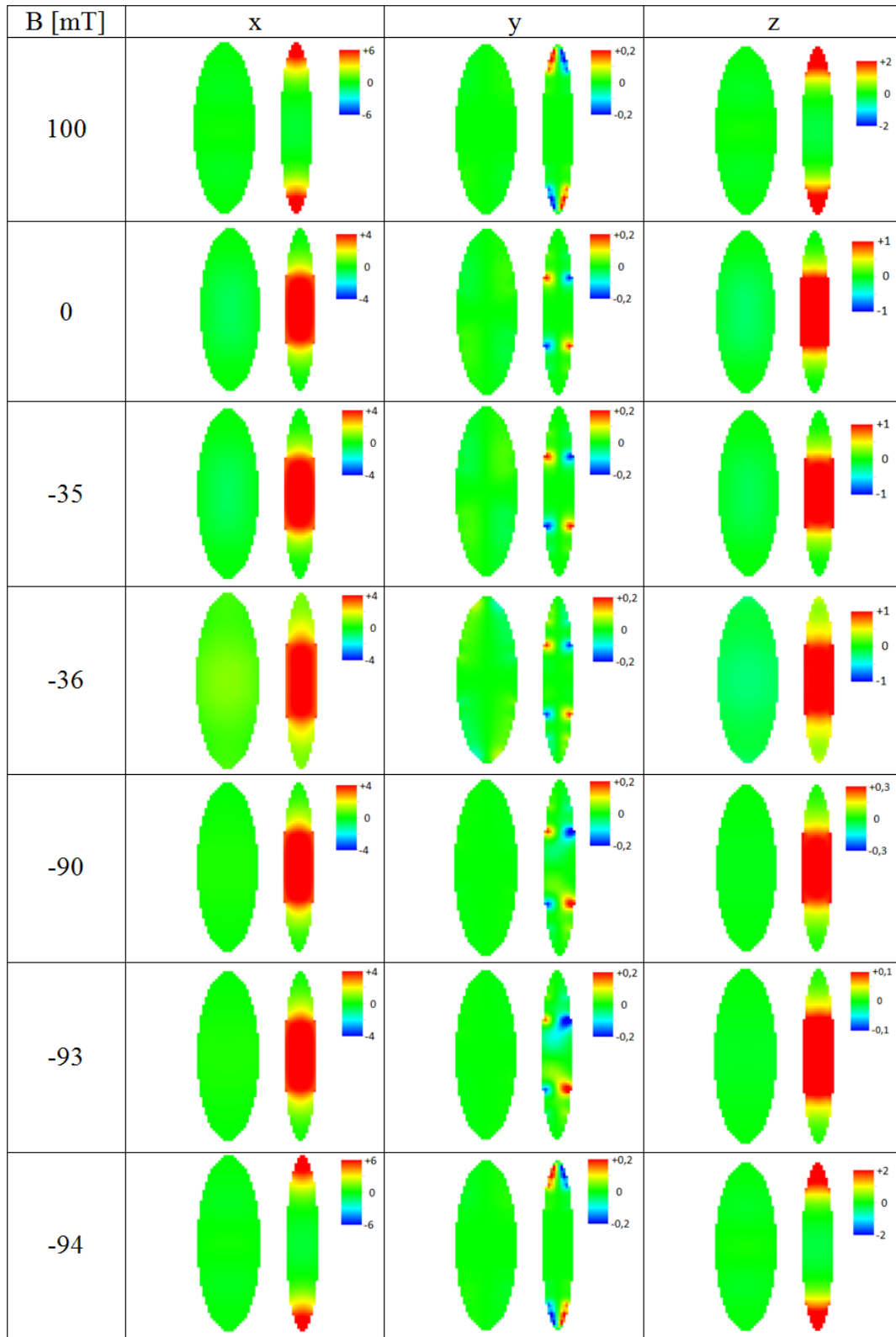
Figure 5.7: Precession amplitude profile for the lowest pseudo-optical mode in chain of ovals of different width at $k = 0$.

An insight into the evolution of the precession amplitude profile for the lowest pseudo-optical mode reveals the tendency of the spins to show a prevailing in-plane

semiaxis of the precession amplitudes (see $B = $ - 93 mT). The y component of the semiaxis is usually much smaller. As before, the z semiaxis becomes semi minor axis of the precession ellipses when approaching the instability, e.g. at $B = $ - 93 mT it decrease by a factor of 20 as compared with $B=$ 100 mT and is about 40 times smaller than the x component of the semi major axis (mind the scale ± 4 for x; $\pm 0, 1$ for z).

5.2   Chain of nanoparticles with different anisotropy

We have seen that making the neighbouring ovals different in their horizontal diameters eased the transition from the FM to the AF configuration. In fact the change in shape entailed a change in the shape anisotropy. Here we shall study the effect of changing the anisotropy itself with the intact shapes as those discussed in the section 4.2. We shall, namely, make the x-axis of every second oval an easy magnetic axis which is feasible with an electric voltage. The corresponding anisotropy parameter is K_1. The anisotropy terms reads in the usual way and is proportional to the squared sin of the angle between the spin and the easy x axis. In fact making the x-axis an easy magnetic axis is similar to making the oval wider, although the physical mechanism and, therefore, the detailed form of the energy function are different. An advantage of making the anisotropy different is that the ovals are geometrically identical and the magnetization in the AF configuration is expected to compensate to zero.

5.2.1   Static

To study the effect of the anisotropy we put our system in the FM configuration magnetized opposite to a constant external field $B=$ 25 mT and vary the parameter K_1. We have checked in previous sections that the configuration is metastable at K_1 = 0 kJ/m^3. Fig. 5.8 demonstrates that at a high enough value of the anisotropy the FM configuration looses its (metastability) and switches to the AF one.
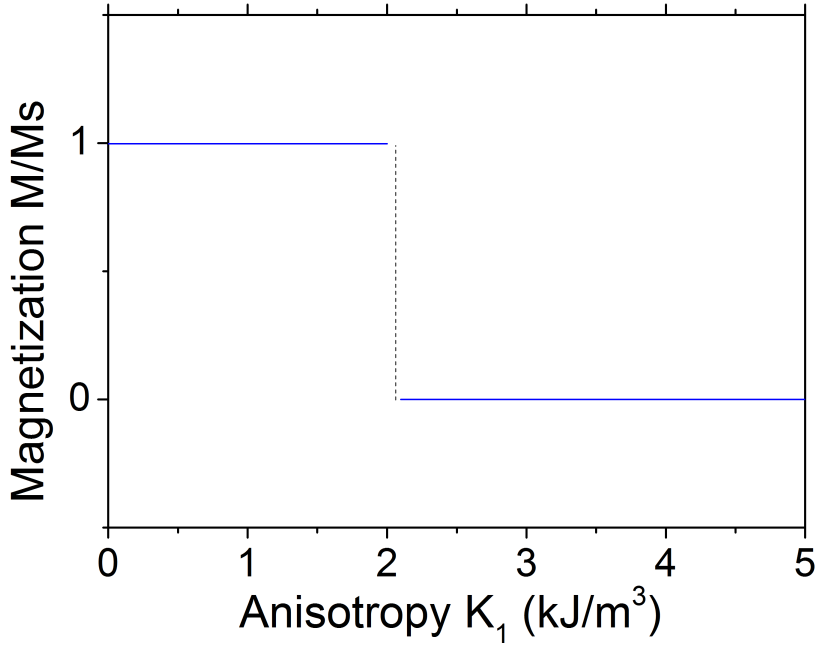
Figure 5.8: Magnetization vs. anisotropy parameter K_1 of every second nanoparticles uned the constant external field B=-25 mT

.

The instability of the initial FM configuration and its transformation to AF occurs at the critical K_1= 2.1 kJ/m^3.

5.2.2   Dynamics

Fig. 5.9(a) exhibits the dispersion relations of the lowest modes in the FM configuration close to its instability before the transition to the AF configuration.
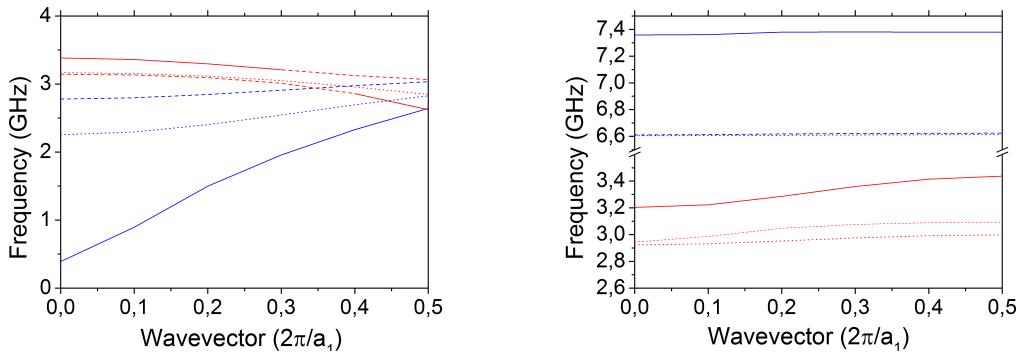

Figure 5.9: Dispersion relation for B=-25 mT acoustic (blue lines) and optical (red lines) BMs (solid lines), EMs S(dashed lines) and EMs AS(doted lines) for (a)FM order for K_1=2 kJ/m^3 and (b) AF order K_1=2.1 kJ/m^3

The unit cell contains two different macrospins so the modes may be in principle

classified as acoustic and optical. It is interesting that this classification turns out fairly adequate in the present case in contrast to the anisotropy difference imposed by the ovals widths. Indeed, e.g. Fig. 5.11 shows a well defined acoustic mode.

A trace of the translational invariance in spite of the ovals difference in anisotropy is a degeneracy of the modes at the Brillouin zone border. Generally the modes exhibit close frequencies that makes the hybridization of those of identical symmetry frequent. They show mostly a weak dispersion, or even no dispersion, except for an acoustic bulk mode that eventually softens at $k = 0$. Its group velocity is positive. With the softening of the mode at $k = 0$ the end of the branch at $k = \pi/a_1$ also goes down making the mode degenerated with the soft mode at the zone border also relatively strongly dispersive with, however, a negative group velocity (see red solid curve in 5.9(a).

After the discontinuous transformation to the AF structure (Fig. 5.9(b) the degeneracy at the zone border disappears and all the modes become weakly dispersive. This is another instance of a variation of the systems' parameters controlling the group velocities of modes and the width of the stop band for the spin waves. The evolution of the lowest modes with increasing anisotropy parameter K_1 can be seen in Fig. 5.10. One can remark that all the modes in the AF structure show a decrease in frequency, although the leading one is an acoustic BM in the Brillouin zone centre. Remarkable is also a quasi-continuity of optical modes across the transformation.
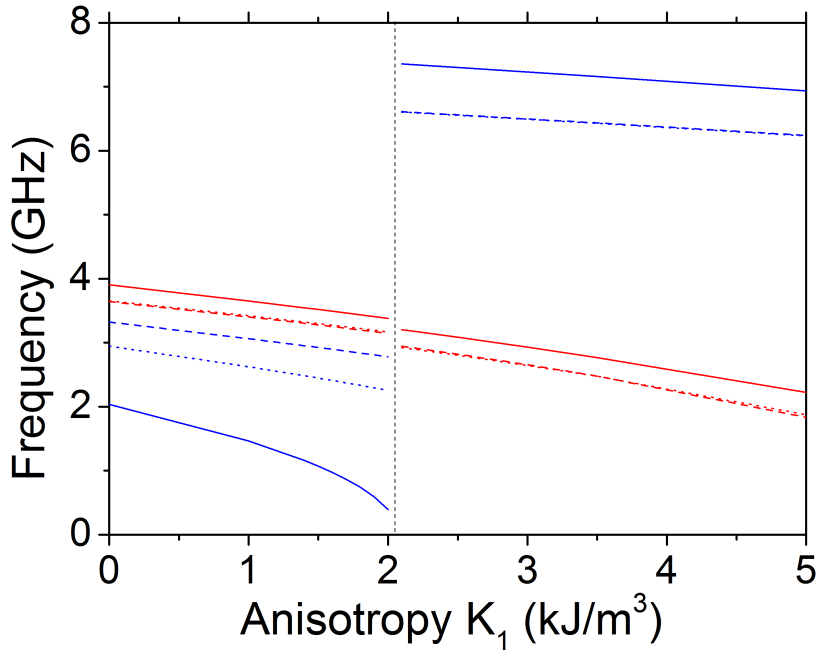

Figure 5.10: Frequency vs. anisotropy at B=-25 mT acoustic (blue lines) and optical (red lines) BMs (solid lines), EMs S(dashed lines) and EMs AS(doted lines) at $k = 0$.

The transformation from FM configuration to AF one takes place at about $K_1 \approx$

$2 \ \mathrm{kJ/m^3}$. The soft mode is an acoustic mode at $k = 0$. The dispersion branches of symmetric and antisymmetric end modes practically coincide in frequency except for the soft acoustic branch in FM configuration. The optical branch shows a little step-like change at the FM $\rightarrow$ AF transition. The frequencies of all the selected modes decrease with increasing anisotropy parameter K_1 in the whole studied region. The evolution of the polarization of the $k = 0$ soft mode as a function of the anisotropy parameter K_1 is depicted in Fig. 5.11.
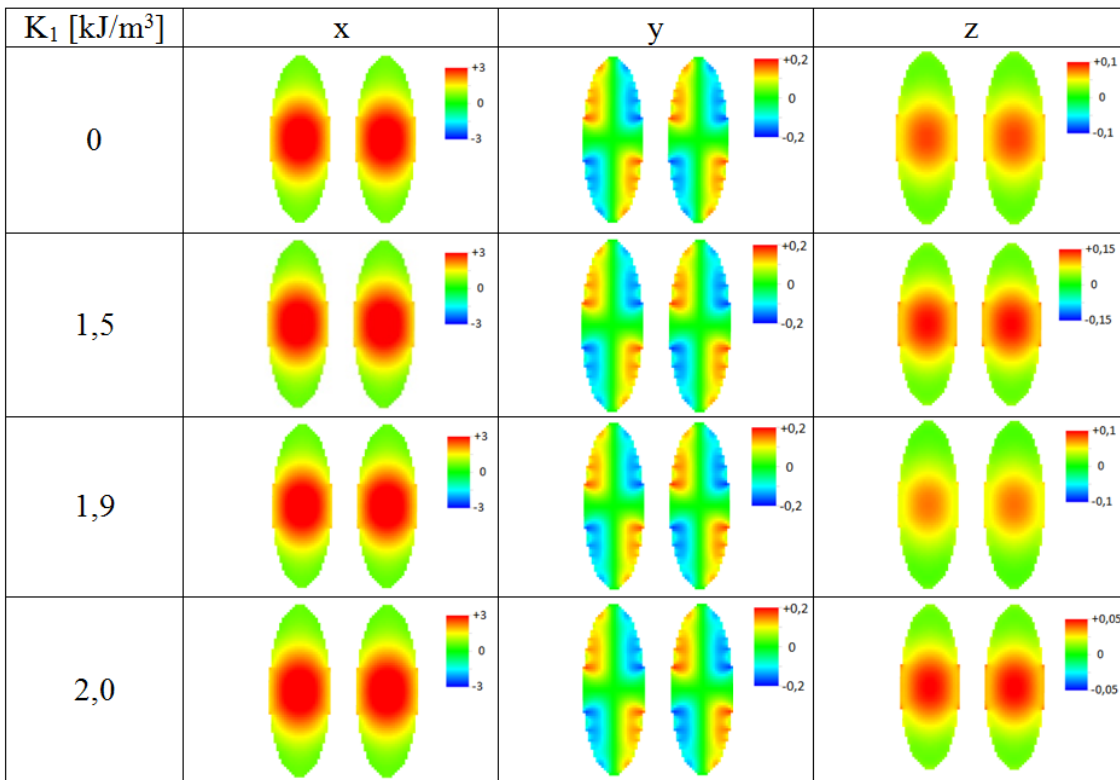

Figure 5.11: Precession amplitude profiles in the lowest acoustic mode at $k = 0$ for a chain with alternating anisotropy

.

One can remark that the precession ellipses are elongated in the (x, y) even at $K1{=}0 \ \mathrm{kJ/m^3}$. The x-component is 30 times longer than the z one there and this ratio increases when approaching the instability.

The AF configuration of the chain with every second oval endowed with an easy x-axis can be recovered with a homogeneous magnetic field, when it becomes strong enough in the direction opposite to the initial FM order. This is illustrated in the Fig. 5.12
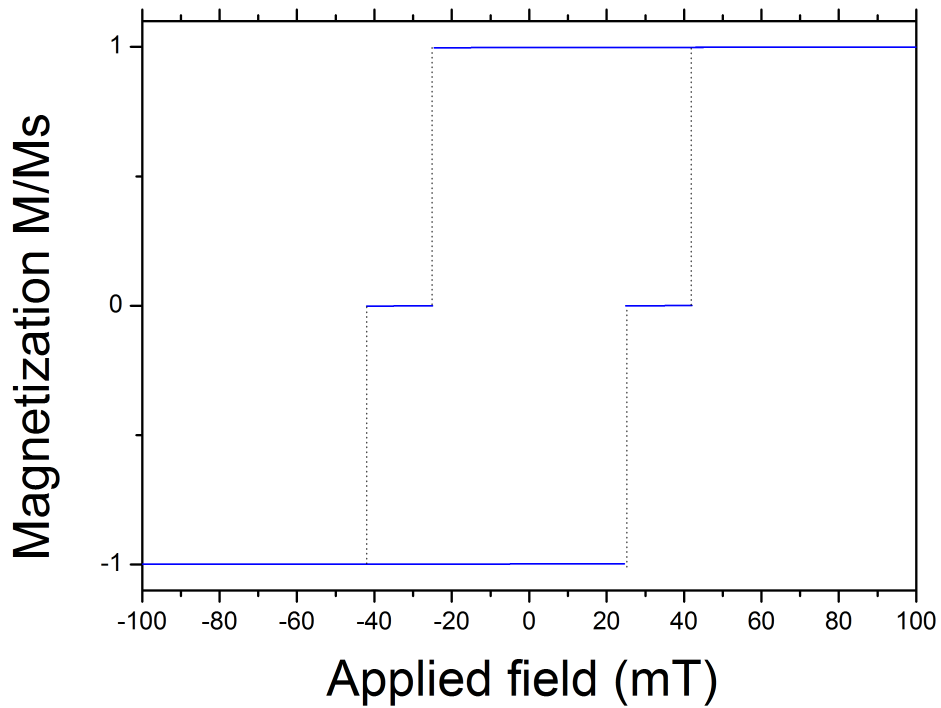
Figure 5.12: Hysteresis loop, magnetization vs. applied field, for a chain of ovals where every second oval shows anisotropy with easy x-axis, K_1= 3.4 kJ/m^3.

The resulting AF is however in a relatively narrow range in the studied example. To enlarge this range one has to increase the anisotropy parameter.

In summary: Making the ovals different, the anisotropy parameter allows one to recover the AF configuration without residual magnetisation. Surprisingly the zone centre modes can be exactly classified as acoustic or optical.

6

From single spin to macrospin

The macrospins as described in previous sections are systems of numerous single ionic spins, treated in a continuum approximation, that collectively behave analogously to a single spin. It is interesting to construct the simplest possible systems of this kind. The motivation for such studies are enhanced by the recent discoveries of molecular magnets where the magnetic interactions can be controlled by the chemical surrounding [28]. Moreover, the model calculations can indicate ranges of parameters for which interesting/useful phenomena are expected and, by this, stimulate experimental studies. In what follows we study the bevaviour of the spins as a function of the parameters of their interactions. In sections 6.1 and 6.2 we avail ourselves of a possibility of considering arbitrary values of the interaction parameters in systems consisting of few spins. This will allow us to give indications concerning design of systems of desired functionality. The result will be compared with the specific case of permalloy where the interaction parameters are well known and dictated by the properties of material. Because the study depends on free parameters their units are not indicated.

6.1   Complex of two-spins: bi-spins

As the first example we will consider a complex of two spins.

6.1.1   Single bi-spin

The geometry of such a pair is adapted to the one considered in the case of macrospins.
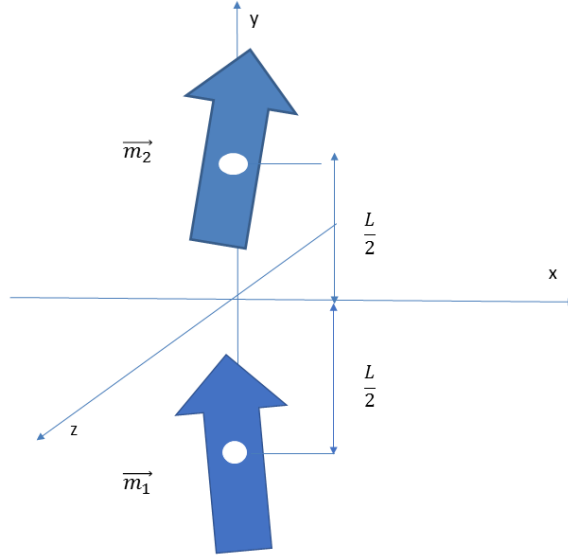
Figure 6.1: Geometry of bi-spin system; the simplest model of macrospin.

The spins are supposed to have a constant unit lengths so that their configuration is described by the polar and azimuthal angles

$$\vec{m}_i = (sin\theta_i cos\phi_i, sin\theta_i sin\phi_i, cos\theta_i), \; i = 1, 2 \tag{6.1}$$

The interactions of spins comprise ferromagnetic exchange and dipole forces. When put into a homogeneous magnetic field H the system has the following total energy.

$$E = -\vec{H} \cdot \vec{m}_1 - \vec{H} \cdot \vec{m}_2 - J\vec{m}_1 \cdot \vec{m}_2 + M^2 \frac{1}{r^3} \left(\vec{m}_1 \cdot \vec{m}_2 - 3 \left(\hat{r} \cdot \vec{m}_1 \right) \left(\hat{r} \cdot \vec{m}_2 \right) \right) \tag{6.2}$$

It is clear that in the absence of the external field the configuration corresponding to the minimum of energy is that of $\theta_i = \phi_i = \pi/2$, i.e. a head-tail parallel column. This is in fact the first manifestation of a shape anisotropy. Assuming a magnetic field parallel to the y axis or $\vec{H} = (0, H_y, 0)$ one can calculate the matrix of second derivatives of the energy (Hessian matrix).

$$\overleftrightarrow{E} = \begin{bmatrix} H_y + J + 2\frac{M^2}{L^3} & 0 & -J + \frac{M^2}{L^3} & 0 \\ 0 & H_y + H_a + J + 2\frac{M^2}{L^3} & 0 & -J + \frac{M^2}{L^3} \\ -J + \frac{M^2}{L^3} & 0 & H_y + J + \frac{M^2}{L^3} & 0 \\ 0 & -J + \frac{M^2}{L^3} & 0 & H_y + H_a + J + 2\frac{M^2}{L^3} \end{bmatrix} \begin{bmatrix} \delta\phi_1 \\ \delta\theta_1 \\ \delta\phi_2 \\ \delta\theta_2 \end{bmatrix} \tag{6.3}$$

The additional parameter $H_a > 0$ corresponds to an anisotropy that makes deviations in z direction more difficult. It will be shown that in the case of a chain of such bi-spins a shape anisotropy will keep the spins in the (x, y) plane. With $H_a > 0$

the stability condition reduces to the following 2 x 2 matrix being positive definite

$$\begin{bmatrix} H_y + J + 2\frac{M^2}{L^3} & -J + \frac{M^2}{L^3} \\ -J + \frac{M^2}{L^3} & H_y + J + 2\frac{M^2}{L^3} \end{bmatrix} \tag{6.4}$$

or

$$det \begin{bmatrix} H_y + J + 2\frac{M^2}{L^3} & -J + \frac{M^2}{L^3} \\ -J + \frac{M^2}{L^3} & H_y + J + 2\frac{M^2}{L^3} \end{bmatrix} > 0 \tag{6.5}$$

and

$$H_y + J + 2\frac{M^2}{L^3} > 0.$$

One can easily see that the bi-spin is stable at $H_y = 0$ when $J > 0$. An instability occurs when the applied field is opposite to the spins, i.e. $H_y < 0$.

We can distinguish two cases.

- A weak exchange

If the exchange parameter is small enough to satisfy the relation

$$-J + \frac{M^2}{L^3} > 0$$

Then the instability condition is

$$H_y + J + 2\frac{M^2}{L^3} = -J + \frac{M^2}{L^3}$$

or

$$H_y = -2J - \frac{M^2}{L^3} = H_c$$

The eigenvector corresponding to the zero eigenvalue then is $(\delta\phi_1, 0, \delta\phi_2, 0) = (1, 0, -1, 0)$, i.e. both spins go into opposite directions. This kind of motion is analogous to a one-node mode in a real macrospin. It ensures a proximity of the head (the *north pole* of one *magnet*) of one spin with the tail (the *south pole* of one *magnet*) of the other. This case, dominated by dipolar interactions, is not typical for macrospins where the exchange interactions are usually strong.

- A strong exchange

When

$$-J + \frac{M^2}{L^3} < 0$$

the exchange interactions prevail. The instability will occur when H_y becomes so negative that

$$H_y + J + 2\frac{M^2}{L^3} = -\left(-J + \frac{M^2}{L^3}\right)$$

i.e.

$$H_y = -3\frac{M^2}{L^3}$$

or

$$H_c = -3\frac{M^2}{L^3}.$$

Noteworthy is that the critical value of the magnetic field now depends on the dipolar interactions only. The eigenvector the corresponding to the vanishing eigenvalue in this case is $(\delta\phi_1, 0, \delta\phi_2, 0) = (1, 0, 1, 0)$.

The reversal of the bi-spin proceeds so that both spins remain parallel, i.e. the exchange energy stays in minimum. The kind of reversal is similar to Kittel mode, or no-node mode, also observed in the oval-section cylinders of permalloy (see section 4.2.3). In what follows we will assume $L = 1$.

For practical reasons the external magnetic field may be declined from the vertical y direction. The critical (coercive) field then changes. The following figure presents the value of the coercive field H_c as a function of the tilt angle between the field and the y axis for the values $J = 1$, $M^2 = 0.5$.
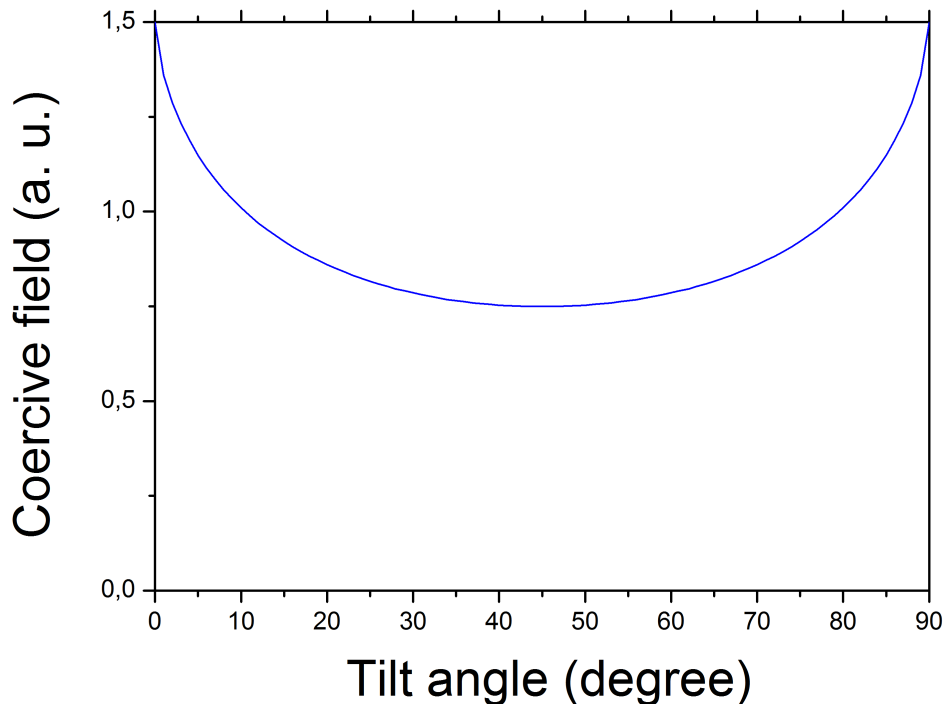

Figure 6.2: Coercive field H_c as a function of the angle of the field with y-axis for $J = 1$, $M^2 = 0.5$.

A decrease in the coercive field is visible for small tilt angles. The narrowest hysteresis occurs for an angle equal to 45° the curve of Fig. 6.2 has a minimum. Then a re-increase is seen. This means that the reversal the bi-spin by a field too

much inclined towards the x axis is more difficult.

We have seen that the shape of the hysteresis loop in permalloy macrospins, in principle quasi rectangular, has been marked by rounding close to the reversal points. The same occurs in the present simple model. The following figure gives the y component of the magnetization at the reversal point with a positive y component of the field $H_y > 0$.
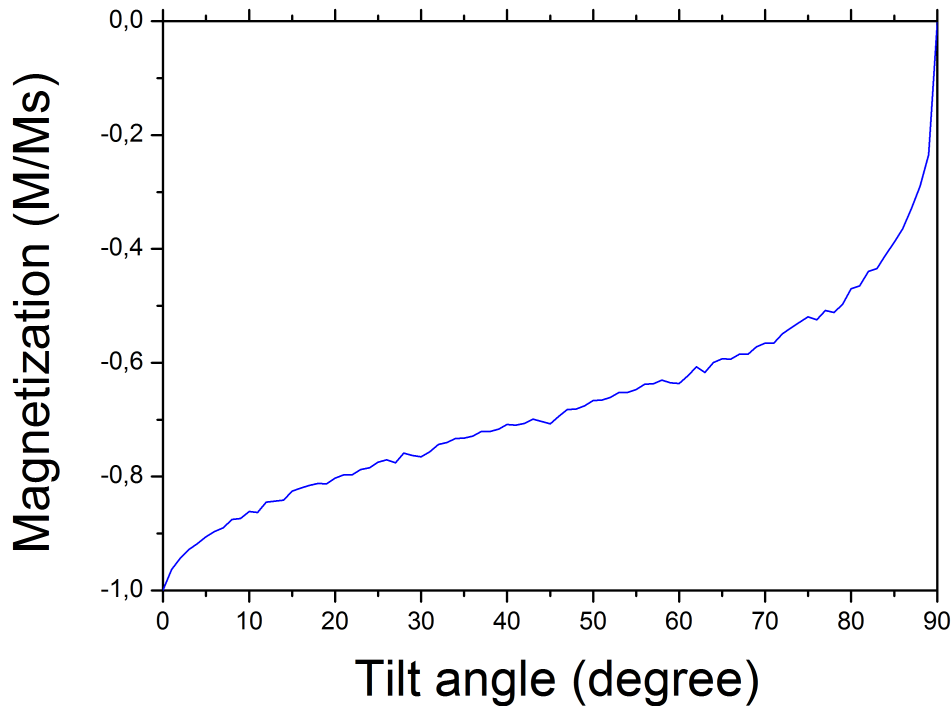

Figure 6.3: Projection of the magnetization on the y-axis at the instability point for $J = 1$, $M^2 = 0.5$ as a function of tilt angle of the field with the y-axis. The projection is negative because we consider a positive y-coordinate of the field applied to bi-spin oriented in y direction. Irregularity of the curve comes from numerical inaccuracies.

Both above Figures have been obtained in the case of $J > M$ in which case the spins are constantly parallel. Consequently the exchange energy does not depend on their angle with the y axis and both figures are the same for every J in the case of the predominant exchange interactions.

6.1.2 Chain of bi-spins

When arranged in an infinite equidistant chain perpendicular to their axes the bi-spins are found to have four possible equilibrium configurations depending on the ratio $d = a/L$, where a is the distance between the neighbouring bi-spins. We always assume that the exchange interactions are active within a bi-spin and they do not exist between different bi-spins independently of the distance.
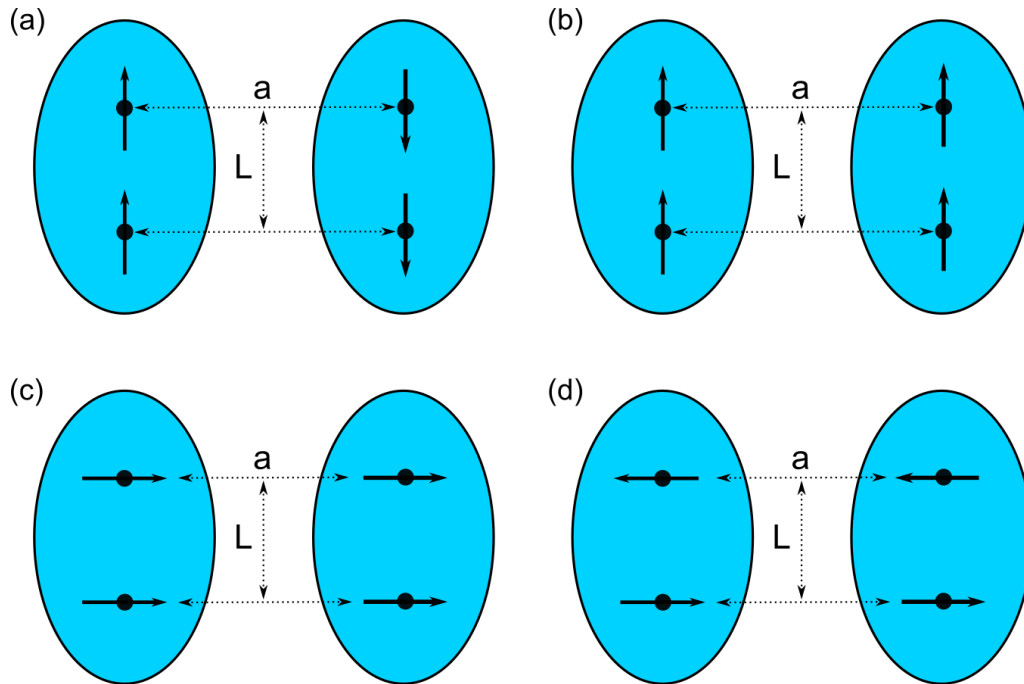
Figure 6.4: Four configurations of the chain of bi-spins: (a) AF, (b)FM , (c) ferromagnetic horizontal FMh and (d) antiferromagnetic horizontal AFh

One can remark that the freedom in selection of distance between neighbouring bi-spins leads to equilibrium configuration encountered in the permalloy macrospins Fig. 6.4 (a,b) as well as horizontal ordering either preserving monodomain character of macrospin (c) or splitting it into two domains (d), where the magnetization of the bi-spin compensates to zero.

6.1.2.1   Statics at $H = 0$ with variable distance

When without external field the FM configuration is always metastable in all the examined cases. The sequence of all the configurations as a function of the distance ratio d depends on the interplay of the parameters J and M^2, but also on the range of dipolar interactions taken into account in the calculations. It is known that these interactions decrease inversely proportionally to the third power of distance, but in real systems they are also screened by the diamagnetism of the magnetic dots and of the substrate. To illustrate the behavior of the chain of bi-spins we present the case with parameters $J = 1$ and $M^2 = 0.5$ and the dipolar interactions extending to the nearest neighbouring bi- spins. The general features are present in this case.

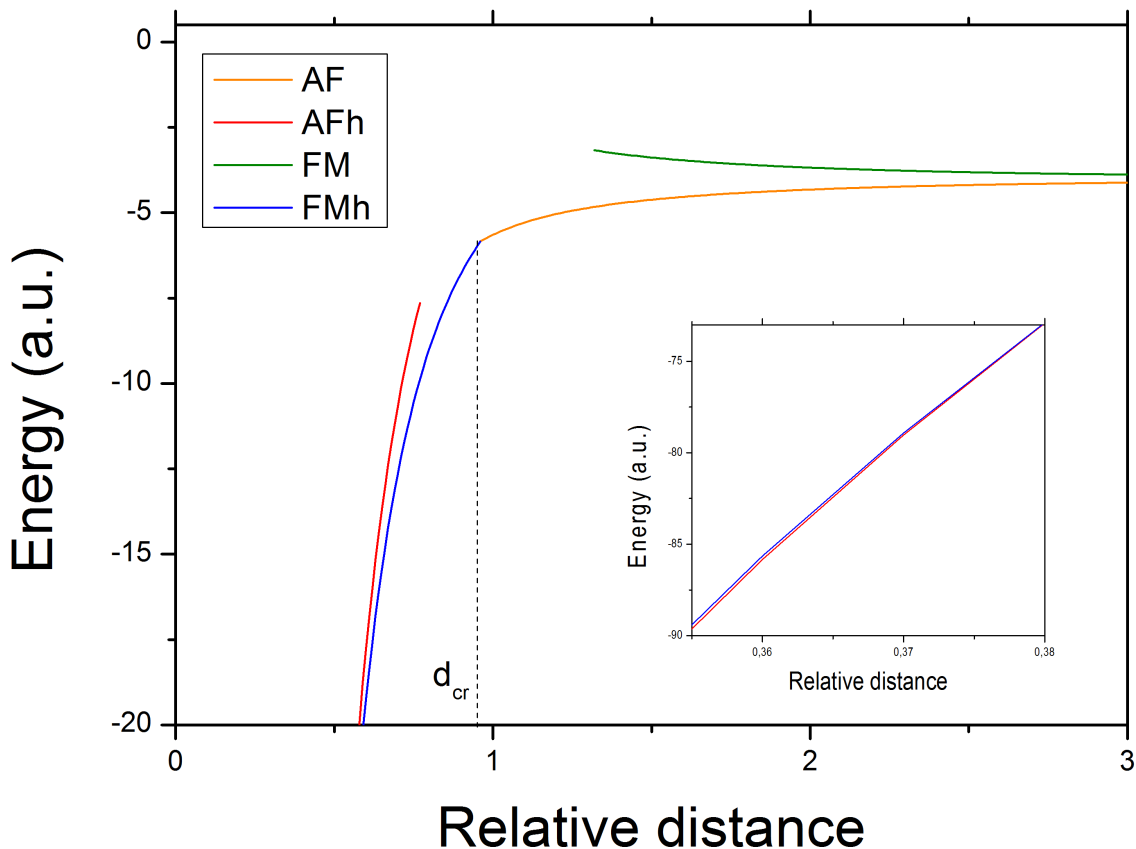The energies of the configurations are shown in the following figure.

Figure 6.5: Energies of bi-spin chain for the configurations with $H = 0$, for $J = 1$ and $M^2 = 0.5$: AF (orange), FM (green) , FMh (blue), AFh (red). Crosing of line AFh and FMh is visible in the inset. Critical value of relative distance d_{cr} corresponds to the second order yet discontinuous transition discussed in section 6.1.2.3

For large enough distances the most stable configuration is AF. The metastable FM configuration looses its stability at $d = 1.315$ where one of the eigenvalues of the Hessian matrix vanishes, so that the minimum transforms into a saddle point. The system drops to the only stable AF configuration. When the lattice constant decreases to $d = 0.961$ the FMh becomes the most stable. The energetic reason for that is clear: the closest dipoles become those which are a apart. Consequently they take a head-tail configuration, whereas the exchange forces within each bi-spin keep the spins parallel. The nature of this transition is extremely interesting as the AF configuration disappears at the same distance as the FMh appear, see Fig. 6.5. This is characteristic of the second order phase transitions. Yet not only is the transition discontinuous: each spin reorients by a right angle, but it even does not fulfil a group-subgroup relation as required by the Landau first necessary condition of the 2nd order phase transition [29, 30, 31]. This will be discussed below. When the lattice constant is shorter than $d = 0.384$ the most stable configuration becomes AFh. One should remark that the latter configuration becomes stable for increasing d with range of dipolar interactions. However it is not stable for the first interacting

neighbours if the exchange interaction constant J is too high. The transition MFh $\rightarrow$ AFh is typically discontinuous. The distance $d = 0.384$ corresponds to the co-existence point of the configurations (see inset in Fig. 6.5). The AFh configuration remains metastable up to the distance $d = 0.777$. On the other hand the metastability of the FMh configuration persists down to the shortest distances in the studied case.

6.1.2.2   Dynamics and transition mechanisms as dependent on bi-spin separation in the chain

The instability points of the chain of bi-spins are marked by an eigenvalue of the Hessian tending to zero, or equivalently, by a soft spin wave. Fig. 6.6(a) presents the dependence of all the eigenvalues of the Hessian matrix on the relative distance d starting from the lowest values and AFh configuiration. The lowest eigenvalue is distinguished by blue color. A discontinuous transition at $d \approx 0.777$ is characterized by jumps of all the eigenvalues, whereas in the second order transition at $d \approx 0.9614...$ the soft mode rebounds in a continuous manner from zero. A continuity of other modes can also be appreciated. The evolution of the eigenvalues starting from the highest values of d and the FM configuration is represented in Fig. 6.6(b). The transition FM→AF at $d \approx 1.315$ is discontinuous, whereas the vicinity of the second order transition at $d \approx 0.9614$ looks exactly the same as in the previous case.

As explained in section 2.2 the Hessian matrix of the magnetic energy allows one to compute the frequencies of the spin waves. An example of comparison of both quantities is given in Fig. 6.7. For our system on the verge of instability of the AF phase at $d \approx 0.9614$. The left panel contains the four eigenvalues of Hessian matrix and the right panel the corresponding frequencies of spin waves. A mode at $k = 0$ tends to zero so it is the soft mode. An insight into the precession profiles allows us to classify the magnons at $k = 0$ as one-node or no-node and as quasi circular precession vs precession elongated in the (x, y) plane. As expected the soft mode is extremely elongated and show no node within the bi-spin. Additionally the precessions on neighbouring bi-spins are shifted in phase by π (optical). The second lowest mode is less elongated, the semi-axis ratio is about 1.41, the precession of both members of the bi-spin is in antiphase (one-node mode) as the precession on neighbouring bi-spins. Both higher modes show almost circular precession, the same in neighboring bi-spins (acoustic), the lower without node and the higher one-node.
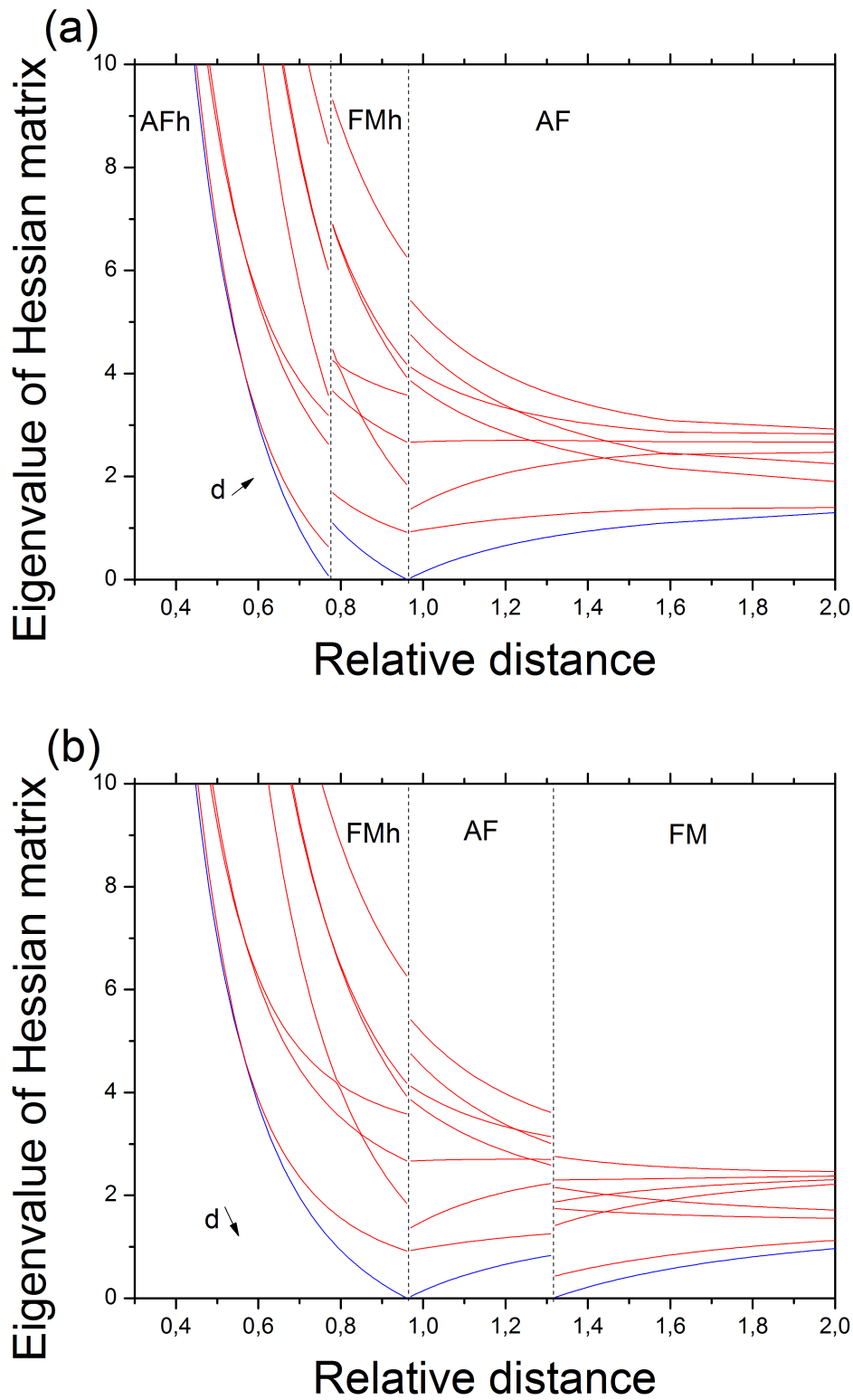
Figure 6.6: Eigenvalues of Hessian matrix of energy in stable and metastable phases of chain of bi-spins as functions of realtive distance d (a) starting from the lowest d in AFm configuration, (b) starting from highest d in FM configuration. Soft mode distinguished with blue color. The eigenvalues have been calculated at $k = 0$, in the unit cell corresponding to the AF configuration, i.e. lattice period equal $2a$. Therefore they represent the zone centre along with zone border modes for the structures of periodicity a.
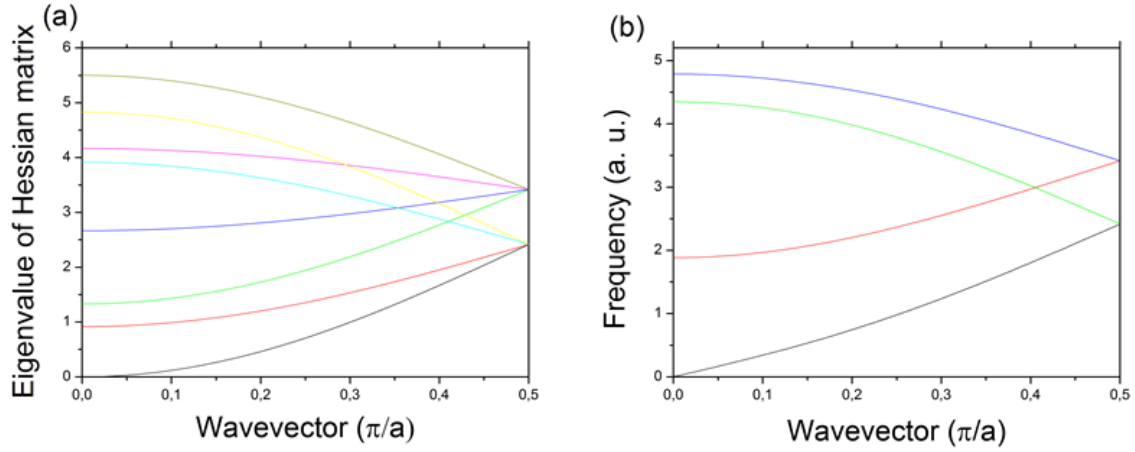
Figure 6.7: (a) Eigenvalues of Hessian matrix and (b) frequencies of spin waves. The color code for the modes at $k = 0$ black: optical, elongated in (x, y) plane, no node; red: optical, slightly elongated in (x, y) plane, one-node; green: acoustic, circular, no node; blue: acoustic, circular, one node.
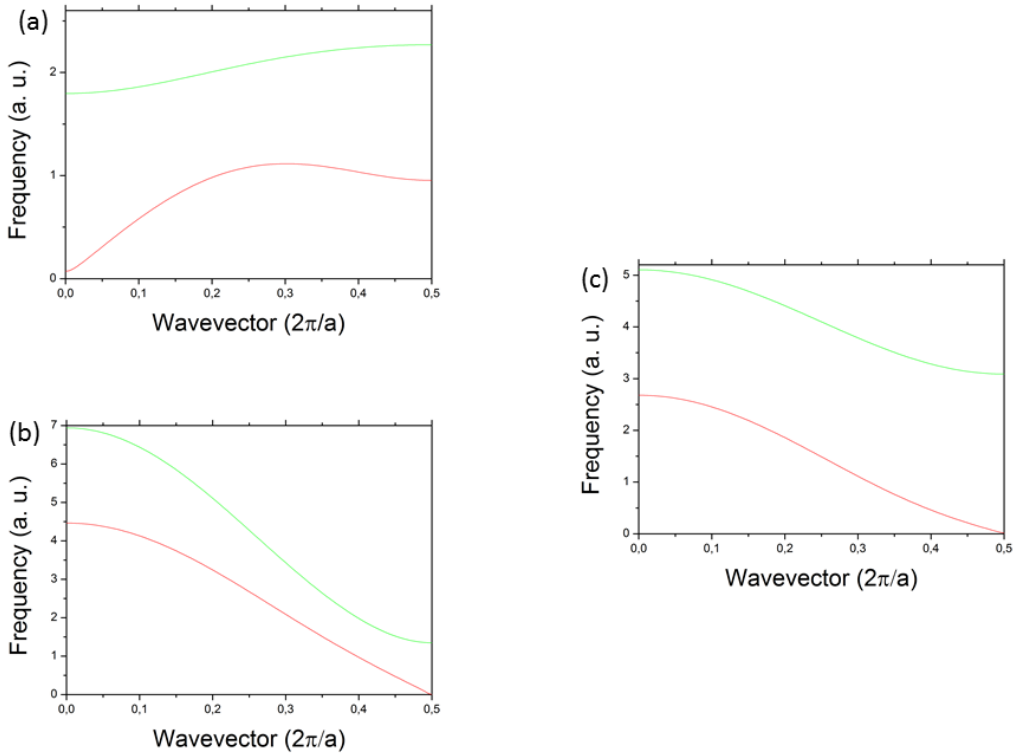

Figure 6.8: The dispersion relations of spin waves (a) in FM configuration, d=1.315, (b) AF configuration $d \geqslant 0.9614$ and (c) FMh configuration $d \leqslant 0.9614$.

The magnons below the second order transition are represented in the right panel of Fig. 6.8. At $k = 0$ the higher mode is almost circular and shows a node, whereas the lower has no node and is elongated in the (x, y) plane by a factor of 1.46. The elongation grows with the k vector to become infinite at $k = \pi/a$, i.e. at the zone

border, where the mode becomes soft. The instability of the FM configuration at $d = 1.315$ is driven by a soft mode at the Brillouin zone centre as seen in the upper left panel of Fig. 6.8. The soft mode is infinitely elongated in the (x, y) plane and has no node. It is interesting that in spite of the fact that it drives an instability leading to AF phase it occurs at $k = 0$, i.e. the neighboring bi-spins precession is in phase. The higher mode is almost circular and with one node at Brillouin zone centre.

6.1.2.3 Discontinuous (but) second order phase transition

The transition AF $\leftrightarrow$ FMh with the changing distance d unifies properties of the first order phase transition and 2nd order phase transition. The energy is continuous. But the configurations are not in a relation group-subgroup, which is analogous to strongly reconstructive martensitic phase transition showing usually a deep hysteresis [32]. It turns out that at $d = d_{cr}$ the energy of the chain does not depend on the angle of the spins with the x-axis if we deviate the spins of neghbouring bi-spins by the same amount in opposite directions (Fig. 6.9). It is clear that if this angle amounts to zero we have FMh structure, and the if reaches 90 deg the structure becomes AF. The plot of energy as a function of the angle for interactions to the nearest neighbours is presented in Fig. 6.10 for three different values of the distance. We have checked that the phenomenon occurs independently of the number of interacting neighbours taken into account.
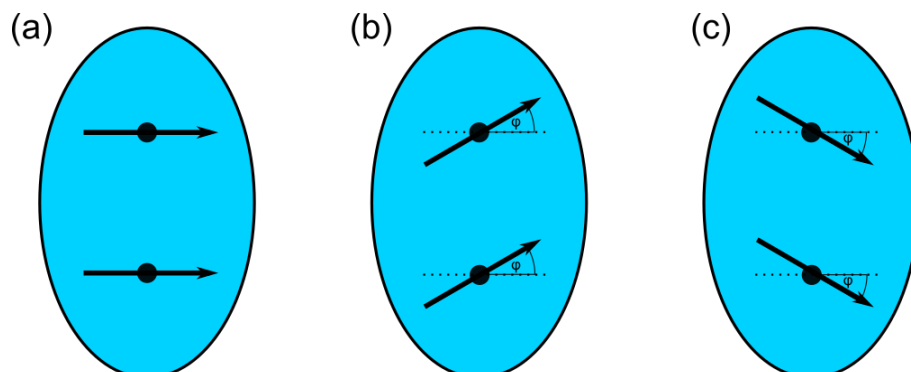

Figure 6.9: Angle deviation of bi-spins at the discontinuous second order transition.
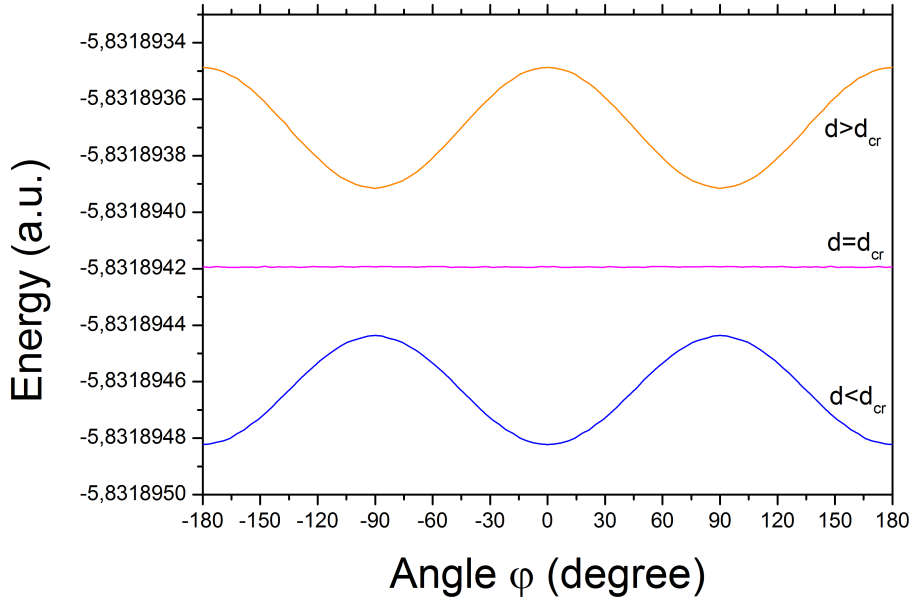
Figure 6.10: Energy of bi-spin chain as a function of angle ϕ of Fig. 6.9 for distances close to critical distance d_{cr}=0.9614.

The plots explain how the minimum at $\phi = 0$ disappears and a minimum for $\phi = \pi/2$ appears at the same time. This is reminiscent of the transcendental order parameter theory given by P. Tolédano [29]. However the Toledano's theory has not invoked phase transitions of second order. The soft modes behave typically for the second order phase transitions as shown in Fig. 6.6. Their frequencies vanish at the same point. This kind of transition, apparently contradictory to the common knowledge associating the second order with continuity is worth further studies that are beyond the scope of the present dissertation.

The studies as dependent on distance d are not current in the existing literature but some piloting experiments with strain have been already done [33]. The collection of phenomena described here indicate an interest in designing systems capable of varying the distance of the macrospins, e.g. by depositing magnetic nanoparticles on an elastic substrate.

6.1.2.4 Hysteresis loop in magnetic field

In the present section we study the behaviour of the chain of bi-spins in analogy to the chain of macrospins. Therefore, we settle the value of the relative distance $d = 2$ where AF configuration is stable at the zero external field $H = 0$ in concurrency with the metastable FM configuration Fig. 6.11(a) gives the energy diagram for the thought experiment in which the external magnetic field parallel to the y axis is applied to the stable AF configuration. When the field attains the value $H = 1.618$ the AF configuration looses its stability and drops to the stable FM configuration magntised parallel to the field. Then we diminish the field. The FM configuration

persists metastable down to $H = -0.9640$. As in the case of elliptical macrospins the stable configuration in these conditions is the FM one aligned along the field. That is why the initial AF configuration cannot be recovered with varying homogeneous magnetic field. Fig. 6.11(b) represents the hysteresis loop for the magnetization along the y axis. With the field being constantly parallel to the y-axis the loop is perfectly rectangular.
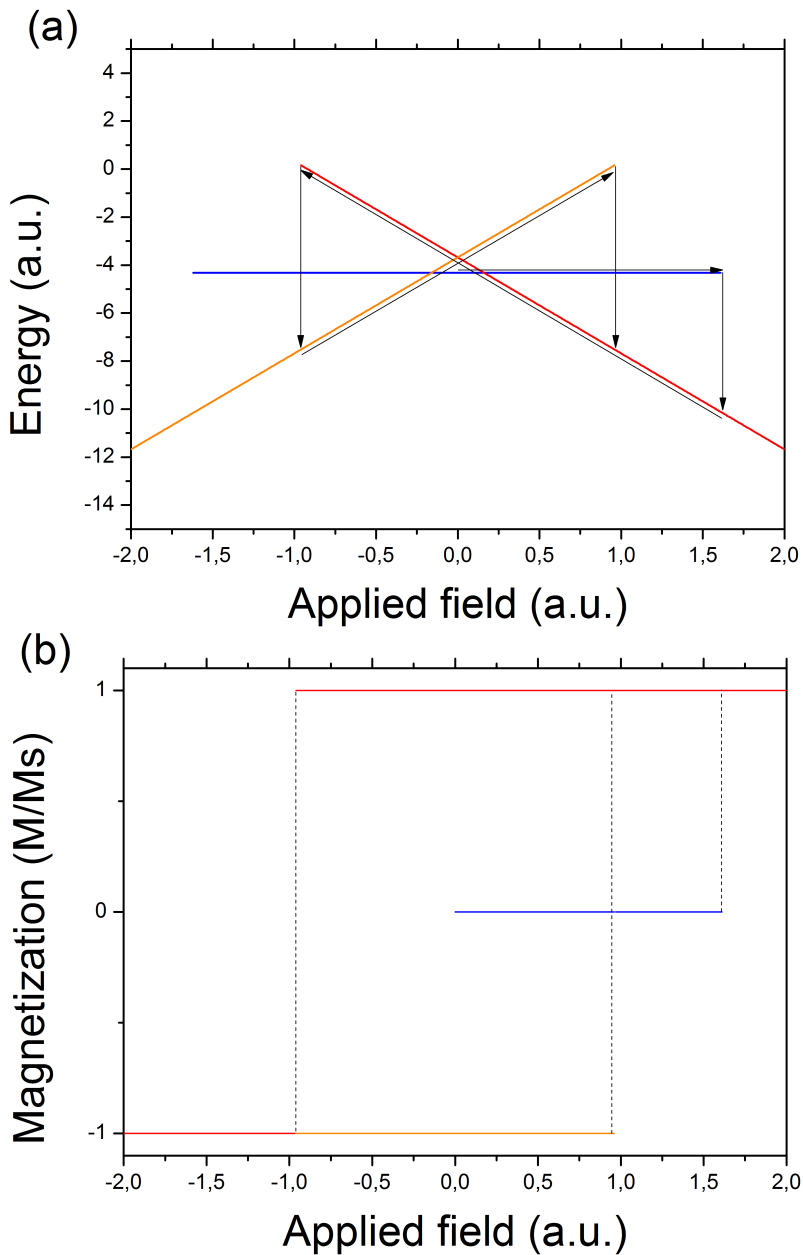

Figure 6.11: (a) Energies of AF and FM configurations of a chain of bi-spins $J = 1.0, M^2 = 0.5$ with relative distance $d = 2.0$. Arrows indicate the sequence of applied fields $H||y$. (b) Hysteresis loop of y-component of magnetization with the same field sequence.

6.1.2.5 Spin waves under magnetic field

Having only two spins in the model of macrospin we can draw all four frequencies of the spin waves as functions of the external field. The behaviour of the frequencies under increasing magnetic field H starting from the AF configuration is shown in Fig. 6.13.

The frequency of the soft mode decreases with increasing external field. An insight into the polarization vectors of the waves shows that for $H = 0$ the soft mode is an optical mode with almost circular precession ellipses of all the spins. The precession in the neighboring bi-spins are shifted in phase by π which is here the definition of the optical mode. With increasing field H the ellipses become more and more elongated in the (x, y) plane and at the same time the precession radius of the spins oriented opposite to the external field increases at the expense of the precession radius of the spins aligned with the field. The second-soft mode (1.0 at $H = 1.66$ and 2.58 at $H = 0$) is acoustic, i.e. the spins in neighbouring bi-spins rotate in phase. In contrast the rotations of the spins within one bi-spin are shifted in phase by π which is analogous to a one node mode. The precession radii of the spins oriented opposite to the field also increase. The magons starting from $H = 0$ with the approximate values $\omega = 1.95$ and $\omega = 2.74$ are zero-node optical and one-node acoustic respectively. The frequencies of both modes increase (hardening) as well as the contribution to the polarization vectors from the bi-spins oriented parallel to the external field. After the jump to the FM configuration the modes change stepwise their character and the frequencies.
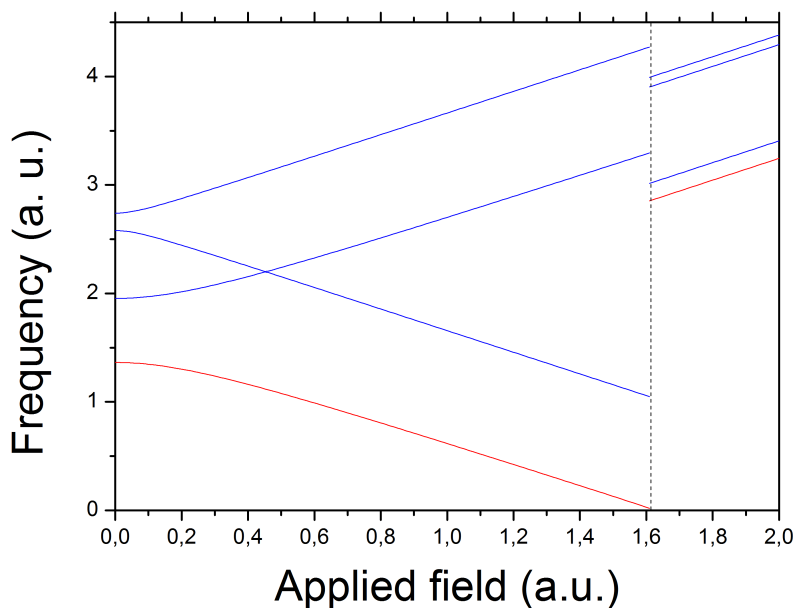

Figure 6.12: Frequencies of spin waves as functions of increasing magnetic field H starting from AF configuration.

The evolution of the dispersion relations of the spin waves with increasing field is depicted in Fig. 6.13. It is remarkable that the dispersion curves flatten significantly with increasing field in AF configuration and become lightly dispersive in FM configuration.
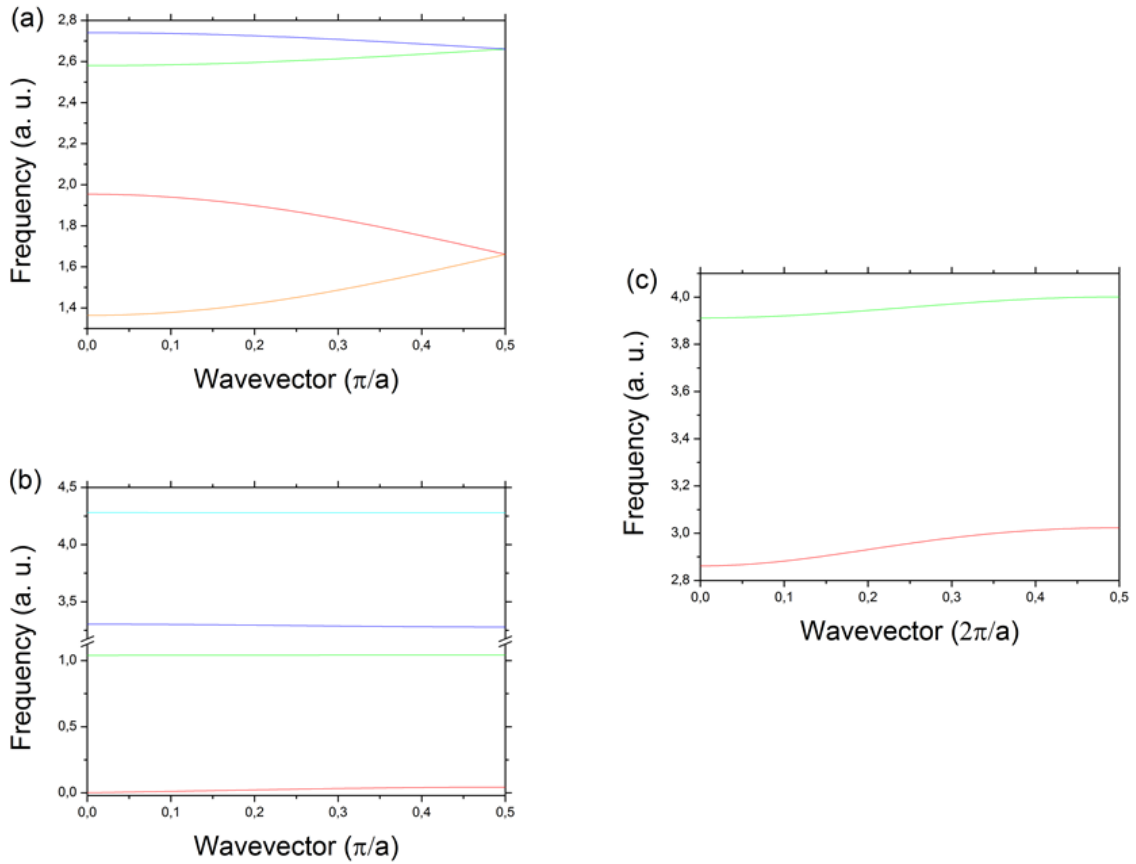

Figure 6.13: Dispersion relations in consecutive stages of transition from AF configuration to FM configuration. (a) AF configuration $H = 0$, (b) AF configuration at verge of stability $H = 1.677$, (c) FM configuration just after transition $H = 1.678$.

The frequencies of the spin waves at the switching between FM configurations are depicted in Fig. 6.14 as functions of the applied field H. Zone centre modes $k = 0$ and the zone border $k = \pi/a$ modes have been shown. Only the soft mode exhibits a curvature the other being fairy linear.
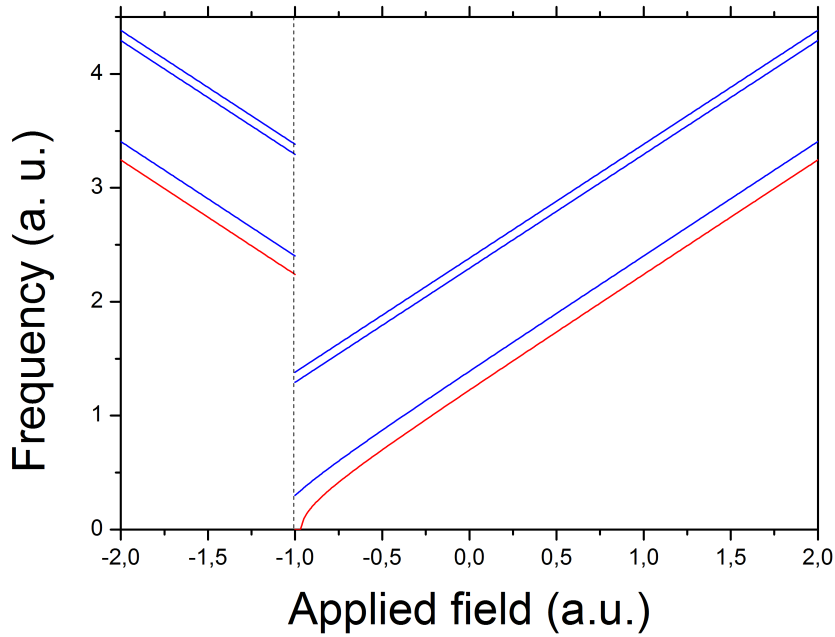
Figure 6.14: Zone center $k = 0$ and zone border $k = \pi/a$ modes frequencies as functions of applied field at switching between two opposite FM configurations.
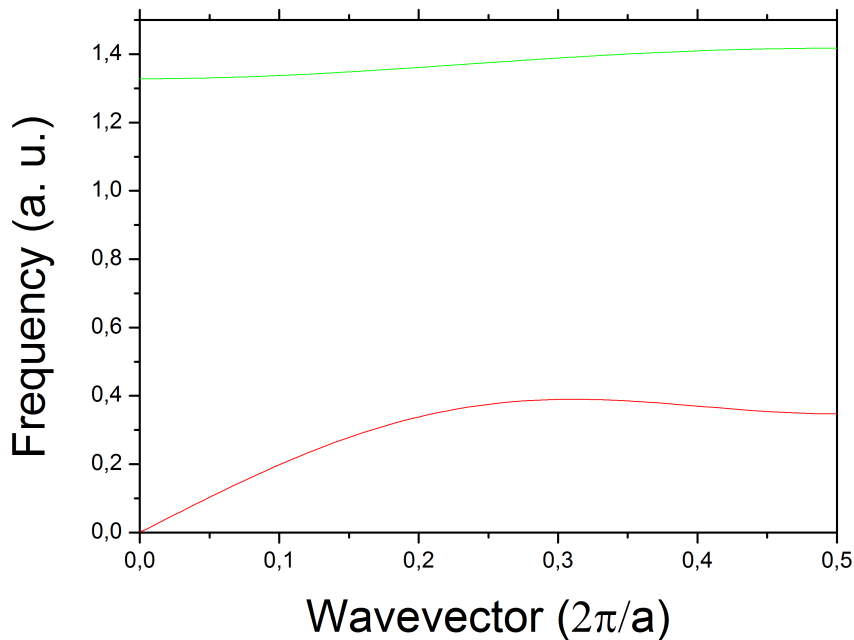

Figure 6.15: Dispersion relations of spin waves in FM configuration at verge of stability.

The dispersion relations of the spin waves at the verge of stability are given in Fig.6.15 The soft mode at $k = 0$ shows no node and a rather strong elongation of the precession ellipse in the (x, y) plane: the theta component of the soft mode tends to

zero. The higher mode in Fig.6.15 involves almost circular precession of both spins in bi-spin but the precession of lower spin is shifted in phase by π, i.e. the mode shows a node across the bi-spin.

Whereas we are not able to model a shape anisotropy with only two individual spins in a macrospin we can, however, introduce a material anisotropy in analogy to section 5.2. As an example we present in Figs. 6.16 the energy diagram and the hysteresis loop with a term

$$E_a = -K_1 m_x^2 = -K_1 (sin\theta, cos\phi)^2 \tag{6.6}$$
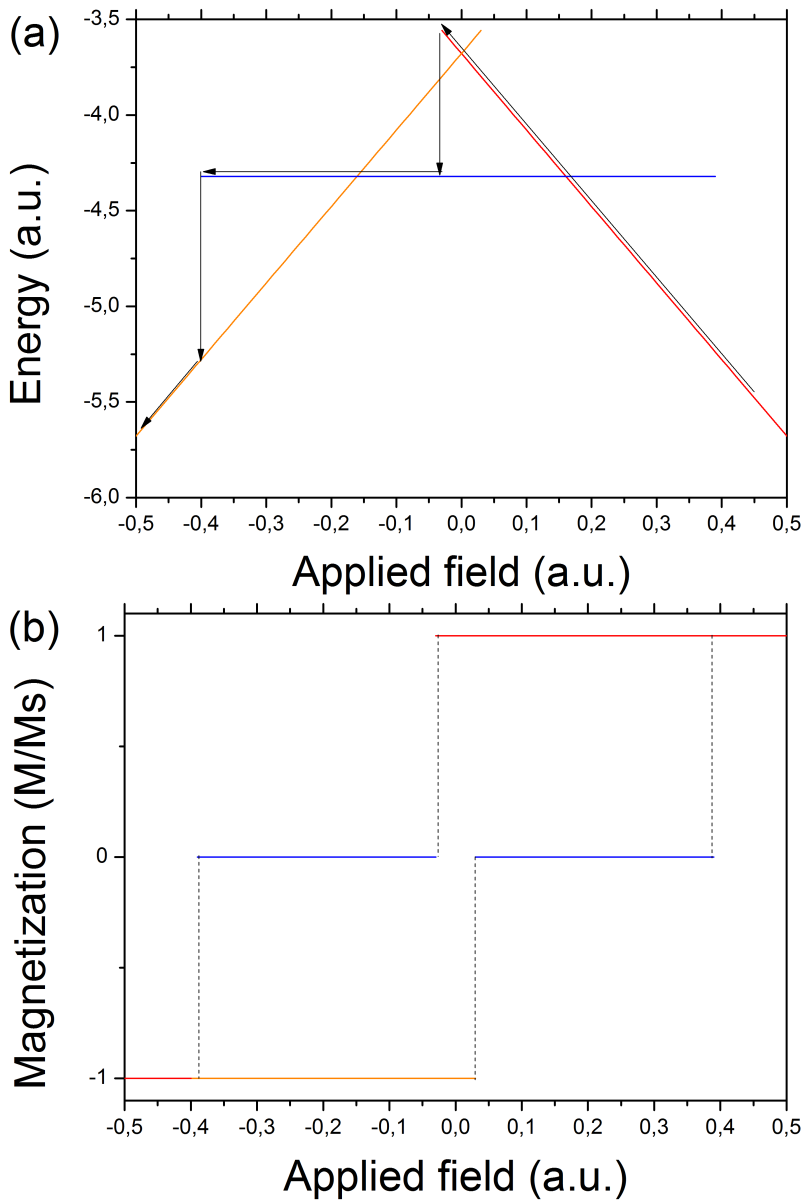
where $K_1 = 0.6$.

Figure 6.16: (a) Energies of AM and FM configuration of a chain of bi-spin. Arrows indicate evolution of applied field. (b) Hysteresis loop of y component of magnetization with the same field sequence.

To close the section on the bi-spin model we present in Fig. 6.16 some examples of hystereses for different distances of the bi-spins. The calculations have been done with the parameters $J = 2, M^2 = 0, 5$. As one can see at the largest distances this simple model reproduces the behaviour of massive macrospins of chapter 4. In particular the loop is fairly rectangular and the initial AF configuration does not reappear under the homogeneous applied field. However, with decreasing lattice spacing one can arrive at a two-part hysteresis loop that drops to the AF configuration either abruptly (Fig. 6.17(b)) or with an oblique region (Fig. 6.17(c))

The results suggest that the distance of the macrospins may be a relevant parameter in designing functional systems transmitting spin waves. In particular the reentrance of the AF configuration may be achieved as a result of the appropriate interplay of exchange and dipolar interactions, as well as of the macrospin separation.
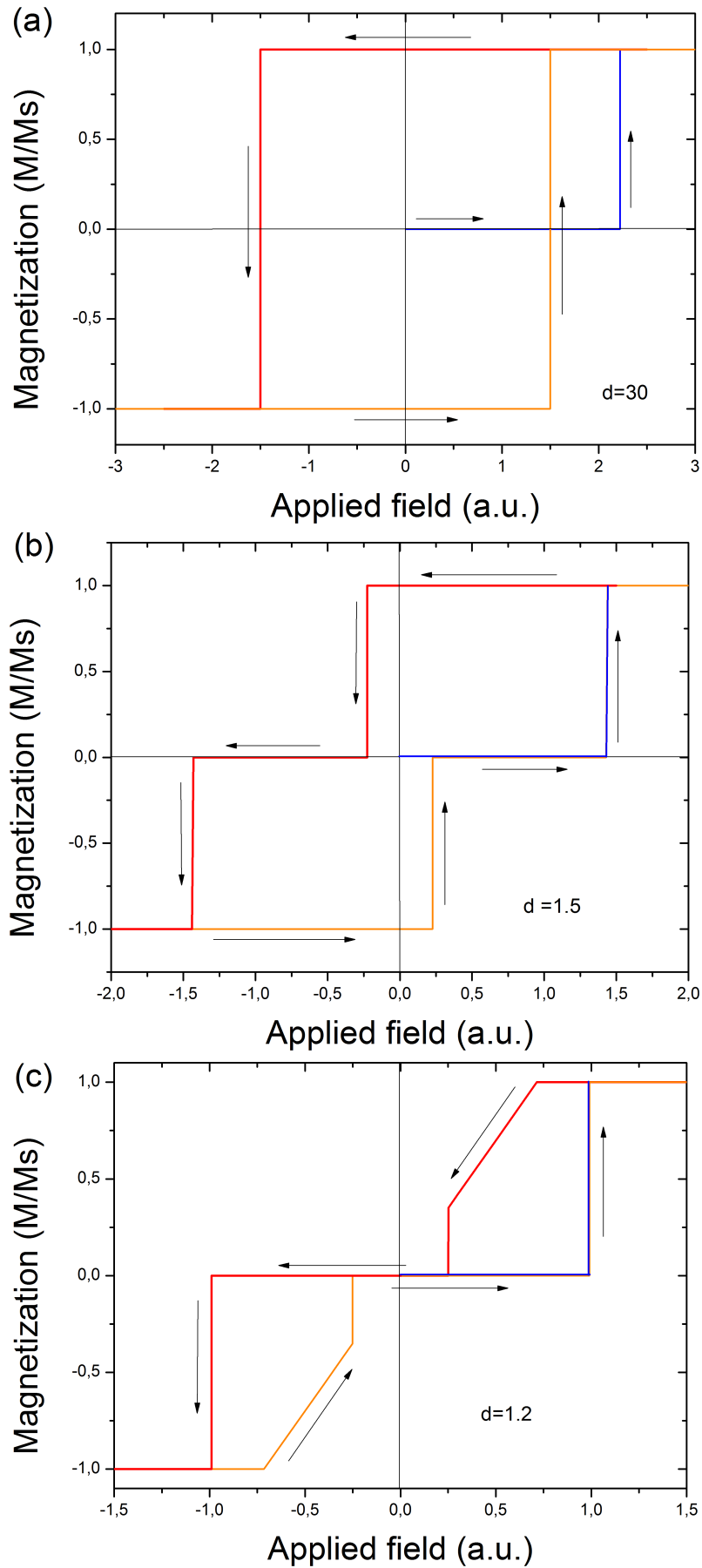
Figure 6.17: Effect of relative distance on shape of hysteresis loop in chain of bi-spins.

6.2 Single spin versus microspin calculations

In the previous sections we studied complexes of few individual spins as the first stage of formation of a macrospin in a "bottom up manner". It is, however, also interesting to what extent the micromagnetic calculations are able to reproduce the results obtained with single spins, i.e. if similar systems can be obtained in a "top-down" strategy. To illustrate this we first considered four individual spins arranged in the corners of a square of edge a. The spins' distance a apart are assumed to interact by both exchange and dipolar forces, whereas those situated on the opposite corners, i.e. the square's diagonal apart are only subject to dipolar interactions. Although it is not sure if such a system can be synthesized chemically we consider it because it follows a usual assumption made in micromagnetic calculations, namely that the exchange interactions extend to the nearest neighbours only. The system shows a very interesting evolution when put in an external field along its diagonal.
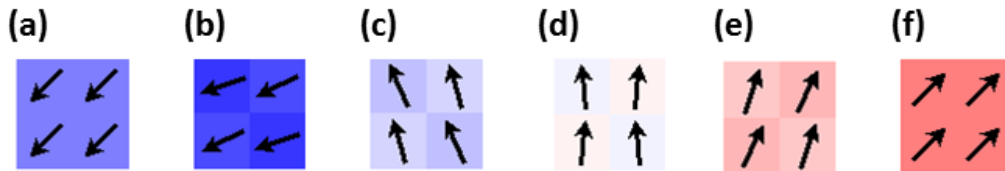

Figure 6.18: Consecuitive stages of magnetization of four-spin system under magnetic field along square diagonal.

The consecutive stages of the four spins are depicted in Fig. 6.18. If the field is strong enough all the spins point exactly along the field. With weakening the field one arrives at a point where the spins decline from the diagonal. This is a typical continuous second order transition with a spontaneous symmetry breaking. The new structure becomes symmetric with respect to the vertical direction when the field vanishes. Following the evolution of the field to negative values makes the angle between the field and the spins obtuse. This is energetically unfavorable and ends up, with increasing the negative value of the field, in a discontinuous transition, to the structure with an acute angle, which subsequently becomes perfectly aligned with the field by a continuous transition. The quantitative evolution is shown in Fig. 6.19(a), where the projections of the total magnetization on the x and y axes are represented separately. The parameters of Fig. 6.19(a) are $J=2$ and $M^2 = 0.5$. It is interesting that the shape of the graph does not change as long as $J > M^2$, i.e. the exchange interactions prevail. The only difference is that the scale on the abscissa changes. In the opposite case, i.e. $J < M^2$ the structure at $H = 0$ is the vortex one which is beyond the scope of the present dissertation.

In contrast with Fig. 6.19(a) the plots 6.19(b) and 6.19(c) are obtained with the data corresponding to the permalloy (in Fig. 6.19(b) the exchange interactions were

reduced by a factor of 10) introduced into a "macrospin" consisting of as few as four cubic cells. In fact it is the system and its states that are reproduced with the OOMMF program in Fig. 6.18. One easily remarks that the curves are identical with only difference in the abscissa scale.

The result proves that the cubic shaped cells in the OOMMF program behave very close to point-like single spins in spite of the fact that they are portions of a medium in a continuous approximation. This also indicates that the single-spin calculations can be informative for some continuous systems. On the other hand it would be interesting to check experimentally the sequence of the transitions on a real square of permalloy to verify how small (large) should the cells be to follow the micromagnetic behavior described.
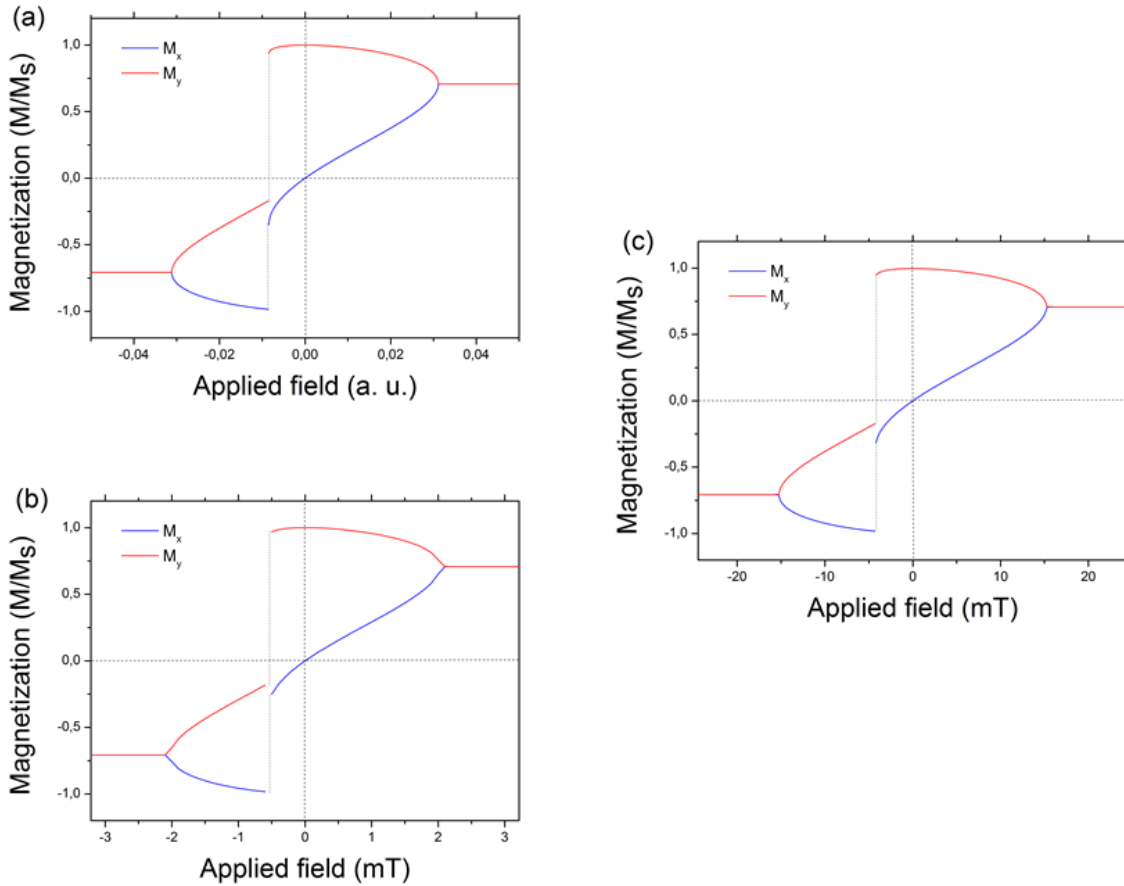

Figure 6.19: magnetization components M_x, M_y (blue, red) in (a) four-spin system of individual single spins $J=1$, $M^2=0.5$, (b) same geometry for microspin pixels with interaction parameters corresponding to permalloy,(c) same geometry for microspin pixels with interaction parameters of permalloy with exchange constant reduced by factor of 10.

7
Summary

The systems studied in this dissertation are assumed to be free of thermal fluctuations. The assumption is valid in low temperatures or when the magnetic moments, e.g. of macrospins, are sufficiently large. The equilibrium states of the systems under such an assumption correspond to minimum of energy instead of thermodynamic potentials involving entropy. Another consequence of the absence of fluctuations is that the solutions of the secular equations show real frequencies and, thus, describe infinitely lived, oscillating excitations. The complex frequencies mentioned in semi-infinite systems of Chapter 3 do not contradict this statement because the attenuation there is a result of energy radiation into the semi-infinite medium by a way of "leaky waves" [14, 15, 34, 35] rather than of dissipation mediated damping. It is known that from among the elementary excitations studied for signal transmission the magnetic ones show the lowest damping and the related large attenuation lengths [36, 37]. The neglect of damping is, therefore, a justified first approximation.

Defects of periodic structures are known to support localized states. This is a result of the fact that complex wave vectors are forbidden in the infinite systems to avoid solutions growing to infinity but they are allowed in semi-infinite media provided that they describe spatially attenuated partial waves. In principle the localized states occur outside the frequency ranges of bulk waves, because in the opposite case the energy is radiated into the medium and the secular state transform into resonances also known as leaky waves. Exceptions are known [17, 16, 38] but rare. However the phenomenon has been found here on the interface of two ferromagnetic chains coupled in an antiferromagnetic manner provided that the radiative bands of both chains are different.

The design of devices capable of transmitting spin waves at a desired speed in a defined frequency range is routinely effectuated with the use of micromagnetic computations. We have employed the techniques to study configurations and spin waves in magnetic particles of a currently available material (permalloy) and of feasible sizes. As the propagative properties change abruptly when switching between stable-metastable ferromagnetic and antiferromagnetic configurations we have studied conditions allowing one to recover the initial antiferromagnetic configuration which is stable in the absence of external field but does not reappear once the ferro-

magnetic configuration is set with a field of sufficient intensity in a chain of identical elliptically shaped macrospins. Two ways of achieving this goal have been proposed: i) making every second ellipse narrower that affects the shape anisotropy and ii) introducing anisotropy difference as a material parameter. It is not surprising that a typical classification of modes at $k = 0$ into acoustic and optical (as is symmetry protected in the phonon case) does not hold when the shapes of macrospins are altered but it is remarkable that this classification works perfectly for the particles of different material anisotropy. The mechanism of FM→AF switching relies on the softening of a mode. One can remark that the soft mode in this transformation is acoustic at $k = 0$, i.e. analogous to the one driving the FM→FM configuration change. Thus, the paths the system follows in the space of its parameters in both transformations begin in the same way. This result comes from the fact that the shape anisotropy does not allow for any soft mode involving out of plane displacements of the magnetization.

An attempt to construct a system mimicking the behavior of a macrospin has turned out successful for as few as two single spins in the macrospin. Not only is this a "toy" model for macrospin considerations but it is also conceivable in the realm of molecular magnets where the interactions are controlled by appropriate ligands. To behave like macrospins the pairs of spins, called here bi-spins, must show an intraparticle exchange ferromagnetic interactions in addition to the ubiquitous dipolar interactions that are also assumed between different bi-spins. Under such assumptions we have availed ourselves of a liberty to vary all the parameters of chains constructed of the bi-spins. A number of stable/metastable configurations have been found as functions of the distance of the bi-spins in the chain. The most striking is a transformation unifying properties of first and second order phase transition with bi-spin distance as a control parameter. This is in fact an example of ideal switching that transforms two very different configurations without hysteresis.

The sparsity of degrees of freedom in the chains of bi-spins allows one to watch the behaviour of all the modes. The rule is that the high frequency modes involve significant out-of plain semiaxes of the precession ellipses whereas the ellipticity (i.e. departure from circularity of the precession ellipse) grows with decreasing frequency so that the semi long axis of the ellipse lies in the plane of the chain. The ellipticity becomes infinite in the soft mode. This is in agreement with the results obtained for massive macrospins. We have demonstrated that the soft mode polarization coincides with the eigenvector of the Hessian matrix associated with the vanishing eigenvalue. A practical realization of a system with variable distance of macrospins would involve macrospins deposited on an elastic substrate deformable by an applied stress.

Using an example of a very small macrospin consisting of four voxels arranged

in a square we have demonstrated that the voxels behave, in spite of being parts of a continuum, in a very close way to a square particle constituted by single spins with ferromagnetic exchange interactions extended to the nearest neighbours. At this example we have also found that the sequence of configurations under a field applied parallel to the square diagonal is quite universal provided that the exchange interactions prevail over the dipolar ones. The system then undergoes one continuous and one discontinuous transition independently of the exchange interaction parameter. The ratio of the field intensities of both transitions does not depend on the interaction details.

Bibliography

[1] Jr W.F. Brown. Micromagnetics. *John Wiley and Sons*, 1963.

[2] M. Grimsditch, L. Giovannini, F. Montoncello, F. Nizzoli, Gary K. Leaf, and Hans G. Kaper. Magnetic normal modes in ferromagnetic nanoparticles: A dynamical matrix approach. *Phys. Rev. B*, 70:054409, aug 2004.

[3] J. M. Ziman. *Principles of the Theory of Solids*. Cambridge University Press, 1979.

[4] C. J. Bradley. *The mathematical theory of symmetry in solids; representation theory for point groups and space groups*. Clarendon Press, Oxford, 1972.

[5] Claas Willem Abert and Michael Hinze. *Discrete Mathematical Concepts in Micromagnetic Computations*.

[6] Theo Gerhardt. *Micromagnetic Simulations of Ferromagnetic Domain Walls in Nanowires*. PhD dissertation, Universitt Hamburg, 2014.

[7] Michael Joseph Donahue and Donald Gene Porter. Oommf: Object oriented micromagnetic framework, Jan 2016.

[8] K M Lebecki, M J Donahue, and M W Gutowski. Periodic boundary conditions for demagnetization interactions in micromagnetic simulations. *Journal of Physics D: Applied Physics*, 41(17):175005, 2008.

[9] Roberto Zivieri and Giancarlo Consolo. Hamiltonian and lagrangian dynamical matrix approaches applied to magnetic nanostructures. *Advances in Condensed Matter Physics*, 2012:1–16, 2012.

[10] Maria Bałanda, Zbigniew Tomkowicz, Wolfgang Haase, and Michał Rams. Single-chain magnet features in 1d [MnR4tpp][TCNE] compounds. *Journal of Physics: Conference Series*, 303:012036, jul 2011.

[11] Sławomir Mamica, Maciej Krawczyk, and Jarosław Wojciech Kłos. Spin-wave band structure in 2d magnonic crystals with elliptically shaped scattering centres. *Advances in Condensed Matter Physics*, 2012:1–6, 2012.

[12] Alexy D. Karenowska, Andrew D. Patterson, Michael J. Peterer, Einar B. Magnsson, and Peter J. Leek. Excitation and detection of propagating spin waves at the single magnon level, 2015.

[13] Leonard Dobrzyński. Interface response theory of discrete composite systems. *Surface Science Reports*, 6(3):119–157, jan 1986.

[14] Paweł Sobieszczyk, Mirosław Gałązka, Dominik Trzupek, and Piotr Zieliński. Propagation of surface waves and surface resonances along cylindrical cavities in materials with any allowed Poisson's ratio - part I: Clean inner surface. *Phys. Status Solidi B*, 252(7):1595–1604, jun 2015.

[15] Paweł Sobieszczyk, Mirosław Gałązka, Dominik Trzupek, and Piotr Zieliński. Propagation of surface waves and surface resonances along cylindrical cavities in materials with any allowed Poisson's ratio - part II: Thin-walled coating. *Phys. Status Solidi B*, 252(7):1605–1614, jun 2015.

[16] S.A. Gundersen, L. Wang, and J. Lothe. Secluded supersonic elastic surface waves. *Wave Motion*, 14(2):129–143, sep 1991.

[17] D. Trzupek and P. Zieliński. Isolated true surface wave in a radiative band on a surface of a stressed auxetic. *Physical Review Letters*, 103(7), aug 2009.

[18] P. Zieliński and L. Dobrzynski. Dynamics of thin epitaxial layers on (001) surfaces of bcc metals: A green-function approach. *Phys. Rev. B*, 41:10377–10386, may 1990.

[19] Allan H. Morrish. *The Physical Principles of Magnetism*. 01 2001.

[20] Sachin Gupta, K. G. Suresh, A. Das, A. K. Nigam, and A. Hoser. Effects of antiferro-ferromagnetic phase coexistence and spin fluctuations on the magnetic and related properties of NdCuSi. *APL Materials*, 3(6):066102, jun 2015.

[21] A. V. Chumak, V. I. Vasyuchka, A. A. Serga, and B. Hillebrands. Magnon spintronics. *Nature Physics*, 11(6):453–461, jun 2015.

[22] György Csaba, Ádám Papp, and Wolfgang Porod. Perspectives of using spin waves for computing and signal processing. *Physics Letters A*, 381(17):1471–1476, may 2017.

[23] Alexander Khitun, Mingqiang Bao, and Kang L Wang. Magnonic logic circuits. *Journal of Physics D: Applied Physics*, 43(26):264005, jun 2010.

[24] A. V. Chumak, A. A. Serga, and B. Hillebrands. Magnonic crystals for data processing. *Journal of Physics D: Applied Physics*, 50(24):244001, 2017.

[25] Qi Wang, Andrii V. Chumak, Lichuan Jin, Huaiwu Zhang, Burkard Hillebrands, and Zhiyong Zhong. Voltage-controlled nanoscale reconfigurable magnonic crystal. *Phys. Rev. B*, 95:134433, Apr 2017.

[26] D. Sander, S. O. Valenzuela, D. Makarov, C. H. Marrows, E. E. Fullerton, P. Fischer, J. McCord, P. Vavassori, S. Mangin, P. Pirro, B. Hillebrands, A. D. Kent, T. Jungwirth, O. Gutfleisch, C. G. Kim, and A. Berger. The 2017 magnetism roadmap. *Journal of Physics D: Applied Physics*, 50(36):363001, 2017.

[27] E. Stryjewski and N. Giordano. Metamagnetism. *Advances in Physics*, 26(5):487–650, sep 1977.

[28] Olivier Kahn. *Molecular Magnetism.* Wiley-VCH, aug 1993.

[29] Pierre Tolédano and Vladimir Dmitriev. *Reconstructive Phase Transitions.* World Scientific Pub Co Inc, jul 1996.

[30] J.-C. Tolédano and P. Tolédano. *The Landau Theory of Phase Transitions: Application to Structural, Incommensurate, Magnetic and Liquid Crystal Systems.* World Scientific Press, August 1987.

[31] Landau L.D. On the theory of phase transitions. *Zh. Eksp. Teor. Fiz.*, 7:19–32, 1937.

[32] A.L. Roitburd. Martensitic transformation as a typical phase transformation in solids. volume 33 of *Solid State Physics*, pages 317 – 390. Academic Press, 1978.

[33] Guohong Dai, Qingfeng Zhan, Huali Yang, Yiwei Liu, Xiaoshan Zhang, Zhenghu Zuo, Bin Chen, and Run-Wei Li. Controllable strain-induced uniaxial anisotropy of fe81ga19 films deposited on flexible bowed-substrates. *Journal of Applied Physics*, 114:173913 to, 11 2013.

[34] Paweł Sobieszczyk, Marcin Majka, Dominika Kuźma, Teik-Cheng Lim, and Piotr Zieliński. Effect of longitudinal stress on wave propagation in width-constrained elastic plates with arbitrary Poisson's ratio. *Phys. Status Solidi B*, 252(7):1615–1619, jun 2015.

[35] Paweł Sobieszczyk, Aleksandra Pajzderska, Dominika Kuźma, Marcin Majka, and Piotr Zieliński. Effect of water deposition on the surface dynamics of mesopores in MCM-41. *Phase Transitions*, 89(4):425–435, 2015.

[36] V. N. Krivoruchko. Spin waves damping in nanometre-scale magnetic materials (review article). *Low Temperature Physics*, 41:670 to 681, 09 2015.

[37] Takashi Manago, Kazuto Yamanoi, Shinya Kasai, and Seiji Mitani. Damping factor estimation using spin wave attenuation in permalloy film. *Journal of Applied Physics*, 117:17D121, 05 2015.

[38] A. A. Maznev and A. G. Every. Bound acoustic modes in the radiation continuum in isotropic layered systems without periodic structures. *Phys. Rev. B*, 97:014108, Jan 2018.